國 立 交 通 大 學

電 控 工 程 研 究 所

碩 士 論 文

利 用 嵌 入 式 繼 光 鏡 顯 微 超 頻 譜 影 像 系 統 進 行 口 腔 癌 檢 測

Detection of oral cancer using embedded relay lens microscopic hyperspectral imaging system (ERL-MHIS)

研 究 生：陳 誌 賢

指導教授：歐 陽 盟 教授

中 華 民 國 一百零一 年 十 月

利用嵌入式繼光鏡顯微超頻譜影像系統進行口腔癌檢測
Detection of oral cancer using embedded relay lens microscopic hyperspectral imaging system (ERL-MHIS)

研 究 生：陳誌賢　　Student：Chih-Hsien Chen

指導教授：歐陽盟　　Advisor：Mang Ou-Yang

國 立 交 通 大 學

電控工程研究所

碩 士 論 文

A Thesis

Submitted to Institute of Electrical Control Engineering

College of Electrical and Computer Engineering

National Chiao Tung University

in partial Fulfillment of the Requirements

for the Degree of

Master

in

Electrical Control Engineering

October 2012

Hsinchu, Taiwan, Republic of China

中華民國 一百零一 年 十 月

利用嵌入式繼光鏡顯微超頻譜影像系統進行口腔癌檢測

學生 ： 陳誌賢　　指導教授 ： 歐陽盟 教授

國立交通大學電控工程研究所

摘要

癌症在國人十大死因的榜首居高不下，其中口腔癌是惡性腫瘤中最可能早期發現，並且藉由早期治療進而痊癒。相較於傳統檢測方法，以肉眼判斷是否有癌症細胞的侵蝕，高光譜影像提供了更多的資訊。我們以嵌入式繼光鏡高光譜成像系統(ERL-MHIS)對細胞切片樣本進行掃描，建立一個三維高光譜資訊矩陣，並且提出了型態與光譜兩類方法進行癌症的辨識。在癌症細胞的影像型態判斷方面，我們提出兩種方法，第一個方法為使用臨界值分離出細胞的基底層，並且使用碎形維度(fractal dimension)計算維度，因為癌症細胞的分裂失去限制，分維的維度值會較正常細胞的維度高。當口腔黏膜細胞發生癌病變時，基底層細胞會持續向內部的固有層持續侵蝕，造成固有層的型態產生變化，因此第二種方法為使用 K 最鄰近分類算法(KNN)對固有層的細胞核影像做分類，並且計算分類結果的準確率。光譜判斷方面，使用了光譜強度的比值、半波寬度(FWHM)、波形下面積與光譜波段範圍內的強度。將分析結果使用高斯分佈計算準確率。我們將準確率高的前三個方法做結合，並且計算新的準確率 98.45%.最後，藉由考慮樣本資料，我們提出雞尾酒方法，將判斷癌症之螢光光譜的準確率提升到 87%。

Early detection of oral cancer using embedded relay lens microscopic hyperspectral imaging system (ERL-MHIS)

student：Chih-Hsien Chen **Advisor：Mang O u-Yang**

Institute of Electrical Control Engineering
National Chiao Tung University

Abstract

Cancer has been the leading cause of death for years in Taiwan. Oral cancer has the greatest possibility for early detection and recovery after early treatment. Compared to the traditional method of using the naked eye to detect oral cancer, the method of using the hyperspectral image of tissue can offer more information. We used the embedded relay lens microscopic hyperspectral imaging system to scan the sections and save the hyperspectral image. In this study, we diagnosed oral cancer using two methods: morphology and spectrum. In diagnosis using morphology, we presented two techniques: calculation of the fractal dimension and classification of k-Nearest Neighbor (KNN). In diagnosis using the spectrum method, we presented six techniques: comparing intensity, ratio of intensity, wavelength of peak, area under spectral curve, maximum after spline and full width at half maximum. We calculated the sensitivity and specificity using Gaussian distribution. Combining the 3 methods of the highest specificity provides a specificity of 98.45%. Finally, in accordance with sample data, we presented a cocktail method to increase the specificity of spectral analysis with fluorescence excitation to 87%.

Acknowledgement

在研究所兩年之碩士生涯，首先要感謝的人為指導教授 歐陽盟博士不辭辛勞指導我的研究方向，不時給予鼓勵與支持而讓我持續保有動力來解決研究過程中所遇到之問題，才能順利完成本論文研究。

感謝 段正仁博士、邱俊誠博士、黃國華博士在繁忙之中抽空給予支援，願意擔任學生之口試委員，在口試當天提供相當多寶貴意見讓學生可以清楚瞭解本研究可以改善之處，提升本論文之品質。

接著也要感謝實驗室博班學長庭緯、耀方、昱達與偉德，不論在課業與研究上面均給予我指導與意見，以及碩士班學長建成，給予研究之建議以及方法；還有碩士班同學與學弟新淼、智翔、子賢、禹舜、幸璁、冠亨、益群、浩志、劉穎、俊誠、胤源、碧秀在程式上面給予我許多支援，以及處理研究相關之大小事，所以讓我在研究所兩年生涯可以過得非常充實以及順利;感謝我的女友筑羽，持續給我鼓勵與支持，讓我以正向的心態努力研究。

還有感謝父母在於金錢以及精神上的鼓勵與支持，得以進入研究所學習更深入之專業技能，讓我可以提升自己，對於在未來踏入競爭如此激烈之社會，有非常大的幫助以及貢獻。因此在未來進入社會階段，必須持續保有一顆感恩的心不斷的提升自己、努力向上，使得自己在社會上可以出人頭地，以報答父母之恩惠。

Content

List of Figures

List of Tables

Chapter 1 Introduction

1.1 Background information

The habits of drinking, smoking and betel-nut chewing, in Taiwan have resulted in an increase in the past ten years in the number of people diagnosed with oral cancer. In the last decade, oral cancer was the third leading cause of cancer deaths in Taiwan and number 6 worldwide [1]. Given the high cost and risk in the therapy of terminal oral cancer, early detection is an important issue. The cure rate is 90% in the first stage of oral cancer, 80–90% in the second stage and 30–50% in the third and fourth stages [2]. Traditionally, the method of detecting oral cancer had been to observe the biopsy of the lesions, and then to use a microscope to determine the change in morphology. With the progress of technology, the hyper-spectral scanning system began to be used in observing oral cancer biopsies.

It took twenty years from the invention of the spectrometer for the development of the hyperspectral system. With the spectrometer, the reflected spectrum of different substances was different and provided observers with richer information. The hyperspectral system had the potential to find the relationship between the biochemical and the morphological, and it offered a noninvasive technology to detect oral cancer. Because of its noninvasiveness, it provided rapid detection of oral cancer.

When the change in tissue biochemistry took place, the detected optical characteristic would be influenced. The hyperspectral information in cancer detection included image and spectrum. The analysis of the image was usually done in real time. First, researchers coated the sample with dye, such as hematoxylin. After the light source irradiated the target, the probe could collect information. In some studies, the most helpful feature would be found in the specific excitation wavelength. The autofluorescent spectrum of tissue had been widely used to distinguish cancer from healthy oral mucosa. The methods of spectral analysis included determining: the ratio of intensity in different wavelengths, the intensity in specific wavelength, and the emission and excitation wavelength ratio.

1.2 Motivation

With respect to the leading causes of disease-related deaths in Taiwan,

cancer was number 1 in the past 29 years; the average yearly number of deaths caused by cancer was 41,046. In other words, one person died every 13 min as a result of cancer. If the cancer could be detected at an early stage, the cure rate would be increased. The widely used method of detection was observing the biopsies by microscope. Using the naked eye, the medical staffs determined whether the cancer cells had diffused. This method has two shortcomings. First, there would be some error caused by lack of experience in judging cancer tissues. Second, the diagnosis was limited to the spectral bands of visible light: 380~780nm. The data for the hyperspectral image had spectral and spatial information, and the range of wavelength included not only visible light but also near-infrared and ultraviolet. The error caused by inexperience could be avoided if the algorithm comparing the characteristic of the spectrum had been entered into the computer.

In judging cancer tissue, the main basis for observers was whether the basal layer had unlimitedly eroded the lamina propria. The probe diagnosing oral cancer was limited to the surface of the mucosa with low transmittance, so observing the spread of cancer was impossible. If we could combine the analysis of morphology and spectrum, the sensitivity and specificity would be improved.

This research used the hyperspectral scanning system to distinguish cancer cells. We used a microscope to enlarge the image of the sample. There were three light sources: a halogen lamp, a fluorescent lamp with 330~385nm excitation and a fluorescent lamp with 470~490nm excitation. We operated the motor to move the relay lens for scanning the image, and we used the hyperspectrometer to transform the image into a hyperspectral image. The EMCCD would store the hyperspectral image as a three-dimensional matrix. The three axes were x, y and λ. There were four layers in the oral mucosa: the lamina propria, the basal-cell layer, the prickle-cell layer and the keratinized layer. The boundary between the lamina propria and the basal layer became blurred because of the cancer cells' erosion. We tried to digitalize the image of the cancer and normal tissue. Lastly, we determined the sensitivity and specificity.

Chapter 2 Review Articles

2.1 Introduction of Anatomy

Anatomy is the study of the internal and external structure of the body. Anatomy can be divided into microscopic anatomy and gross anatomy according to the methods of research. Microscopic anatomy uses the microscope to observe the fine structure unobservable with the naked eye. It includes cytology and histology. Gross anatomy means using the naked eye to observe the structure of the body. It includes surface anatomy, regional anatomy and systemic anatomy.

With respect to the three dimensions, section pertains to the method of understanding the body's position. Because of the sections, we do not have to understand the structure of the body via surgery. The planes are the transverse plane, the frontal plane and the sagittal plane [3].

Table 2-1: The plane of body.

Plane	Direction	description
transverse	Frontal or coronal	The body is divided into upper and lower part.
Frontal plane	Transverse or horizontal	The body is divided into front and rear part.
Sagittal plane	Sagittal	The body is divided into left and right part.
Midsagittal plane	Sagittal	The plane goes through the midline to divede the body into left and right part equally.

2.1.1 Oral cavity

The anatomical locations are the gingival, hard palate, soft palate, maxillar fold, cheek mucosa, dorsal side of the tongue, lateral border of the tongue, ventral side of the tongue, transition of the tongue to the floor of the mouth, the floor of the mouth, the mandibular fold, the lower inner lip mucosa, and the vermilion border of the lip [4].

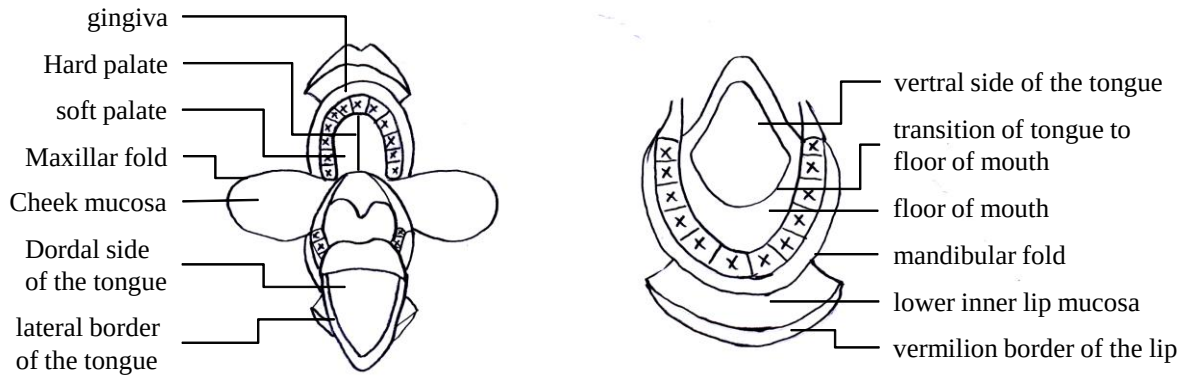

Figure 2-1: The 13 anatomical location.

The stratified squamous epithelium lies in the oral cavity. The glands located below the mucosa can secrete serous and mucous. The skeletal muscle fibers compose the main part of the tongue. In some parts of the oral cavity, the deep tissues are composed of bones, including the hard jaws and teeth.

The lips cover the opening of the mouth. The squamous epithelium covers the lips, which contain the glands and underlying muscle. The vermilion is the region between the outer surface and the inner surface. The squamous epithelium of the vermilion contains the rete ridge system. The salivary gland emits secretions to the surface, and the opening of Fordyce's spots is on the surface of the mucosa. In the depth of the lips, the orbicularis oris muscles surrounding the mouth are responsible for the opening and closing of the mouth.

The squamous epithelium, which internally lines the cheeks, is rich in glycogen. Because of the long-term friction of the teeth and cheek biting, there are some horny regions. There are buccal glands, Fordyce's spots and cheek muscle under the mucosa.

The bottom of the mouth is covered by a non-keratinized stratified squamous epithelium that connects with the ventral epidermal of the tongue. The bottom of the mouth is rich in minor sublingual glands, and there are major sublingual glands at the ventral epidermis of the tongue.

The tongue, which has a high degree of genital muscle, enters the mouth from the floor of the mouth. The ventral epidermis of the tongue is covered by a non-keratinized stratified squamous epithelium that connects with the bottom of the mouth. The back of the tongue is covered by a keratinized stratified squamous epithelium.

The dorsal surface of the tongue is divided into the front two-thirds and the

other one-third by the circumvallate papilla, which is like a flattened dome. The epithelial of the circumvallate papilla contains taste buds that can detect bitterness [3].

2.2 Introduction of Histology

Histology is the science of the microstructure of the biological. Histology is an important study of the physiological and the medical because it combines biochemistry, molecular biology and physiology. Since the invention of the optical microscope and use of tissue sections started the research of histology, the knowledge of cells has been established. Originally, tissues were divided into four types: epithelial tissues, muscular tissues, nervous tissues and connective tissues.

Now, electron microscopy, cell culture technology of cloning and protein sequencing, and molecular genetics provide new understanding of the cell. We can classify cells according to their main function, such as epithelial cells, supporting cells, contractile cells, nerve cells, germ cells, blood cells, immune cells and hormone-secreting cells. However, one cell that may have multiple functions will be grouped into more than one cell type, for instance, many hormone-secreting cells are also epithelial cells, a white blood cell is not only a blood cell but also an immune cell, etc.

Table 2-2: The classification of cells.

cell	example	function
Epithelial cells	The skin, the lining cells of blood vessels	Barrier, absorption, secretion
Supporting cells	Cartilages, bones	The composition and maintenance of body
Contractile cells	Muscle	Movement
Nerve cells	Brain	Direct communication between cells
Germ cells	Sperm	Breeding
Blood cells	White blood cells, erythrocyte	Protection, carry oxygen

Immune cells	White blood cells, lymphoid tissue	Protection
Hormone secreting cells	Thyroid, adrenal	Indirect communication between the cells

If all the cells in the tissue have the same structure, the tissue is called simple tissue. But most tissues containing different functional cells are called compound tissues. For example, nerve tissue contains supporting cells, immune cells and epithelial cells [5].

2.2.1 Oral mucosal tissue

In a section of healthy oral mucosa, the epithelial tissue showing the hierarchical arrangement includes: the basal-cell layer, the prickle-cell layer and the keratinized layer. The basal-cell is a cubic or a columnar cell in the bottom of the epithelial tissue. Because of the ability of hyperplasia, the nucleus of basal cells that have been coated by some dyes, present a dark color. Above the basal-cell layer, the prickle-cells connect to other prickle-cells by the intercellular bridge. The keratinized layer is in the outermost layer. The keratinized layer is the last level of differentiation in epithelial tissue. According to the keratinized layer, the oral mucosa has resistance to friction.

2.2.2 Oral squamous cell carcinoma

Cancer is a genetic disease, but it is not heritable. It is caused by carcinogenic factors and genetic changes. The normal cycle of its growth has been uncontrolled, leading to an abnormal proliferation. The cancer tissue grows rapidly and can spread to other parts of the body through the blood and lymph. The cancer cells may destroy the organ that has been eroded, and they may be life-threatening.

Oral squamous cell carcinoma (OSCC), also called oral cancer, is an invasive lesion at the oral mucosa. The causes of oral cancer include smoking, drinking, chewing betel nuts, and viral infection. Symptoms include: leukoplakia and erythroplakia on the surface of the oral mucosa, an unexplained tumor, mucosal ulceration that does not heal for a long time, unexplained bleeding and restricted activity of the tongue.

When we observe the lesions of cancer tissue in the oral mucosa, we can determine the changes of type and structure. The changes of type include: increased activity of cell division, the ratio of nucleus and cytoplasm, the number of nuclei chromosomes and the normal space between the cells. The

change of structure means the direction of cell proliferation is uncontrolled. The lamina propria is eroded by the cancerous tissue. In histology, we can classify oral cancer by the degree of differentiation, including well differentiation, moderate differentiation and poor differentiation. The hyper degree of differentiation signifies better healing after surgery.

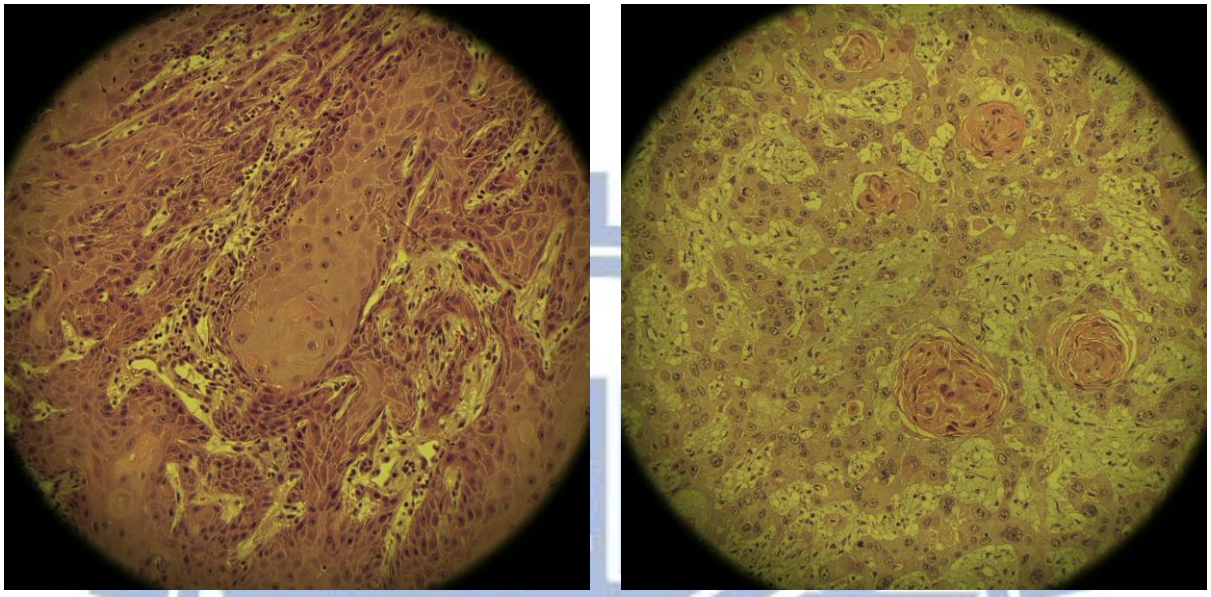

(a) (b)

Figure 2-2: (a) Well differentiated keratinizing squamous cell carcinoma. (b) Poorly differentiated keratinizing squamous cell carcinoma.

2.2.3 Process of making sections

When we examine the tissues by light microscope, paraffin embedding is the standard method for making the tissue samples. It is inexpensive, easy to use, and can be done automatically by machine. After the tissues were dissected, the samples were fixed in paraformaldehyde overnight. The samples were dehydrated by placing them in ethanol until the water in the tissue and fixative was removed. The alcohol was then replaced by organic solvents. Finally, the sample was moved into paraffin at the melting point of paraffin. At a normal temperature, the paraffin would solidify, and the sample could be cut into thin slices (2–3μm) without variant.

Since cells are colorless, the sections must be stained before observation by the light microscope. The staining methods include: empirical stains, histochemical stains, enzyme histochemical stains and immunocytochemistry. The combination of hematoxyline and eosin is the most useful agent in the detection of the sections. It is easy to use and inexpensive. The nucleus is

stained purple or black, and the cytoplasm is stained red or pink.

2.3 Development of diagnosing cancer using hyperspectral image

2.3.1 Diagnosis of cancer from image

A fluorescent image was produced in the tissue that the light source irradiated. Because imaging provided two-dimensional information, we could easily mark the areas of lesions in the specific excitation wavelength. The fluorescence imaging techniques enabled real-time detection of cancer simple; it is inexpensive and has high sensitivity and specificity. Many studies have been performed using fluorescence imaging [6] to detect cancer in different organs, such as oral cancer and cancer of the lungs [7-12], the bladder [13], the colon [14-20] and the gastrointestinal tract [21-24].

Ina *et al*. used the laser-scanning fluorescence 351–364nm and 488nm excitation to detect cervical cancer [25]. Due to the essential dye, Mitotracker Orange, they could see the precancer's cytoplasmic fluorescence in the bottom of the epithelium. They found that the intensity of fluorescence decreased with the development of cancer cells. In this study, only 10 patients were diagnosed, and the sample number was low.

Darren *et al*. observed the fluorescence images of oral lesions and normal tissues; the images were obtained from 56 patients and 11 normal volunteers [26]. They classified the images as normal and cancer in different fluorescence excitation wavelengths, 365, 380, 405 and 450nm, with the ratio of normalized red-to-green fluorescence and the autofluorescent image. The data were divided into two sets: a training set and a validation set. The training set included: 20% invasive cancer, 28% dysplasia and 52% normal; the validation set included: 14% invasive cancer, 25% dysplasia and 61% normal. With 405nm excitation, the autofluorescent image showed obvious decreased intensity. It had the highest sensitivity (95.9%) and specificity (96.2%) in the training set, and 100% sensitivity and 91.4% specificity in the validation set. They provided a noninvasive and sensitivity tool to diagnose oral cancer. They detected oral lesions using the decrease in autofluorescence images without observing the spectrum.

Catherine *et al*. used a hand-held device to evaluate oral cancer by location, fluorescence visualization (FV) status, histology and loss of heterozygosity (LOH) [27, 28]. First, they marked a blue line on the surface of the tumor diagnosed by the naked eye. After the light illuminated the tissues, the tissues provided direct visualization, and they marked a green line in the FV loss (FVL) area as the tumor margins. Lastly, they used LOH to analyze the FVL biopsies

from the tumor margins. In a total of 44 patients, the sensitivity was 98% and the specificity was 100%. However, they did not analyze the spectrum of biopsies.

2.3.2 Diagnosis of cancer from spectrum

Diagnosis based on spectrum has the potential to determine the change of material in the cancer cells. The spectrum was classified as the halogen spectrum and the fluorescence spectrum. When the halogen irradiated the section, we recorded the transmittance as the halogen spectrum. When the light source excited the tissue, the fluorescence spectrum was emitted by the tissue. The spectral data were saved to a computer to be analyzed. Many studies have been performed using the spectrum method to distinguish between normal cells and cancer cells, and the method includes: Principal Components Analysis (PCA) [29-31], emission wavelength ratios [32-35], change of intensity [36-40] and artificial neural networks [41, 42].

Irene *et al.* evaluated low-grade and high-grade dysplasia of Barrett's esophagus (BE) by fluorescence, scattering properties, and enlargement and crowding of nuclei [43]. They tried to distinguish high-grade dysplasia from low-grade dysplastic and nondysplastic BE, and high-grade and low-grade dysplasia from nondysplastic BE. There were two peaks in the fluorescence with 337nm excitation; the decrease between the two peaks occurring in the 420nm was caused by the absorption of oxyhemoglobin; they combined the corresponding reflectance spectrum to compensate for the decrease.

At 337nm excitation, the line-shape of the spectrum shifted to the right during the progression from nondysplastic to low-grade, to high-grade dysplasia. At 397nm excitation, the increase of intensity was found in the wavelength range 600–750nm. After the corresponding fitting of the reflectance spectrum, the scattering coefficient reflectance spectrum, μs, changed in different grades of dysplastic tissue. They also showed the enlargement of nuclei could be the characteristic, defining diameter > 10 μm as enlargement of the nuclei. The analysis combining 3 techniques had a sensitivity of 93% and a specificity of 100%. Their analysis combined the spectrum and image, but the enlargement would be hard to define because of the irregular shape of the nuclei.

Hamed *et al.* detected cancer by using integral, support vector machines (SVM), spectral standard deviation and the normalized cancer index (NDCI) [44]. The halogen spectrum was normalized to calculate the reflectance using the following equation:

$$R(\lambda) = \frac{I_{raw}(\lambda) - I_{dark}(\lambda)}{I_{white}(\lambda) - I_{dark}(\lambda)} \quad (2\text{-}1)$$

where R(λ) is the reflectance value, $I_{raw}(\lambda)$ is the raw-data radiance value, $I_{dark}(\lambda)$ is the dark current and $I_{white}(\lambda)$ is the white board radiance. The wavelength range was 1000–2500nm, and they found the area under the spectral curve was higher in cancer than in normal tissues, while the slopes at 1200–1400nm were lower in cancer tissues. They also used SVM to classify tissue into normal and cancer tissues. They also compared the spectral standard deviation using the following equations, (2–2) in two dimensions and (2–3) in three dimensions:

$$SD(i, j) = C\sum_{k=k1}^{k2}\{\sum_{i=i-i1}^{i+i1}\sum_{j=j-j1}^{j+j1}[R(i, j, k) - R_{av}]^2\}^{\frac{1}{2}} \quad (2\text{-}2)$$

$$SD(i, j) = C\{\sum_{i=i-i1}^{i+i1}\sum_{j=j-j1}^{j+j1}\sum_{k=k1}^{k2}[R(i, j, k) - R_{av}]^2\}^{\frac{1}{2}} \quad (2\text{-}3)$$

where SD was the standard deviation, k was the number of wavelength bands, k1 and k2 were the range of wavelength bands, i and j were spatial coordinates, i1 and j1 were the area size of the predefined neighbor, C was a coefficient, R was the reflectance and R_{av} was the mean of reflectance. The NDCI was calculated using the following equation:

$$NDCI = C_1\sum_{k=k1}^{k2}(d(R_k))^2 + {}_2\sum_{k=k3}^{k4}(d(R_k))^2 \quad (2\text{-}4)$$

where NDCI was the normalized cancer index, C1 and C2 were coefficients, R_k was the normalized reflectance in wavelength k, $d(R_k)$ was the derivative of R_k , k_1, k_2, k_3, and k_4 were the wavelength bands. Lastly, the specificity was 88% using integral, 80% using SVM, 82% using spectral standard deviation and 93% using NDCI. However, they only analyzed the halogen spectrum without the fluorescence that could show the change of biochemistry.

Kevin *et al.* used the colonoscopy to detect colorectal cancer from two imaging modalities: visible and NIR autofluorescence imaging and hyperspectral reflectance imaging [45]. For normalization, they subtracted the background intensity and divided the corresponding brightfield images. In the autofluorescence imaging, they found that normal tissues emitted more autofluorescence than the cancer tissues in 515nm excitation did, but the normal tissues emitted less autofluorescence than the cancer tissues did in 567nm

excitation. Therefore, they divided the fluorescence intensity at the second peak with 567nm excitation by the fluorescence intensity at the first peak with 515nm excitation to diagnose the colorectal cancer, and the ratio was less than 1.96 in normal mucosa and more than 1.98 in cancer, as shown in Table 2-3. In the hyperspectral reflectance imaging, the result of a total of 7 samples (T1-T7) showed a great correlation between different stages of cancer except for tissue sample T5. However, the number of samples was too low to prove the method was successful.

Table 2-3: Tissue type, disease state, and 516/515nm ratio.

Sample	Tissue type	Disease state	567/515nm ratio
T1	Rextum	Carcinoma	2.0003
T2	Sigmoid Colon	Dysplasia adenoma	2.0655
T3	Colon	Normal mucosa	1.9563
T4	Sigmoid Colon	Dysplasia adenoma with possible cancer	2.0927
T5	Right Colon	Normal mucosa	1.9563
T6	Descending Colon	Moderately differentiated adenocarcinoma	1.9864
T7	Colon	Normal mucosa	1.9562

Kojiro *et al.* analyzed the fluorescence spectrum of oral squamous cell carcinoma in 404nm excitation [46]. The samples were all in hamsters, and the oral squamous cell carcinoma was induced by chemicals. With 404nm excitation, they found the intensity increased at 634 and 672nm peaks and decreased at 520 and 582nm peaks, as shown in Table 2-4. They said the decrease at 520nm was due to the reducing oxidized forms of riboflavin in tumor tissues; the increase at 630nm was due to the accumulation of porphyrin in the tumor tissues. After they defined the intensities of the peaks at 582, 634 and 672nm as A, B and C, respectively, they calculated A/B, B/C and A/C, as shown in Table 2-5. The value of A/B and A/C decreased during the progression from control to hyperplasia, to early cancer, to invasive cancer.

Table 2-4: Fluorescence intensities with 404nm excitation.

	Peak A (582nm)	Peak B (634nm)	Peak C (672nm)
Control (n=6)	24.9±3.8	5.3±0.7	0.9±0.3
Hyperplasia (n=10)	21.7±4.7	6.4±2.4	1.2±0.3
Early cancer (n=5)	17.1±5.8	5.1±1.1	1.4±0.6
Invasive cancer (n=3)	13.0±9.0	27.0±19.1	8.1±4.7

Table 2-5: Ratio of fluorescence intensities with 404nm excitation.

	A/B	B/C	A/C
Control (n=6)	4.7±0.5	6.2±1.6	8.0±9.4
Hyperplasia (n=10)	3.4±0.7	5.5±1.6	18.8±4.4
Early cancer (n=5)	3.4±1.0	4.2±1.4	13.6±4.5
Invasive cancer (n=3)	0.8±0.7	6.5±8.5	1.5±0.7

Brigitte *et al.* analyzed the fluorescence spectrum of colorectal cancer with 375–478nm excitation [47]. When they evaluated the spectrum from 478 to 700nm, they found that the ratio of the intensity in the 500–549nm to 657–700nm was a characteristic of the presence of cancer cells, and the critical value was 2.25. The sensitivity of this analysis was 97%, and its specificity was 95%. However, the number of the spectrum was less than 15 in one sample, too low to prove the method was successful.

Chapter 3 Methodology

3.1 Embedded Relay Lens Microscopic Hyperspectral Imaging System (ERL-MHIS)

In the measurement process, the system (ERL-MHIS) contained two light sources, one microscope, one spectrometer, EMCCD saving hyperspectral data, and a computer displaying and analyzing the spectrum. The light sources included a halogen spectrum and a fluorescence spectrum with 330–385nm and 470–490nm excitation. The microscope (IX701, Olympus) enlarged the image of the target area on the sample and transferred the image to the spectrometer. Lastly, the halogen spectrum and the fluorescence spectrum were saved as a 1004x1004x1002 three-dimensional matrix by the EMCCD.

The relay lens was between the microscope and the spectrometer. The function of the relay lens was to transfer the image from the object plane to the image plane. By moving the relay lens, we transferred the image without the relative movement between the microscope and the spectrometer.

The hyperspectral data were saved in a personal computer (PC) for analysis. The PC also controlled the ERL-MHIS. A self-written code controlled the motor to move the relay lens for scanning the image of the target area, and set the integration time of EMCCD; the hyperspectral data were also analyzed by the PC.

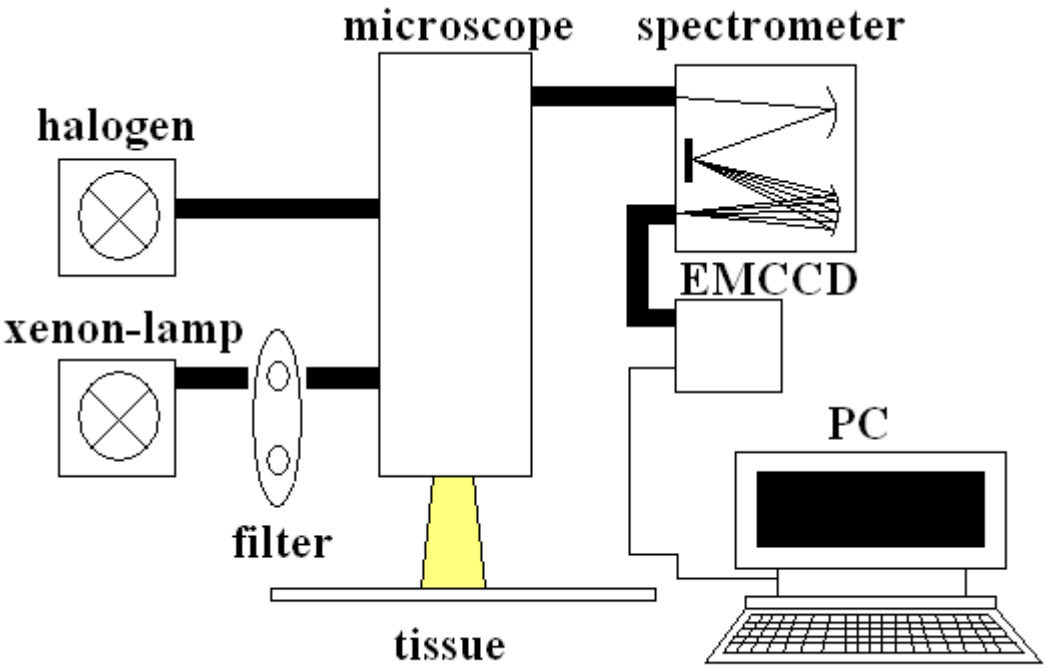

Figure 3-1: The embedded relay lens microscopic hyperspectral imaging system (ERL-MHIS).

3.2 Process of hyperspectral data

Generally, the hyperspectral image was saved in binary format, including band sequential (BSQ), band interleaved by pixel (BIP) and band interleaved by line (BIL). BSQ, the data of the same wavelength in the hyperspectral image, were stored in one file. For getting the spectral information of the points in the image, BSQ was the best choice. When we used the BIP format, we stored the first pixel of all wavelengths in the first file, the second pixel of all wavelengths in the second file, the third pixel of all wavelengths in the third file, and so on. According to BIL format, we stored the information of the same split in one image for one file. BIL was the compromise between BSQ and BIP, and it was also the most commonly used.

In the spectra of halogen, we calculated the penetration after removing the light and dark noise. In the halogen, the center of the image had the strongest brightness because of the light source. The light noise was caused by the uneven light source. We calculated the transmittance and removed the dark and light noise using the following equation:

$$T(\lambda) = \frac{I_{raw}(\lambda) - I_{dark}(\lambda)}{I_{light}(\lambda) - I_{dark}(\lambda)} \qquad (3\text{-}1)$$

where T(λ) is the transmittance value, I_{raw}(λ) is the raw data, I_{dark}(λ) is the dark noise, and I_{light}(λ) is the light noise. In the same way, the hyperspectral data in the fluorescence needed to have the dark noise removed.

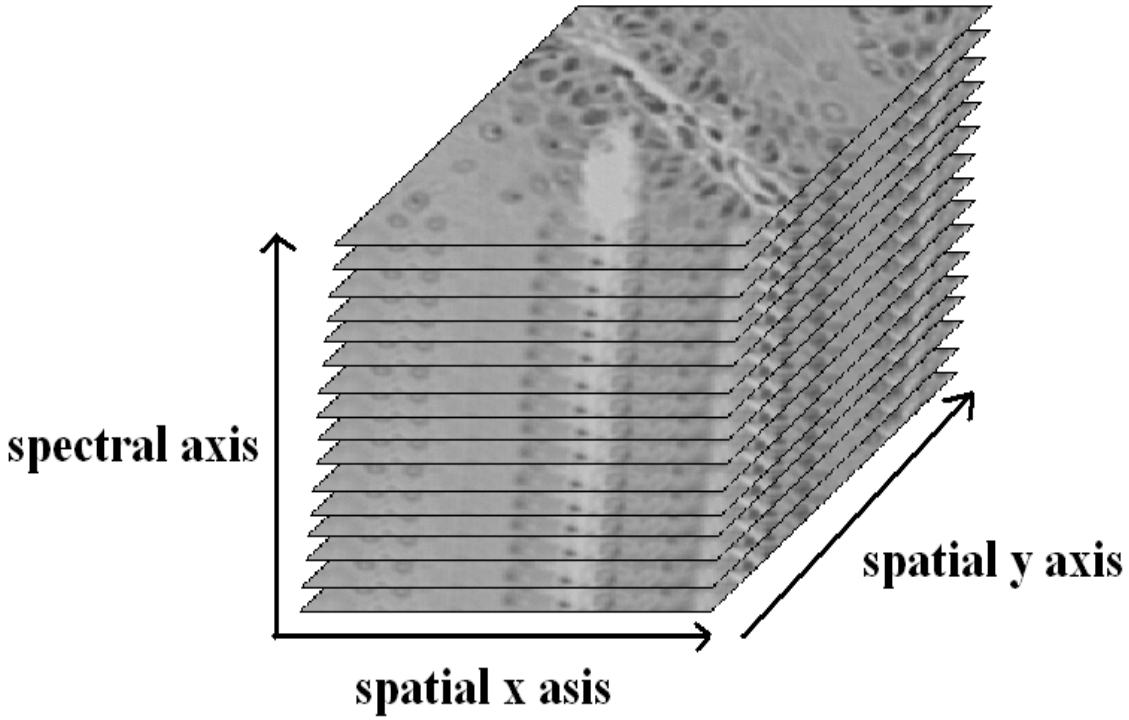

Figure 3-2: The three dimensional matrix of hyperstral image.

In our research, the original information pertaining to the hyperspectral image was a three-dimensional matrix, and the three axes were x, y and λ. For the matrix, x was 1004, y was 1004 and λ was 1002. It meant the image was 1004 pixel size and 1002 bands. For easy analysis, we transformed the three-dimensional matrix to 1004 files by BIL format.

3.3 Patients and samples

We investigated 33 patients in our research, including 32 men and 1 woman: 10 patients with good differentiation, 19 patients with moderate differentiation, and 4 patients with poor differentiation. The biopsy locations involved: 15 sections at the tongue, 6 biopsies at the buccal mucosa, 5 biopsies at the gum, 3 biopsies at the palate, two biopsies at the pyriform sinus, one biopsy at the upper lip, and one biopsy at the bucca and retromolar trigone.

We took two images from each sample: normal and cancer. According to the different light sources: one halogen and two kinds of fluorescent, we had three sets of hyperspectral data in one image, so we had a total of six sets of hyperspectral data on one patient. Because we had the data of light source for only the sample numbers 1~12, we only analyzed the sample numbers 1 to 12 using topology, and analyzed all samples using spectrum.

3.4 Morphological methods for diagnosing oral cancer

In cancerous tissue, the erosion of cancer cells is uncontrollable. It changes the image of the epithelial tissue in the cancer tissue. We tried to digitalize these changes, so we proposed two methods to analyze the erosion of cancer cells in histology. In normal tissue, there are clear borders between different layers, as shown in Figure 3-3a. In cancerous tissues, cancer cells erode other cells, as shown in Figure 3-3b, and it causes unclear borders between different layers. Therefore, we calculated the fractal dimension of the basal-cell layer in normal cells and of cancer cells in cancerous tissue. We also found a change of morphology in the lamina propria between normal and cancerous tissue, such as the increasing number of nuclei. Therefore, we classified the image of nuclei as basal cells and lamina propria by K-nearest neighbor. In cancerous tissue, because of the change of morphology in the lamina propria, the correct rate of classification was low.

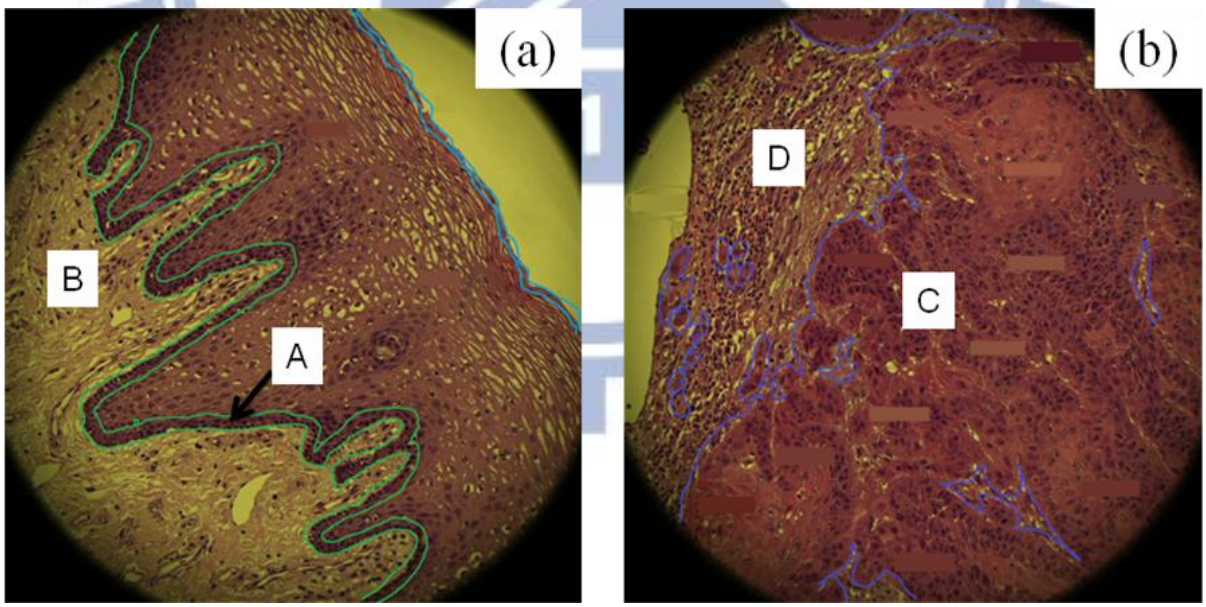

Figure 3-3: The image (a) of normal tissue and (b) cancer tissue. A: basal-cell layer B: lamina propria in normal tissue C: cancer cells D: lamina propria in cancer tissue.

3.4.1 Fractal Dimension

In the topological dimension, 0 was used for points, 1 for lines, 2 for surface and 3 for volumes. Generally, the value of dimension meant the number of coordinate axis to determine the location of one point for the graphics.

Differing from the topological dimension, the fractal dimension can be a non-integer value. The fractal dimension can be divided into regular and irregular. The dimension of regular fractal, like the Koch curve and the Cantor set, was calculated using the formula (3-2). D was the dimension, m was the number of new sticks and the 1/c signified the scaling factor.

$$D = \ln m \Big/ \ln(1/c) \tag{3-2}$$

When we observed the biopsies of cancerous tissue, the cancer cells in the basal-cell layer eroded the lamina propria. If we only leaved the image of the basal-cell layer, we could determine the erosion of the cancer cells by calculating the fractal dimension of the basal-cell layer. The image of the basal-layer in cancerous tissues was more complex than in normal tissues. In other words, the fractal dimension of the basal-cell layer calculated was higher in cancerous tissues than in normal tissues.

We superimposed the image of the hyperspectral data on the wavelength range 500~580nm because the largest difference in the spectral intensity between the basal-cell layer and the lamina propria was there. Then we fuzzified the image superimposed by hyperspectral data in the wavelength range 500~580nm to decrease the effect of nuclei by moving the average. Because the spectral intensity of the basal-cell layer was lower, we tried to use the threshold method to leave the basal-cell layer. The value of the threshold method was decided by the nuclei chosen by hand. Closing was the method to fill the interruption and gap in morphological image processing. We used the closing to remove the small cracks of the basal-cell layer. Lastly, we calculated the fractal dimension by the formula (3–2).

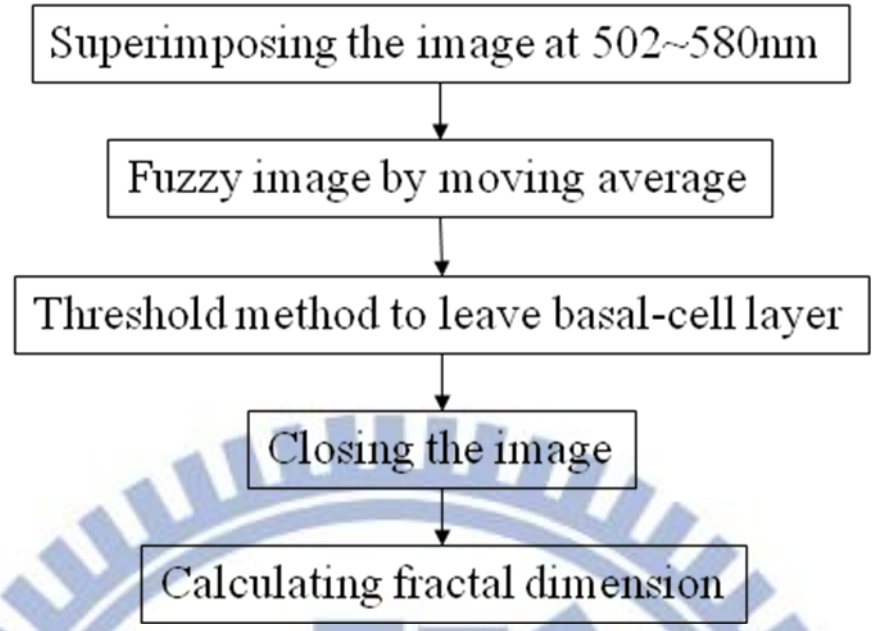

Figure 3-4: The flow chart of analysis by fractal dimension.

3.4.2 Classification by K-Nearest Neighbor

K-nearest Neighbor (KNN) is one of the machine-learning algorithms, and it is instance-based learning. KNN classifies the test data by the closest training data in the feature space. When inputting test data, we calculated the distance between the input and all training data. In the k sets of closest training data, if the majority belonged to a category, the test data also belonged to the category.

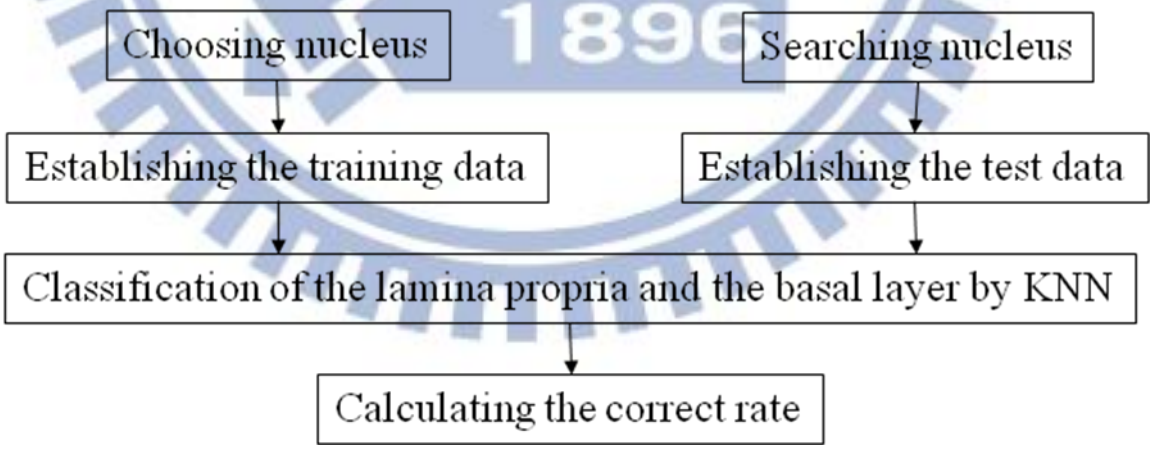

Figure 3-5: The flow chart of analysis by KNN classifying.

When we observed the section of cancer tissue, we determined the change of the image in the lamina propria because of the erosion by the cancer cells. Because the morphology of the samples was one by one case, we constructed the training data and used the KNN digitalizing the change of the image in the lamina propria. If we classified the nuclei in the basal-cell layer and lamina

propria by KNN, the correct rate of classification was lower in cancer cells because of the change of the image in the lamina propria by the erosion of the cancer cells. First, we had to establish the training data and test data. To establish the training data, we chose nuclei of the basal-cell layer and of the prickle-cell layer in normal tissue and cancer cells in cancerous tissue, which we labeled as group A. Then we chose some nuclei of the lamina propria, which we labeled as group B. In every coordinate, we got an 11x11 matrix, similar to the size of a cell, and expanded the matrix to the one-dimensional matrix, as in Figure 3-5; we recorded the one-dimensional matrix as training data. To establish the test data, we moved an 11x11 matrix to scan the image. When the intensity of the 5x5 matrix in the center was lower than 80% intensity of the average in the 11x11 matrix, we recorded the 11x11 matrix as a nucleus. After the matrix scanning of the image, we expanded the 11x11 matrix as an one dimensional matrix, as in Figure 3-5, and recorded the one dimensional matrix as test data.

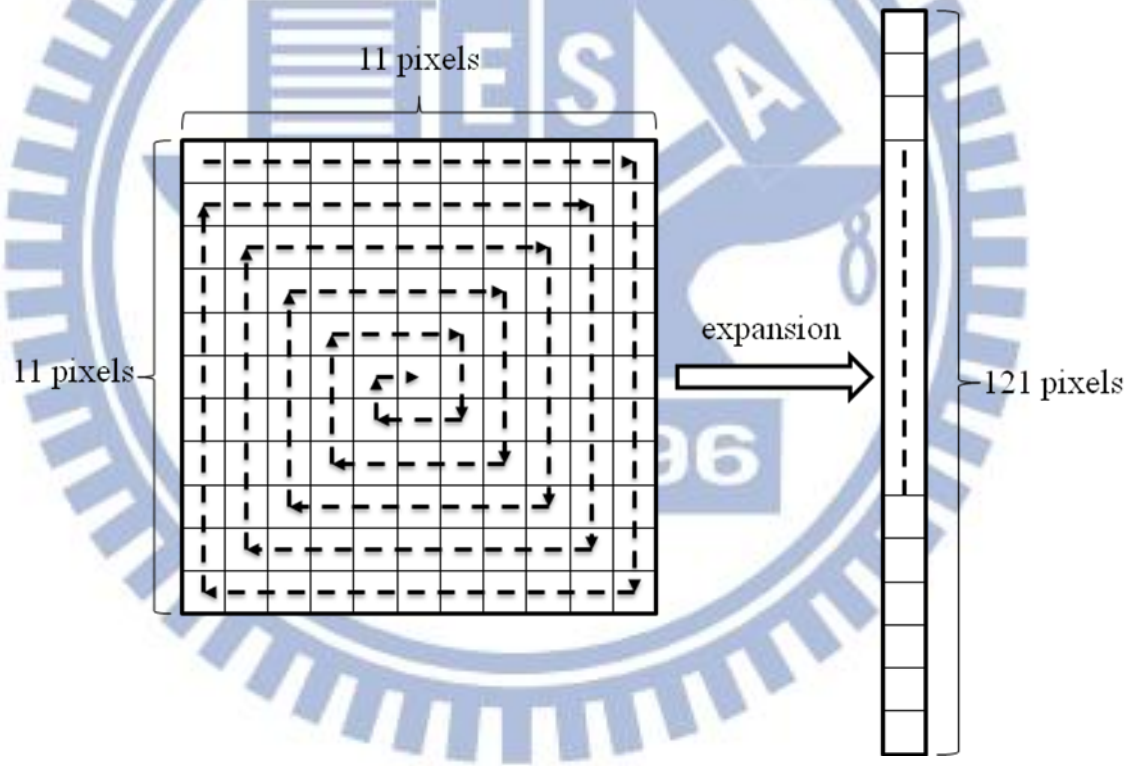

Figure 3-6: Expanding an 11x11 matrix to one dimensional matrix.

According to the training data, we could classify the test data by KNN, and the vector difference between the test data and each set of training data in the feature space was calculated. Lastly, we calculated the correct rate of the lamina propria classified by KNN.

3.5 Spectral methods for diagnosing oral cancer

Before analyzing the spectrum, we needed to remove the noise. For instance, the spectrum in halogen dark and light noise needed to be removed; the spectrum in fluorescence only removed the dark noise because there was no data for the light source.

After removing the noise, we marked nuclei in the image of the sample and recorded these coordinates. According to the coordinates chosen by hand, we got the spectrum of these nuclei. We had three methods to analyze these spectral data: four in halogen, four in fluorescence 330~385nm excitation and three in fluorescence 470~490nm excitation.

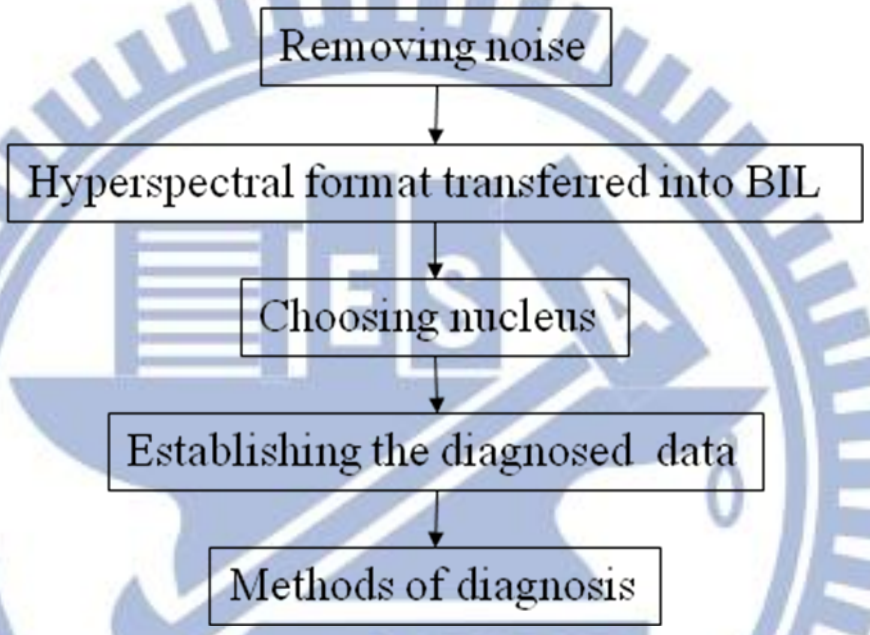

Figure 3-7: The flow chart of spectral analysis.

3.5.1 Intensity in the specific wavelength range

In some wavelength ranges, the spectral curve showed an obvious characteristic. For searching the specific wavelength range, we compared the spectral intensity every 30nm wavelength range; then we could find the specific wavelength range of the largest difference in intensity. For example, the transmittance of halogen in normal cells was higher than in cancer cells in the 460~480nm, as shown in Figure 3-8a, and we also compared the fluorescence intensity 470~490nm excitation in the wavelength range 540~560nm, as shown in Figure 3-8d.

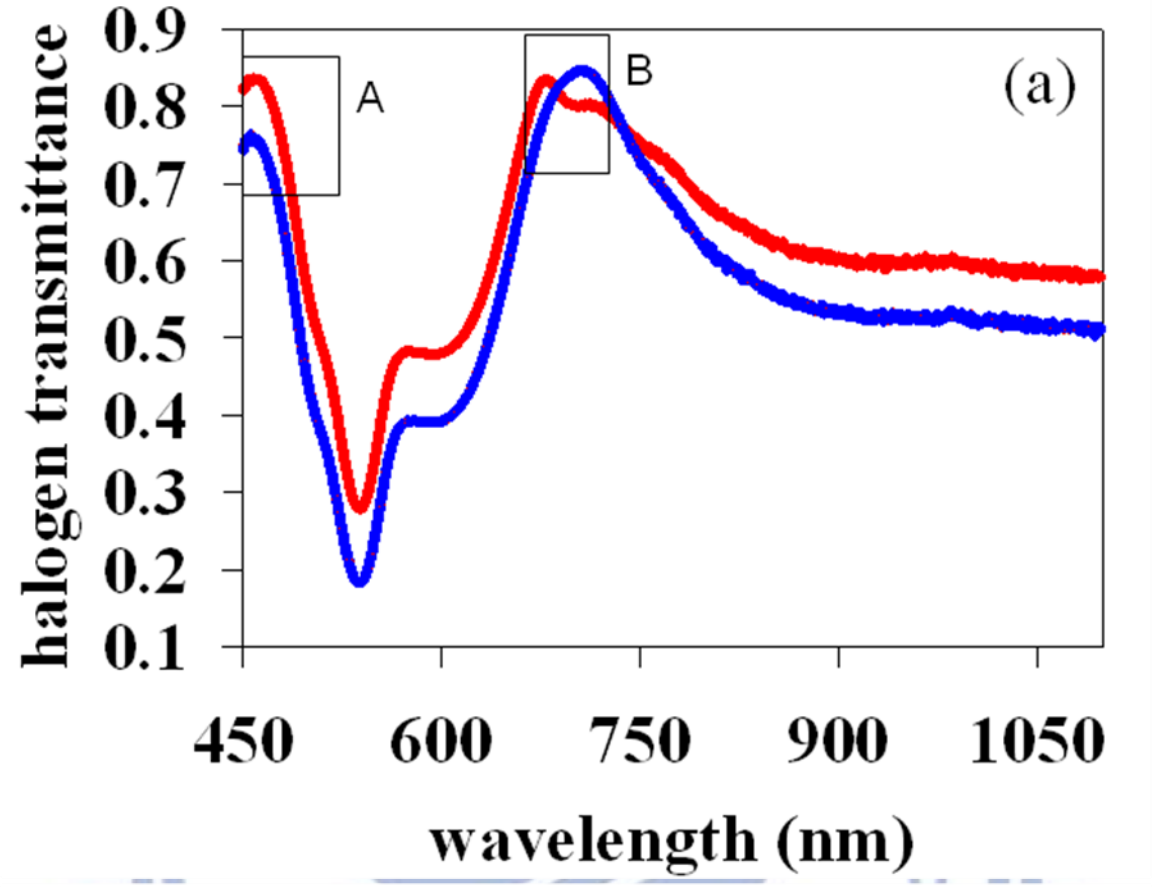
halogen transmittance
0.9
0.8
0.7
0.6
0.5
0.4
0.3
0.2
0.1
A
B
(a)
450
600
750
900
1050
wavelength (nm)

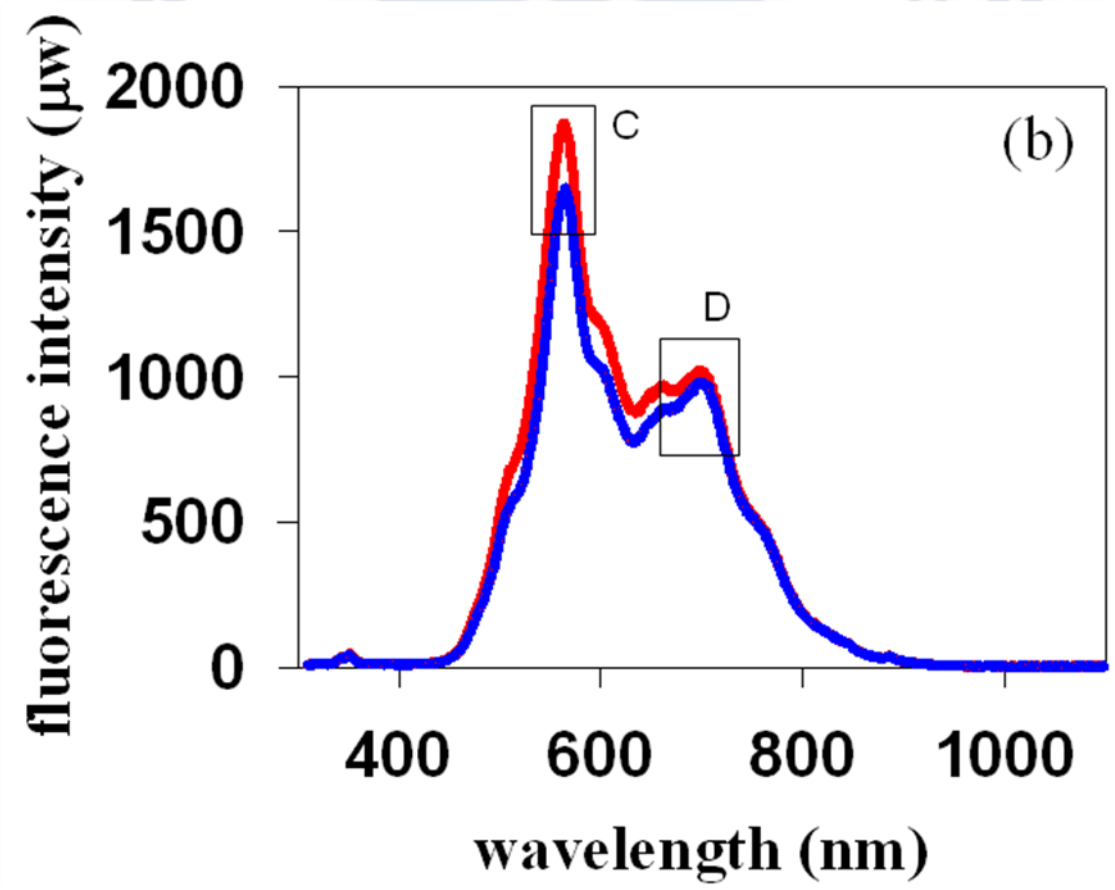
fluorescence intensity (μw)
2000
1500
1000
500
0
C
D
(b)
400
600
800
1000
wavelength (nm)

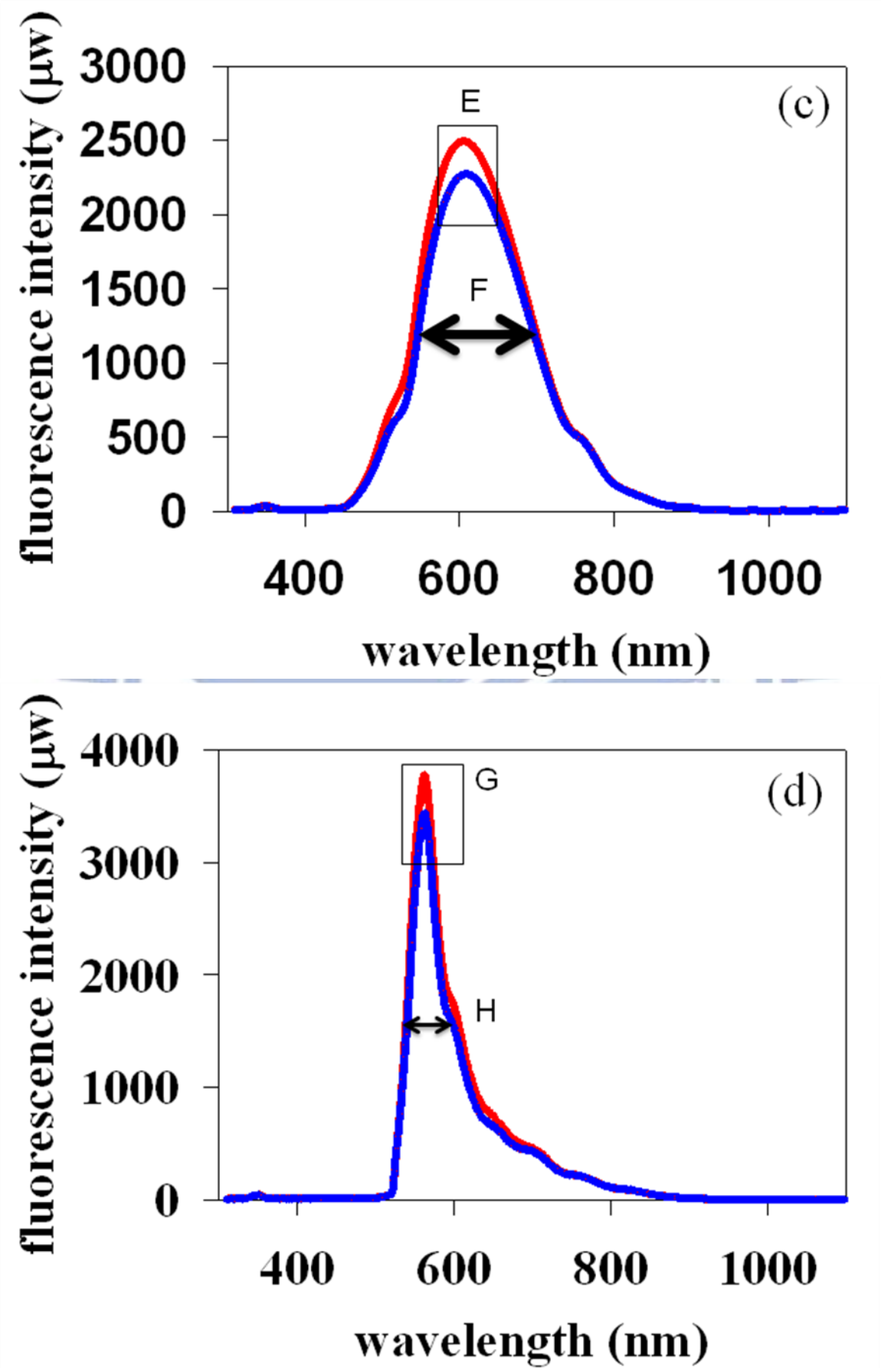

Figure 3-8: The spectrum of one sample (a) Halogen transmittance. (b)

Fluorescent intensity with 330-385nm excitation. (c) Fluorescent intensity compensated by spline with 330-385nm excitation. (d) Fluorescent intensity with 470-490nm excitation. Red line is normal cells, and blue line is cancer cells. A: the peak in wavelength range 460~480nm. B: the peak in wavelength range 700~710nm. C: the intensity in wavelength range 540~570nm. D: the intensity in wavelength range 680~710nm. E: the maximum of spectral curve. F: the full width at half maximum (FWHM) of spectral curve. G: the peak in wavelength range 540~570nm. H: the FWHM of spectral curve.

3.5.2 Ratio of intensity in two different wavelength ranges

Generally, there were some peaks in the spectral curve. We calculated the ratio of the intensity in different peaks or specific wavelength range. In our research, we calculated the ratio of average halogen transmittance in the range 460~480nm to the 700~710nm.

3.5.3 Wavelength of the specific peak

The wavelength of the peak may be different in each spectral curve. In halogen, we compared the wavelength of the maximum in the wavelength 700~710nm. We tried to find the movement of the peak caused by the cancer cells.

3.5.4 Area under spectral curve

By the integration of the spectral curve, we calculated the area under the curve. Before the integration, we needed to normalize the spectral curve. First, we recorded the maximum of the spectral curve, and then we divided the intensity by the maximum. We wanted to diagnose cancer cells by the change of area under the spectral curve.

3.5.5 Maximum of spectral curve compensated by spline

In fluorescence 330~385nm excitation, two peaks occurred in the wavelength range 540~560nm and 700~710nm. The decrease between the peaks that might have been caused by the absorption of hemoglobin, and the spectral curve of fluorescence excitation approximates Gaussian distribution and parabolic[43]. We compensated the decrease and fitted the spectral curve as parabolic by spline. Spline used the slope of the left and right borders to fit a parabolic by the interpolation, as shown in Figure 3-9. After compensation by spline, we recorded the maximum of this curve.

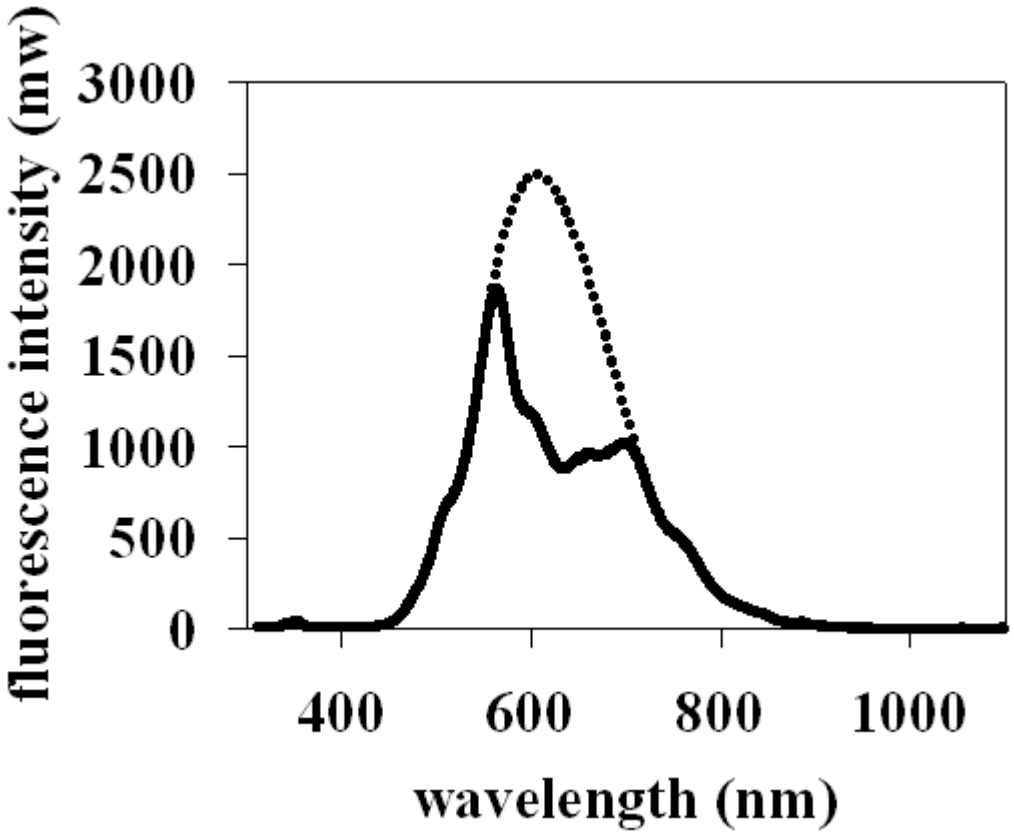

Figure 3-9: Spectrum compensated by Spline. Solid line is fluorescent spectrum with 330-385nm excitation, dotted line is the spectrum curve compensated by Spline.

3.5.6 Full Width at Half Maximum (FWHM) of spectral curve

Full width at half maximum (FWHM) refers to the distance between half width of a peak, figure 3-10. After the spectral curve in fluorescence 330~385nm excitation was compensated by spline, we calculated the FWHM of the curve.

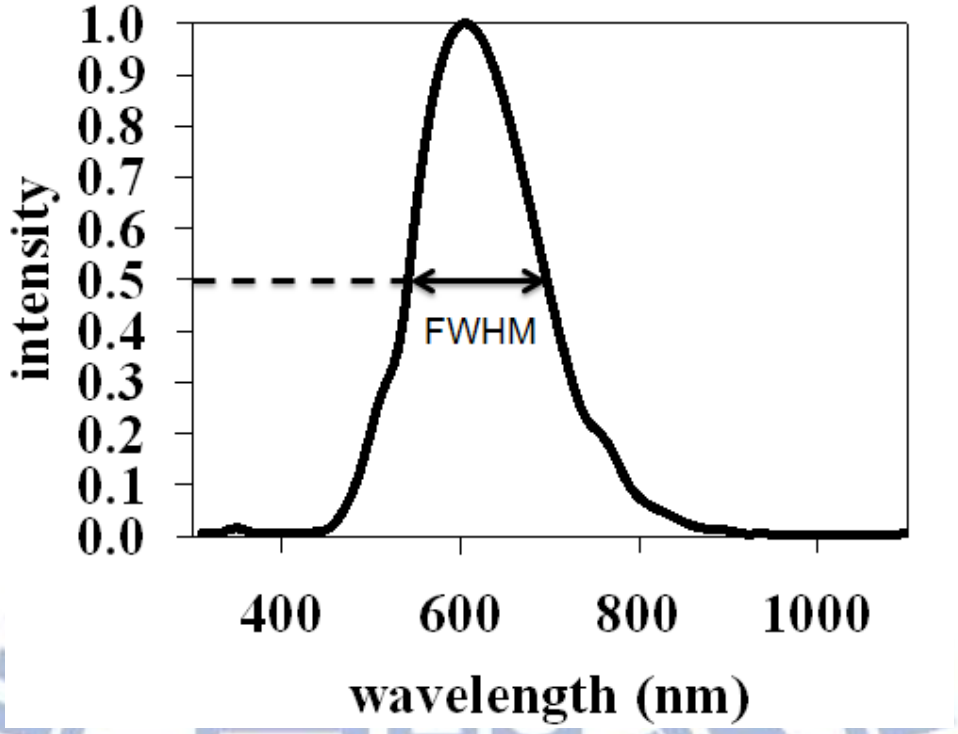

Figure 3-10: Full width at half maximum.

3.6 Sensitivity and specificity

Sensitivity means the correct rate of determining the normal cells as normal cells, and specificity means the correct rate of determining the cancer cells as cancer cells. We used the Gaussian distribution to calculate the sensitivity and specificity of our analysis. First, we computed the mean and variance of the result in the analysis; then we could determine the Gaussian distribution using the formula (3-3). μ was the mean, and σ was the variance.

$$f(x) = \frac{1}{\sigma\sqrt{2\pi}} e^{-\frac{(x-\mu)^2}{2\sigma^2}} \quad (3\text{-}3)$$

By the Gaussian distribution, we determined the critical value of the method, for example, by using the intersection of two curves. We defined the right region as normal tissue and the left region as cancerous tissue. Then we could determine the sensitivity and specificity: sensitivity was the ratio of the area under the solid line and on the left of critical point to the area under the solid line, as shown in Figure 4-9; specificity was the ratio of the area under the dotted line and on the right of critical point to the area under the dotted line, as shown in Figure 3-11. Figure 3-12 shows how to calculate sensitivity and specificity.

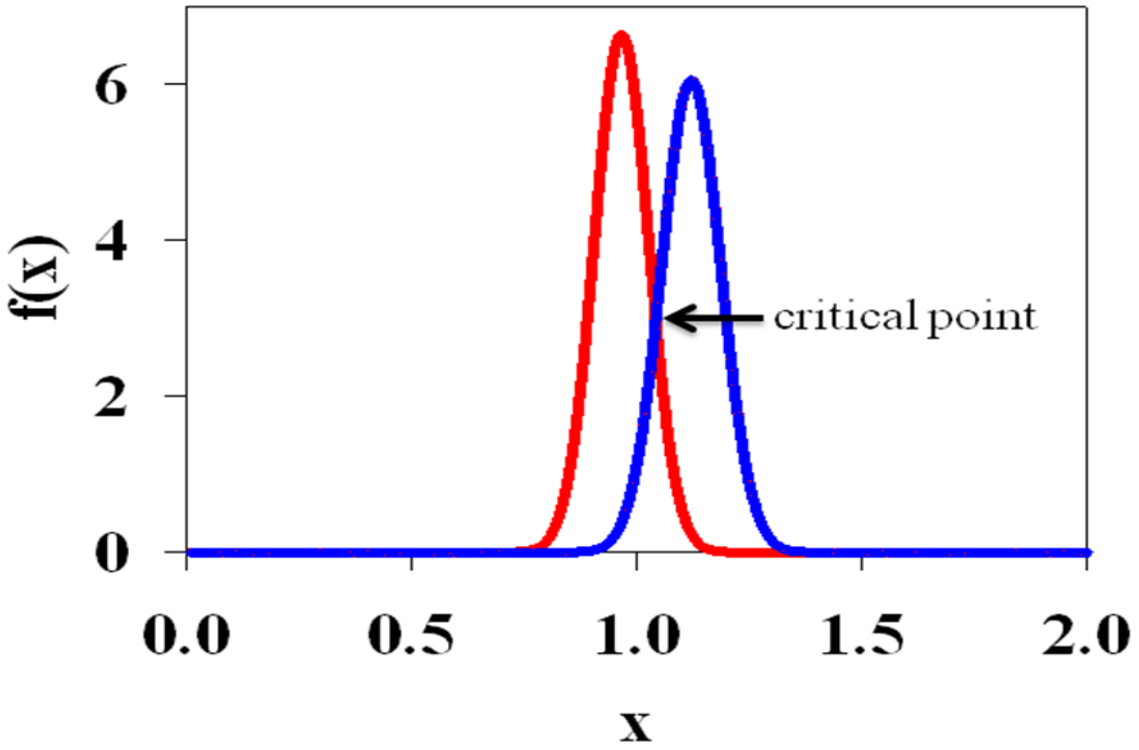

Figure 3-11: The Gaussian distribution of the analysis. Red line is normal cells, and blue line is cancer cells.

		Patients with oral cancer	
		Condition Positive	Condition Negative
Test Outcome	Test Outcome Positive	True Positive (TP)	False Positive (FP)
	Test Outcome Negative	False Negative (FN)	True Negative (TN)
		Sensitivity =TP/(TP+FN)	Specificity =TN/(FP+TN)

Figure 3-12: Calculation of sensitivity and specificity.

Chapter 4 Results

4.1 Experiments

This is the flow chart of our experiment. First, we used the hyperspectral scanning system to transfer the optical image of the sample into a hyperspectral matrix. The hyperspectral scanning system includes: a microscope, three light sources, a motor, a relay lens, a spectrometer and an EMCCD. We use the microscope to enlarge the image of the sample. There are three light sources: halogen lamp, fluorescent at 330~385nm excitation and fluorescent at 470~490nm excitation. The motor was used to move the relay lens for scanning the image, and we used the spectrometer to transform the image into the hyperspectral image. Lastly, the EMCCD stored the hyperspectral image in a three-dimensional matrix. The three axes are x, y and λ.

After we transferred the format of hyperspectral data to BIL, we chose the nuclei in the image. These data on nuclei, which were chosen by hand, and used to diagnose cancer cells using the spectral method; they would also serve as the training data in the method of topology. There are two kinds of cancer cell diagnoses: the difference of spectral curves and the change of topology. In the diagnosis by the difference of spectral curves, we have 11 methods to compare the spectrum of normal cells and cancer cells: 4 methods in halogen, 4 in fluorescence 330~385nm excitation and 3 in fluorescence 330~385nm excitation. In the diagnosis of the change in topology, we present two methods: calculating the fractal dimension of the image and the correct rate of the classification by KNN. Lastly, we can plot the Gaussian distribution curve of the value generated by the methods, and calculate the sensitivity and specificity of this method.

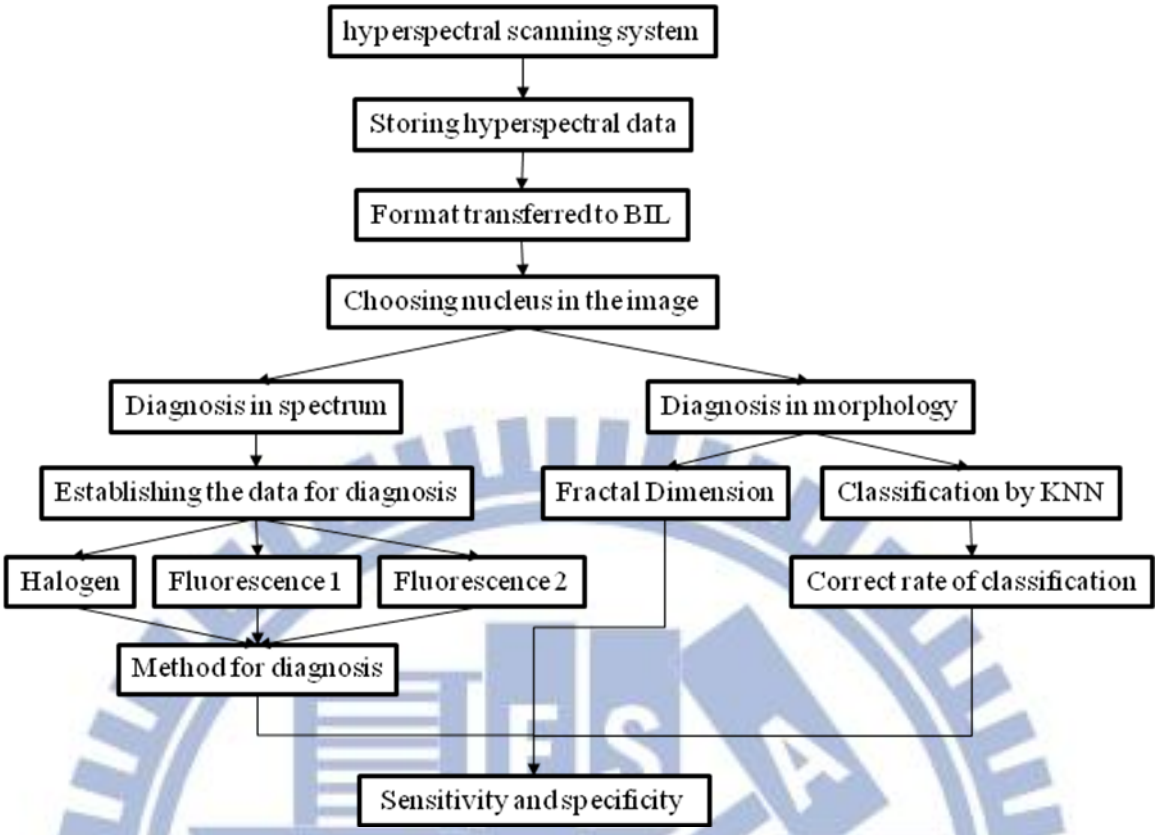

Figure 4-1: The flow chart of experiment.

4.2 Morphological analysis of oral cancer

Before our analysis in topology, we needed to remove the light noise. Because we only had the spectrum of light source in samples numbered 1 to 12, we only analyzed the sample numbers 1 to 12 in topology.

4.2.1 Calculation of Fractal Dimension after Threshold Method

Figure 4-1 shows the result of the threshold method for the samples numbered 1 to 12. After using the threshold method, the basal-cells in normal tissue and the cancer cells in cancerous tissue were set to 1 or white, and the others to 0 or black. The figures on the left in Figure 4-1 are all normal tissue; the figures on the right are cancerous tissue.

We can determine that the threshold method images exhibit a large difference between normal cells and cancer cells. The white area in the normal tissue shows a continuous curve, and the white area in the cancerous tissue shows a discontinuous curve and spreads over the whole image. Table 5-1 shows the fractal dimension of the image after using the threshold method.

According to the Gaussian distribution, we can determine 1.75 as the critical value. If the fractal dimension is lower than 1.75, we identify the image as normal tissue; on the other hand, if the fractal dimension is higher than 1.75, we identify the image as cancerous tissue. The sensitivity is 83.44%, and specificity is 91.46%.

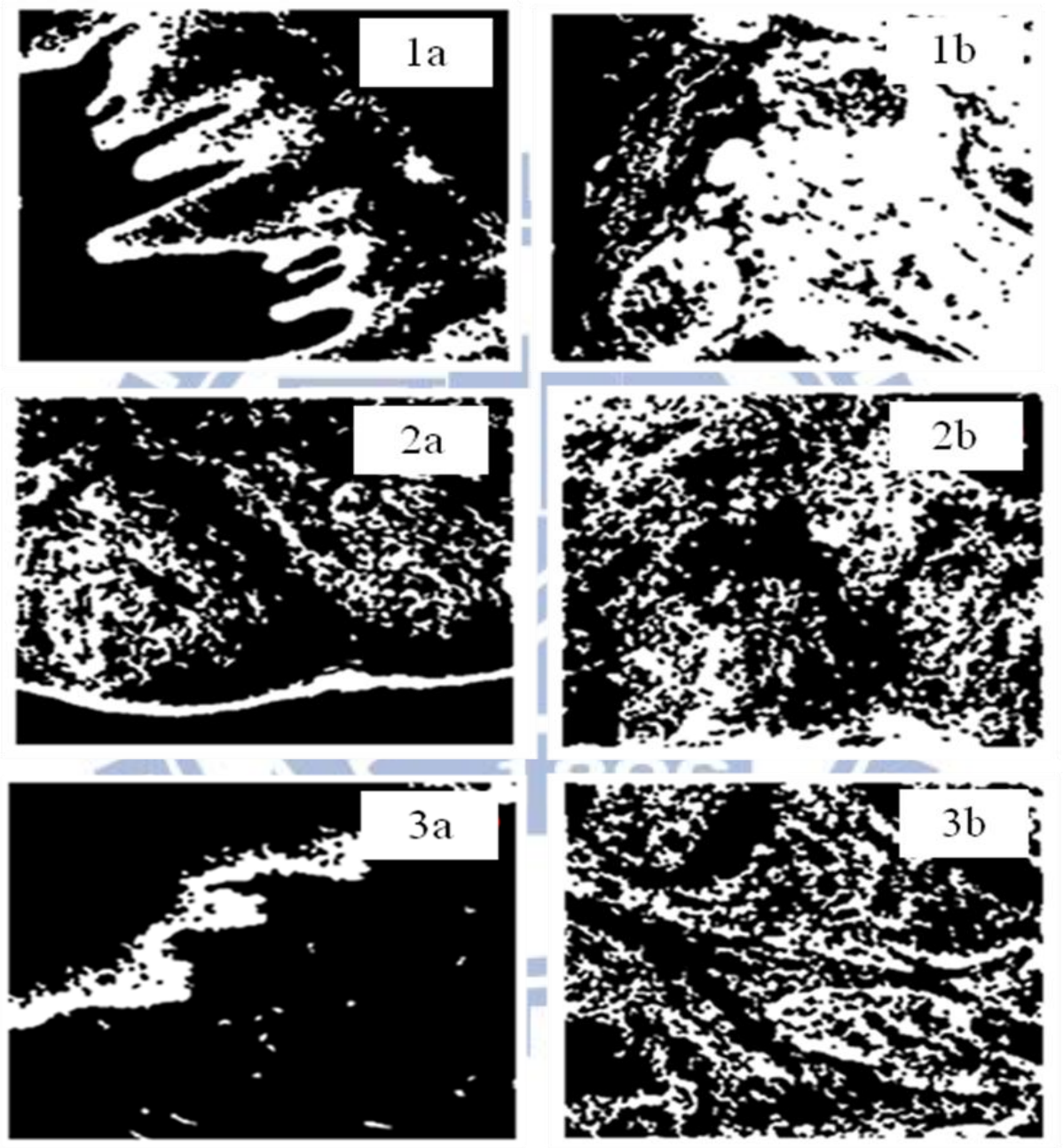

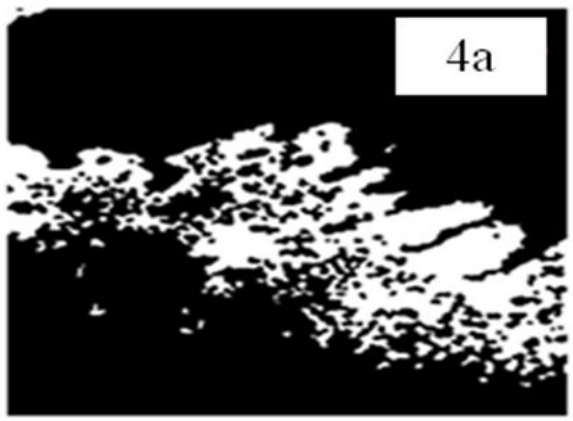
4a

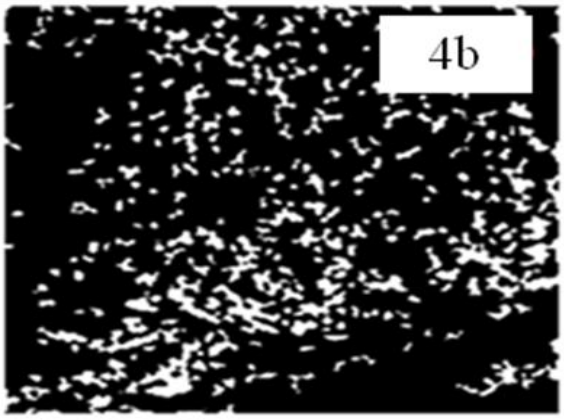
4b

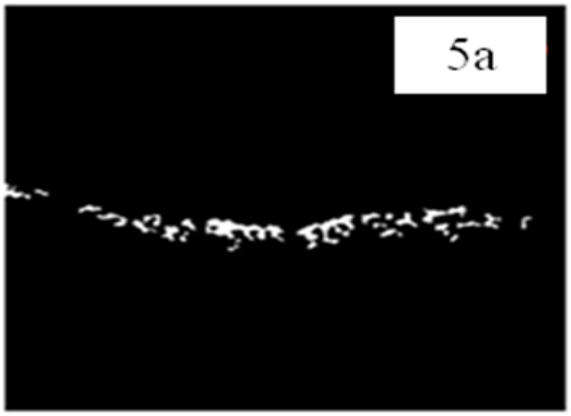
5a

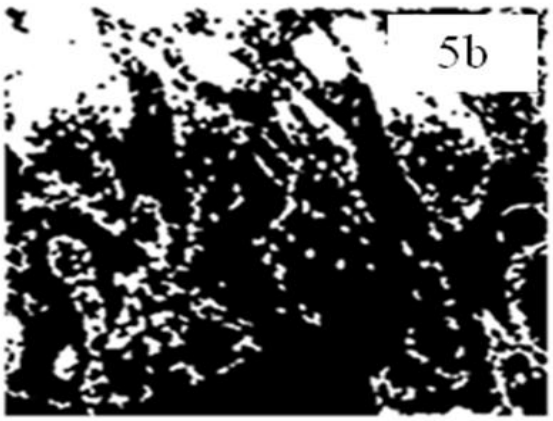
5b

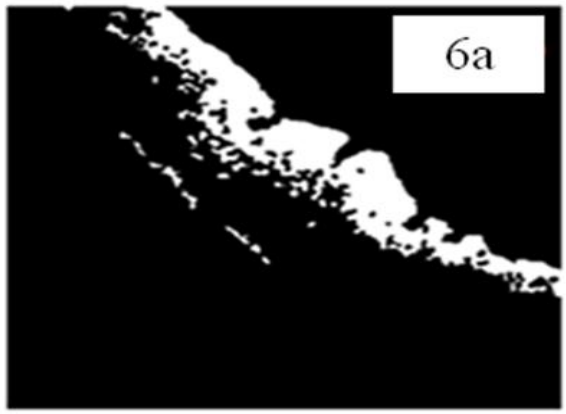
6a

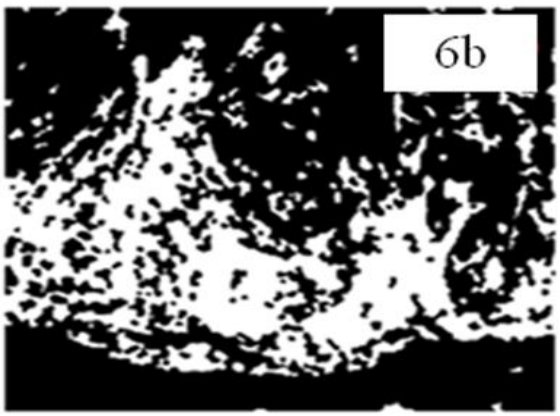
6b


7a


7b

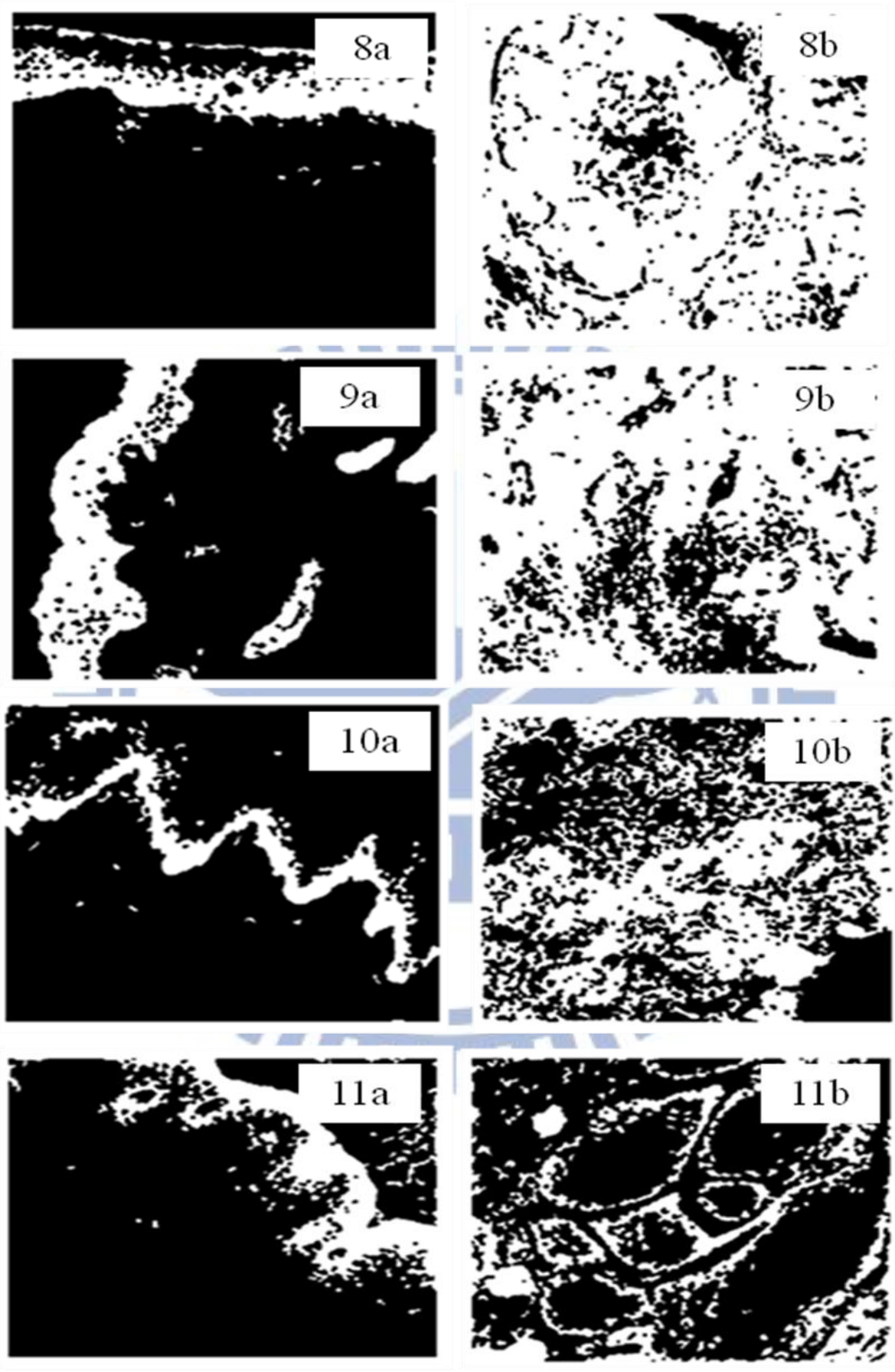
8a
8b
9a
9b
10a
10b
11a
11b

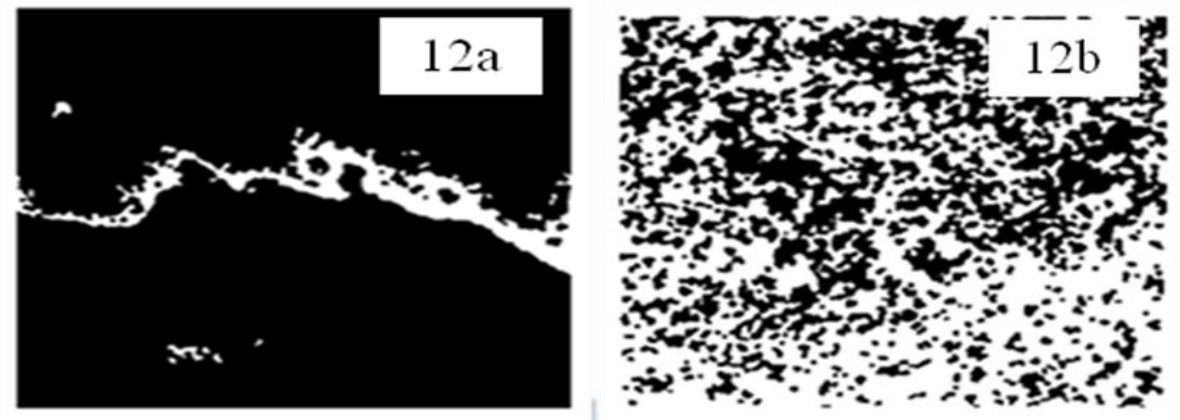

Figure 4-2: After threshold method, the basal cells are white, and the others are black in the images. The number 1 to 12 of figure means the number of the sample. The label (a) means normal tissue, and the label (b) means cancer tissue.

Table 4-1: The fractal dimension of sample numbered 1 to 12 after threshold method.

Number of patients	**1**	**2**	**3**	**4**	**5**	**6**	**7**	**8**	**9**	**10**	**11**	**12**
(a) Normal cells	1.73	1.73	1.57	1.73	1.24	1.59	1.65	1.66	1.68	1.59	1.66	1.50
(b) Cancer cells	1.90	1.82	1.81	1.67	1.78	1.80	1.85	1.97	1.95	1.89	1.76	1.91

4.2.2 K-nearest Neighbor Classification

According to the training data chosen by hand, we can classify the nuclei as basal-cell and lamina propria. Figure 4-2 shows the result of classification by KNN. A red point means basal-cell and a blue point means lamina propria. Table 4-2 shows the correct rate of classification in lamina propria by KNN. After the calculation of Gaussian distribution, we determined the critical value as 0.76. This means if the correct rate is lower than 0.76, then we indentify the sample as cancerous; conversely, if the correct rate is higher than 0.76, we indentify the sample as normal tissue. The sensitivity is 81.36%, and the specificity is 55.34%.

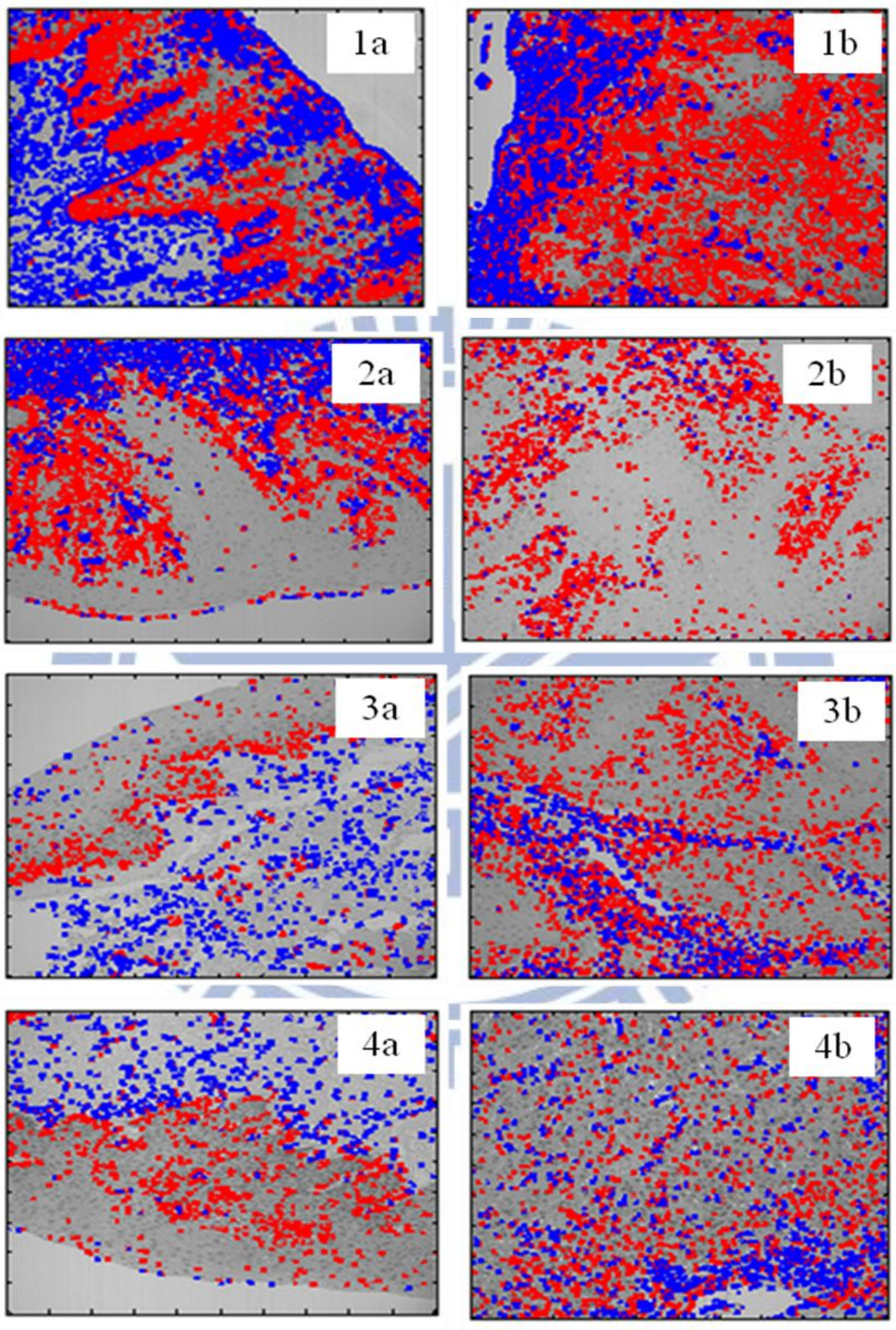
1a
1b
2a
2b
3a
3b
4a
4b

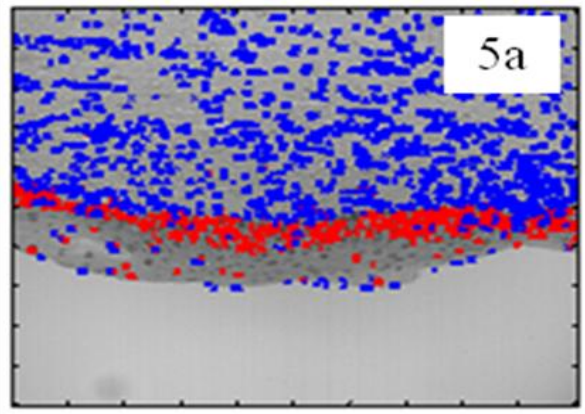
5a

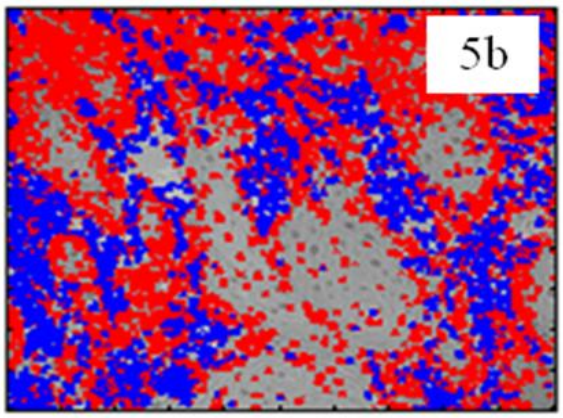
5b

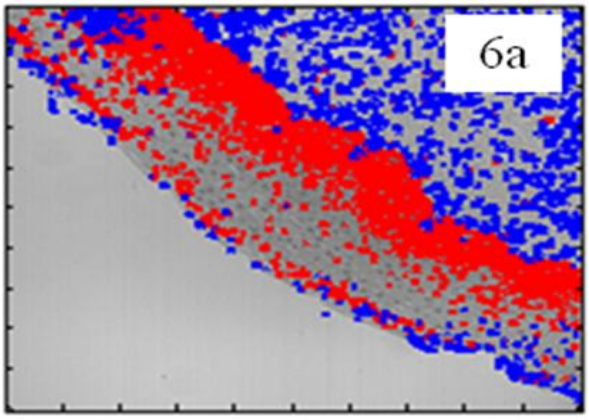
6a

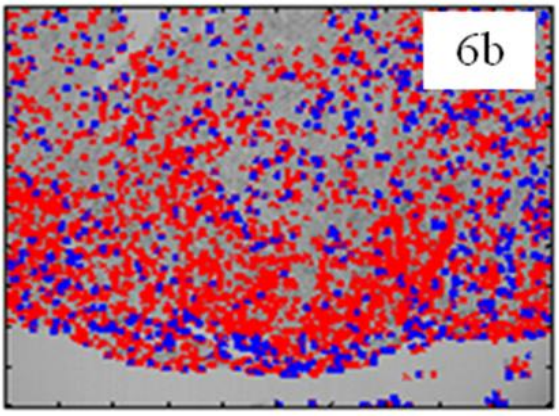
6b

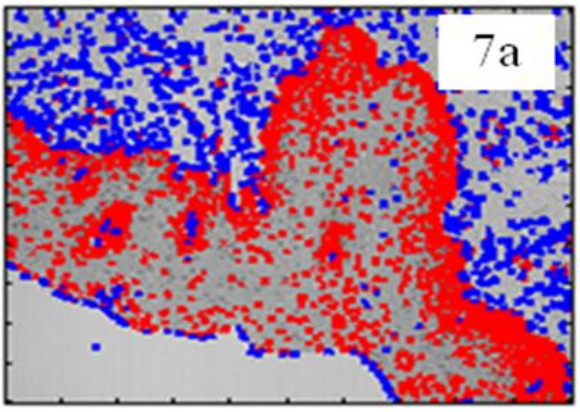
7a

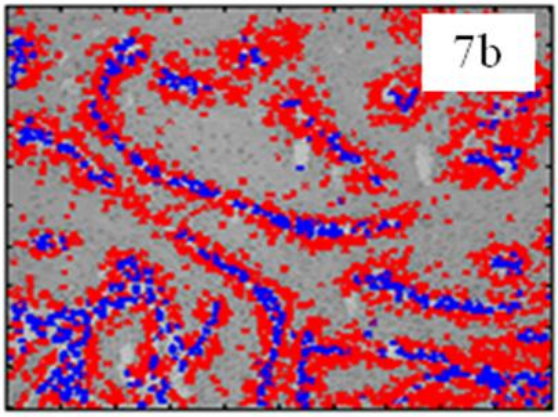
7b

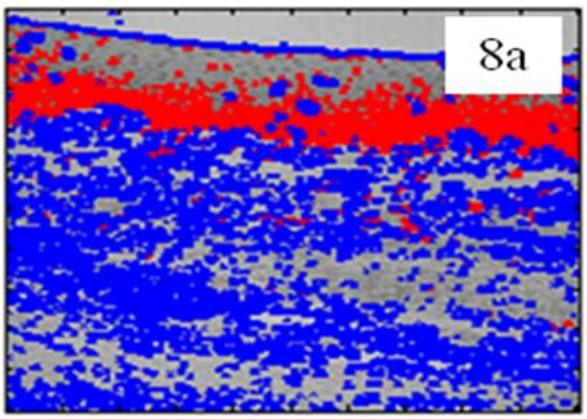
8a

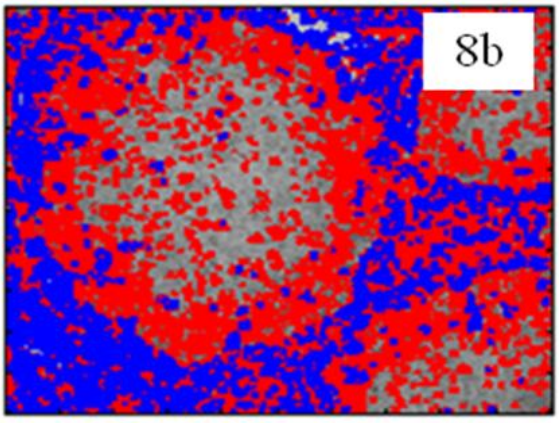
8b

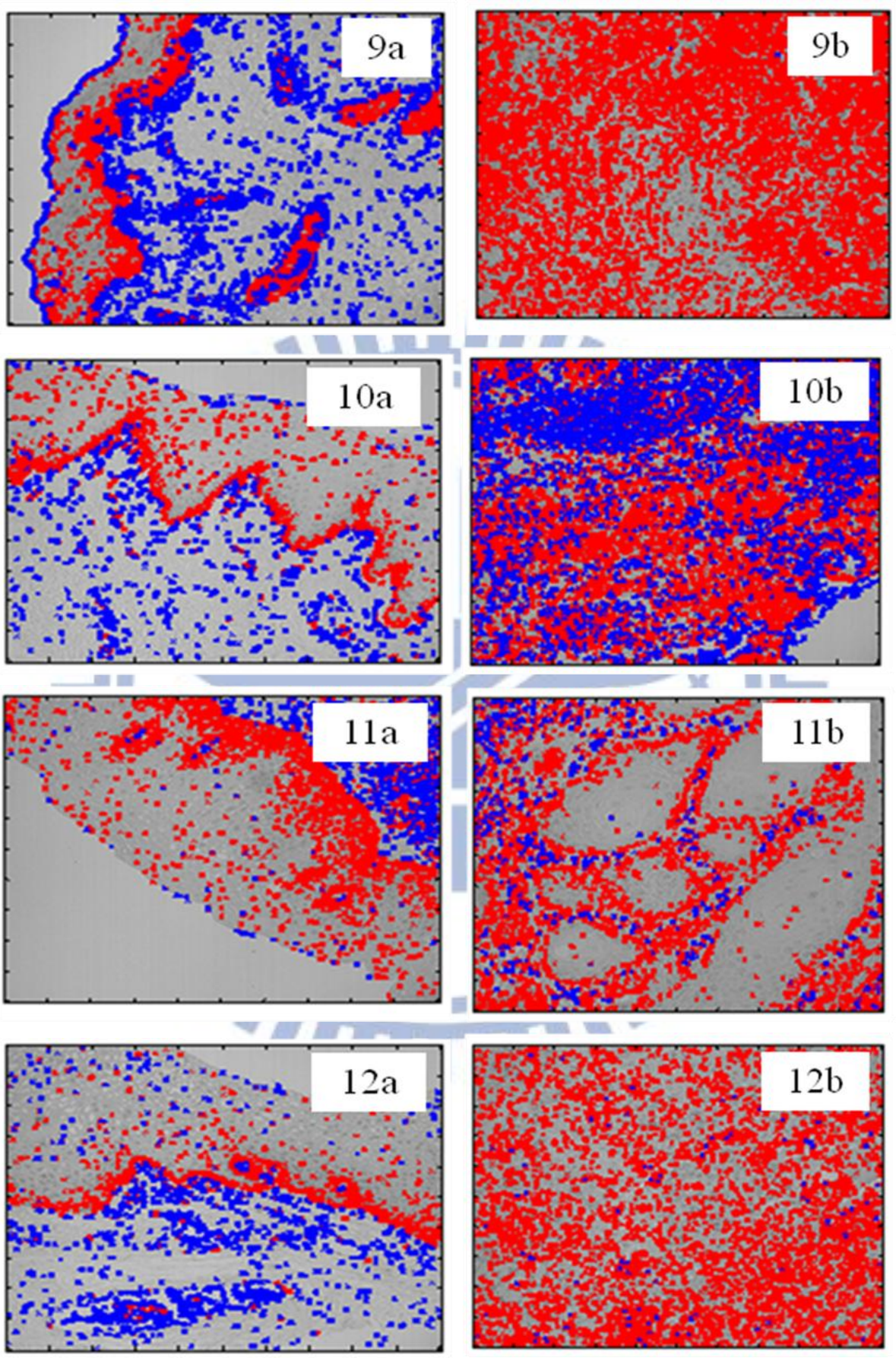
9a
9b
10a
10b
11a
11b
12a
12b

Figure 4-3: The result of classification by KNN in the sample numbered 1 to 12. The number 1 to 12 of figure means the number of the sample. The label (a) means normal tissue, and the label (b) means cancer tissue.

Table 4-2: The correct rate of classification by KNN in the sample numbered 1 to 12.

Number of patients	**1**	**2**	**3**	**4**	**5**	**6**	**7**	**8**	**9**	**10**	**11**	**12**
(a) Normal cells (%)	80.9	58.3	94.7	87.8	95.0	89.4	86.3	92.2	87.8	91.2	64.9	89.2
(b) Cancer cells (%)	49.8	87.9	73.0	81.6	62.9	80.7	79.9	47.4	100	50.9	70.4	93.6

4.3 Spectral analysis of oral cancer

We chose nuclei in the image as the data for diagnosis of cancer cells by hand, and the number of the data is shown in Table 4-3. Except for sample number 5, we have at least 100 sets of data in one sample. Because we have three light sources, we have to diagnose cancer cells in three kinds of spectrum. We have 11 methods to diagnose cancer cells in spectrum: 4 in halogen, 4 in fluorescence 330~385nm excitation and 3 in fluorescence 470~490nm excitation.

Table 4-3: The number of spectral data.

Number of patient	**Normal tissue (nuclei)**	**Cancer tissue (nuclei)**	**Number of patient**	**Normal tissue (nuclei)**	**Cancer tissue (nuclei)**
1	557	458	**18**	184	301
2	133	150	**19**	358	739
3	260	164	**20**	416	551
4	265	210	**21**	236	371
5	82	221	**22**	450	584
6	167	140	**23**	424	262
7	376	404	**24**	279	239
8	202	182	**25**	167	248
9	150	563	**26**	309	449

10	241	263	**27**	425	449
11	334	278	**28**	399	316
12	242	413	**29**	311	330
13	215	120	**30**	315	387
14	393	759	**31**	229	632
15	313	342	**32**	507	296
16	432	351	**33**	359	693
17	623	565			

4.3.1 Transmitting spectral mode

Figure 5-3 shows the penetration in halogen for the samples numbered 1 to 12. The penetration means we removed the light noise and black noise from the spectral data, and we only have the data of light source in the samples numbered 1 to 12. The maximum of penetration is 1, and the minimum is 0. We have four analytical methods in the spectrum of halogen. Method 1-1 is calculating the penetration in the wavelength range 460~480nm. Method 1-2 is calculating the ratio of the penetration in the range 460~480nm to the penetration in the range 700~710nm. Method 1-3 is calculating the intensity of the peak at 700~710nm.

Table 5-2 shows the specificity of each method in halogen. Except for sample number 2, we can see that methods 1-1 and 1-2 have the highest specificity, the means of which are 87.15 and 86.27, respectively, so we combined methods 1-1 and 1-2 to analyze the spectrum in halogen. If we ignore sample number 2, the mean of specificity is 98.45.

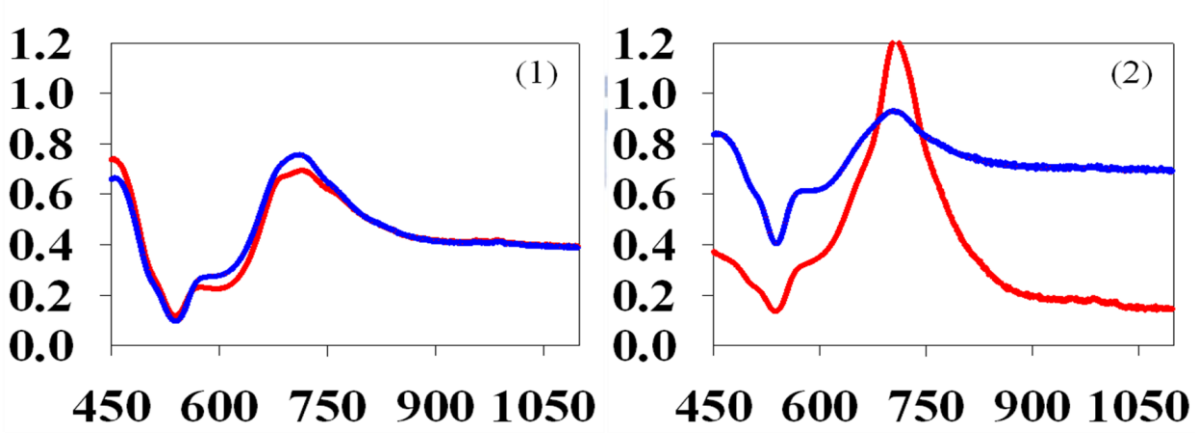

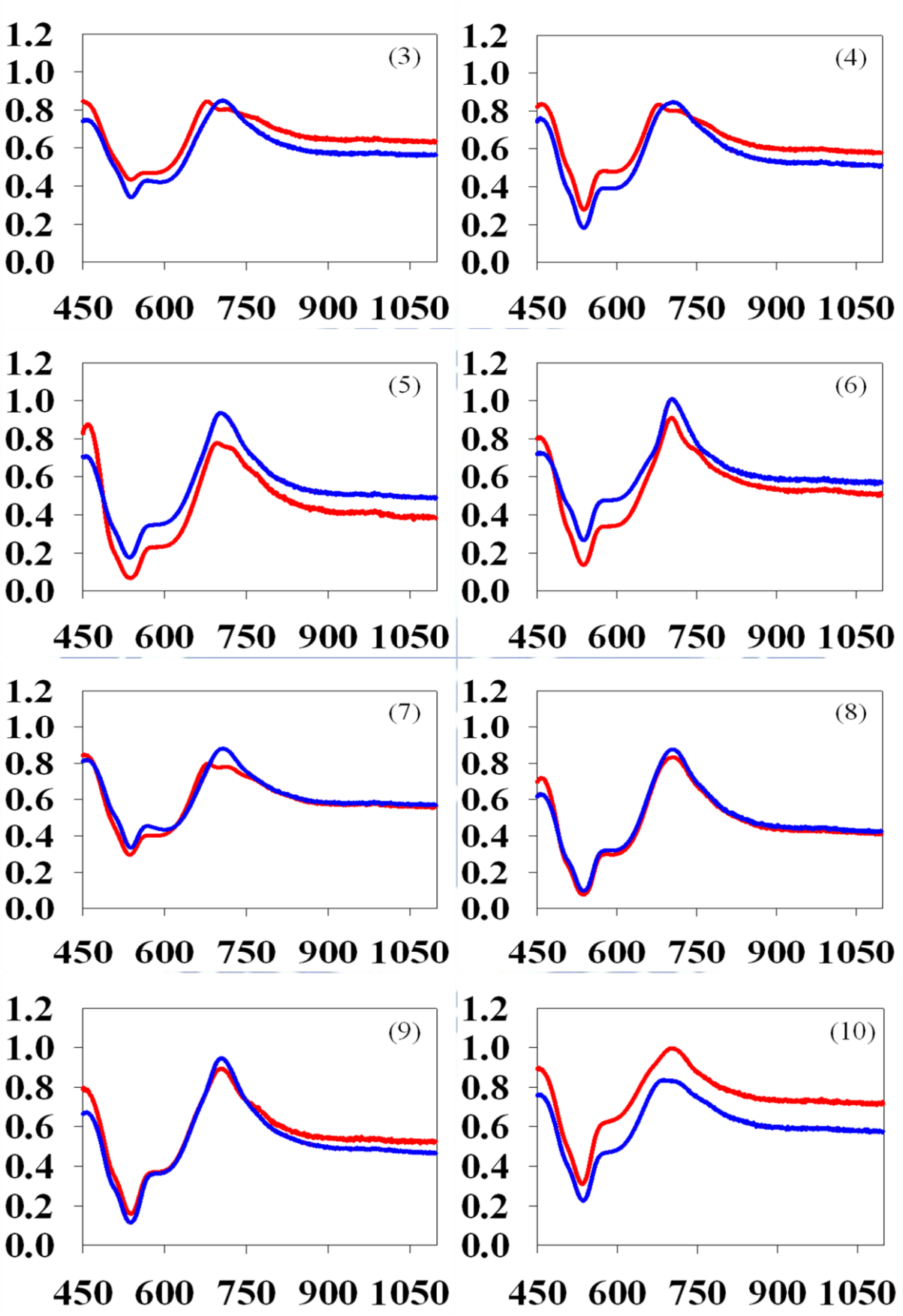
(3)
(4)
(5)
(6)
(7)
(8)
(9)
(10)
1.2
1.0
0.8
0.6
0.4
0.2
0.0
450 600 750 900 1050

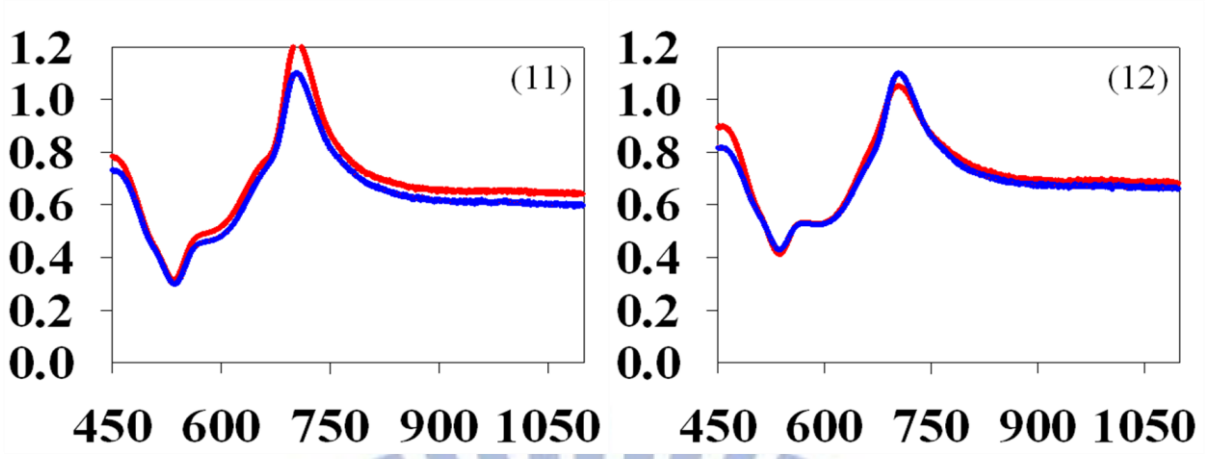

Figure 4-4: The spectral curve of the sample numbered 1 to 12 in halogen. The red line means normal cells, and blue line means cancer cells. The number means the number of patients. X axis is wavelength (nm), and Y axis is halogen transmittance.

Table 4-4: The correct rate of classification by KNN in the sample number 1 to 12.

Number of patient	Specificity of method 1-1 (%)	Specificity of method 1-2 (%)	Specificity of method 1-3 (%)	Specificity of method 1-1+1-2 (%)
1	92.5	90.4	43.4	97.4
2	0	0	42.0	0.0
3	99.6	98.9	77.1	100.0
4	98.0	90.4	65.8	100.0
5	95.1	99.7	71.1	100.0
6	92.3	88.4	74.4	92.2
7	83.6	86.6	76.1	97.3
8	96.6	86.4	35.0	100.0
9	99.8	93.7	64.2	100.0
10	99.9	65.2	37.7	100.0
11	94.7	69.9	71.3	96.1
12	96.6	79.4	66.7	100

4.3.2 Fluorescence with 330~385nm excitation

Figure 4-5 shows the fluorescence intensity of 33 samples in fluorescence

330~385nm excitation, and Figure 4-6 shows the spectral curves that have been compensated by the spline. We have four methods to compare the normal cells and cancer cells. Method 2-1 compares the ratio of the intensity in the range 540~570nm to the intensity in the range 680~710nm. Method 2-2 calculates the area under the spectral curve that has been normalized by the intensity at 540~570nm. Method 2-3 compares the maximum of the spectral curve that has been compensated by spline. Method 2-4 compares the full width at half maximum (FWHM) of the spectral curve compensated by the spline.

Table 4-5 shows the specificity of the method analyzing the spectrum in the fluorescence 330~385nm excitation. We can see a large difference between the specificity of each sample; it signifies that these analyzing methods are not strong enough.

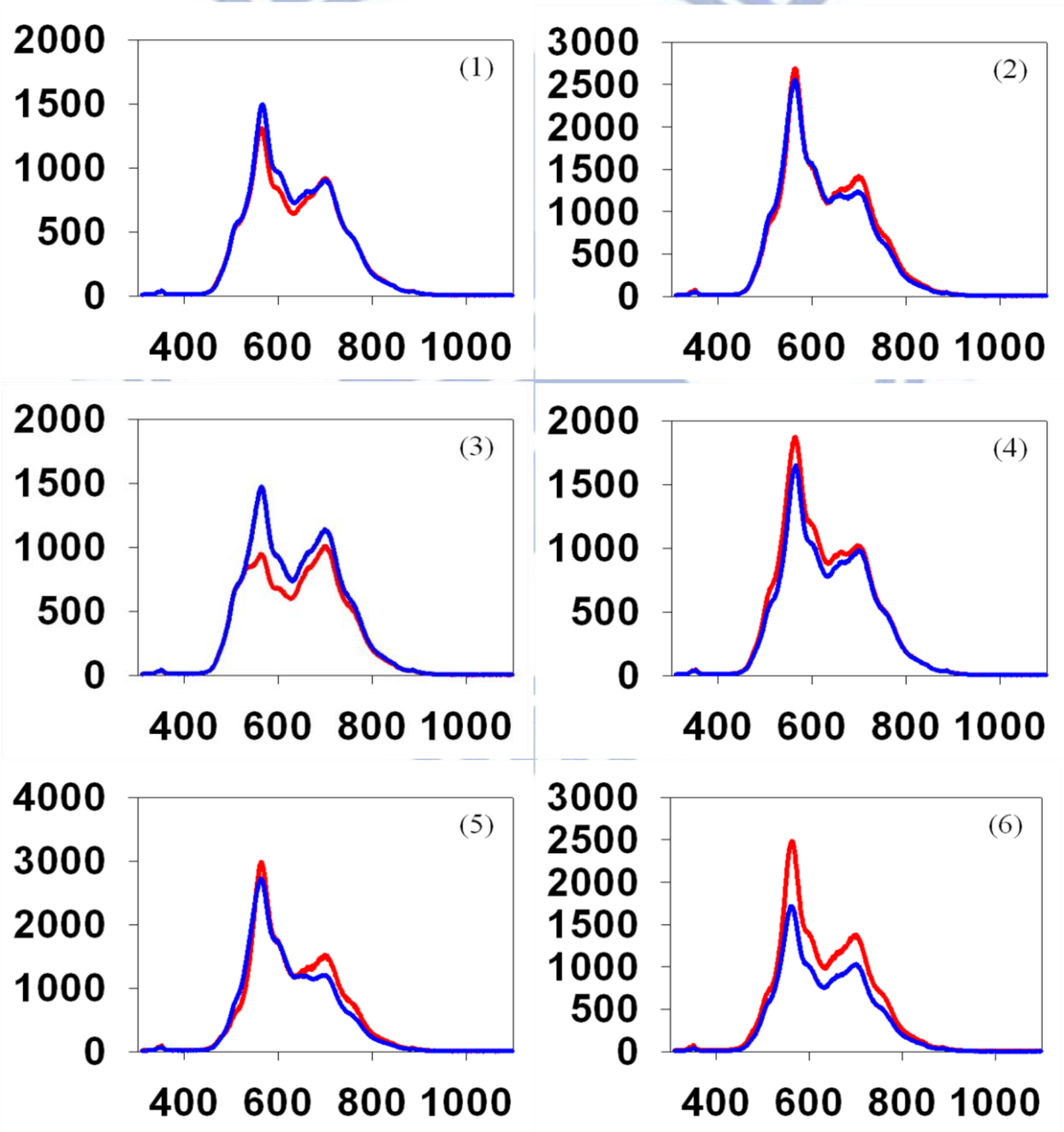

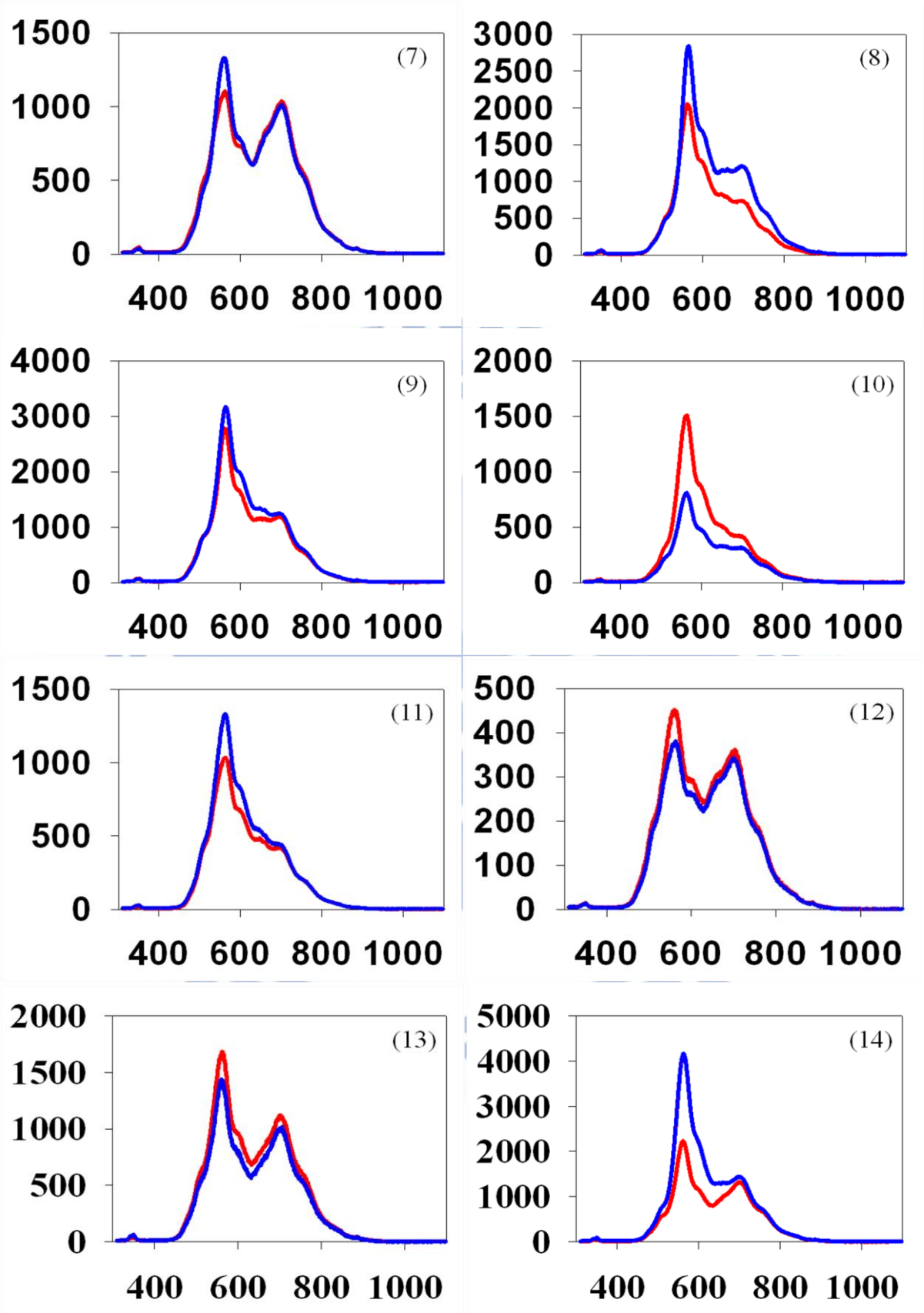
(7)
1500
1000
500
0
400 600 800 1000
(8)
3000
2500
2000
1500
1000
500
0
400 600 800 1000
(9)
4000
3000
2000
1000
0
400 600 800 1000
(10)
2000
1500
1000
500
0
400 600 800 1000
(11)
1500
1000
500
0
400 600 800 1000
(12)
500
400
300
200
100
0
400 600 800 1000
(13)
2000
1500
1000
500
0
400 600 800 1000
(14)
5000
4000
3000
2000
1000
0
400 600 800 1000

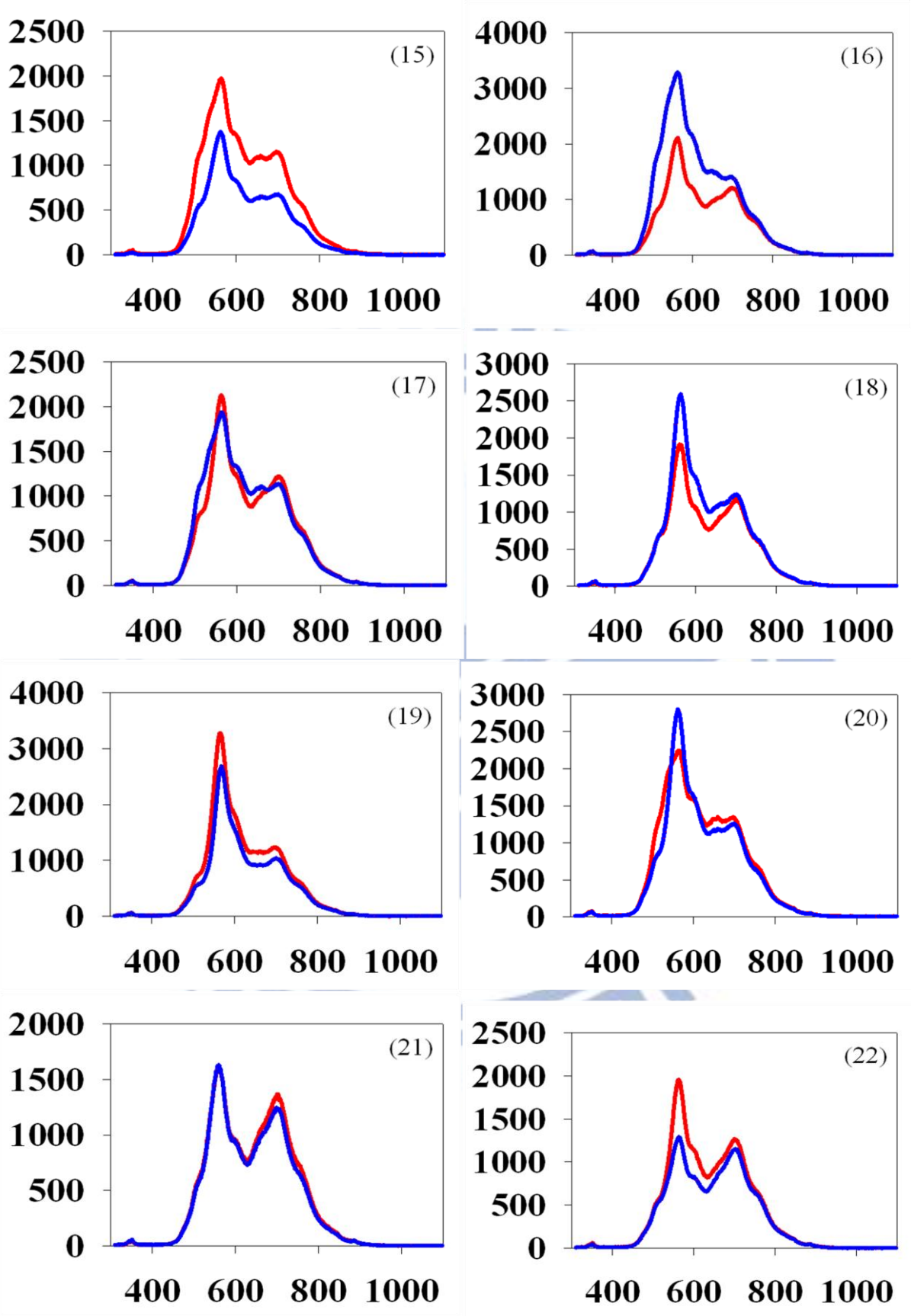
(15)
(16)
(17)
(18)
(19)
(20)
(21)
(22)
400 600 800 1000

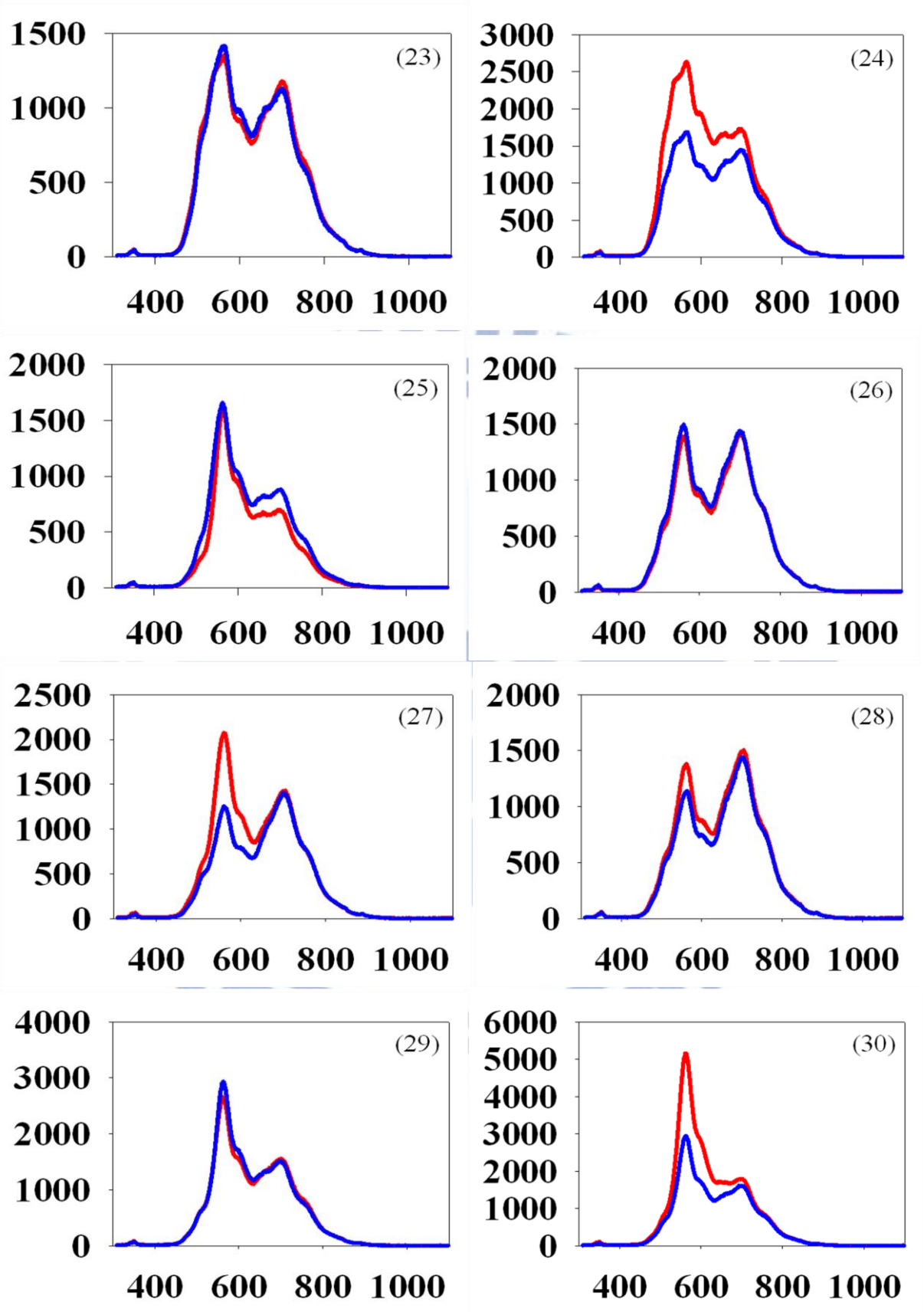
(23)
1500
1000
500
0
400 600 800 1000
(24)
3000
2500
2000
1500
1000
500
0
400 600 800 1000
(25)
2000
1500
1000
500
0
400 600 800 1000
(26)
2000
1500
1000
500
0
400 600 800 1000
(27)
2500
2000
1500
1000
500
0
400 600 800 1000
(28)
2000
1500
1000
500
0
400 600 800 1000
(29)
4000
3000
2000
1000
0
400 600 800 1000
(30)
6000
5000
4000
3000
2000
1000
0
400 600 800 1000

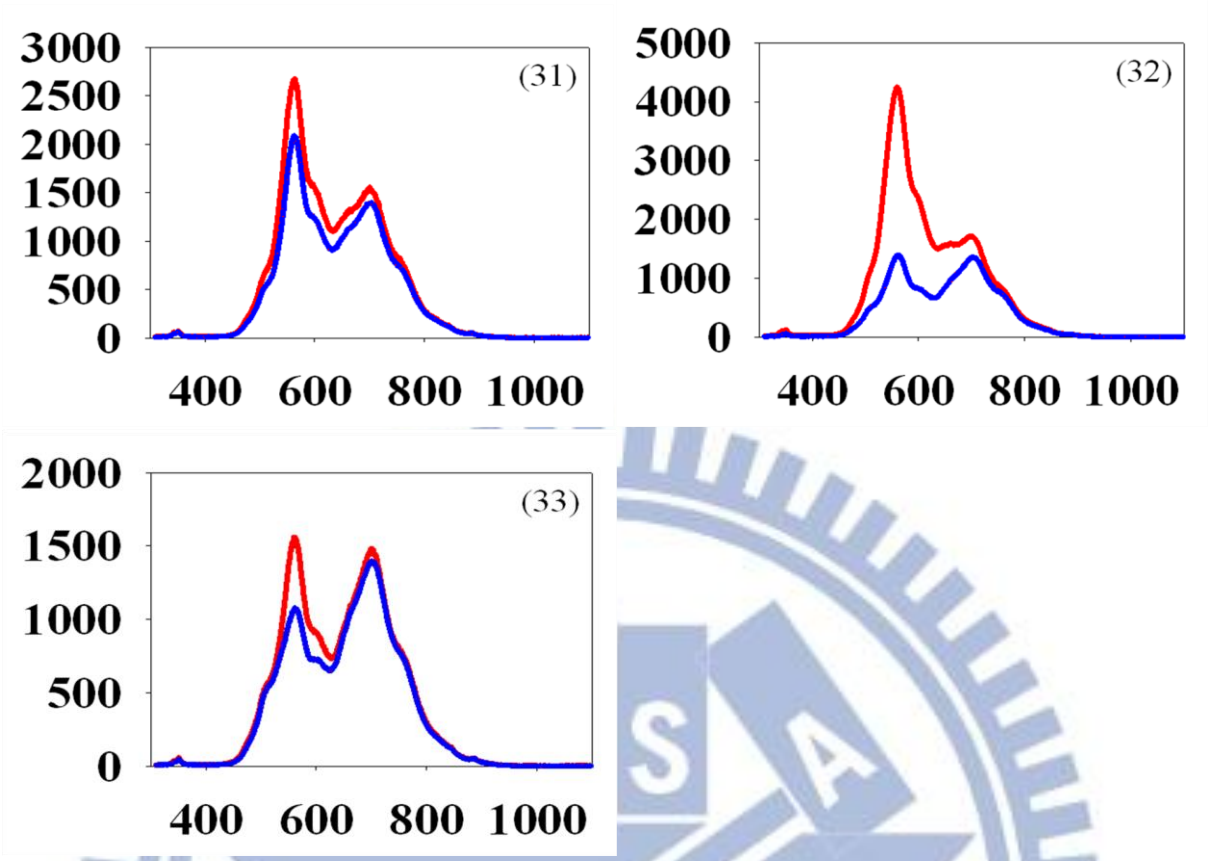

Figure 4-5: The spectral curves of each sample in fluorescence 330~385nm excitation. The number of figure means the number of the sample. The red line means normal cells, and blue line means cancer cells. The number means the number of patients. X axis is wavelength (nm), and Y axis is fluorescence intensity (μ w).

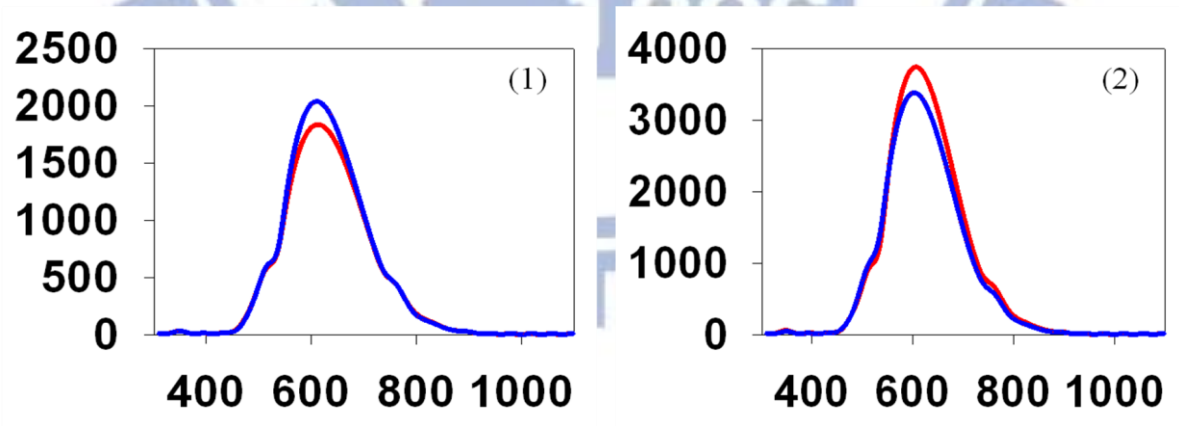

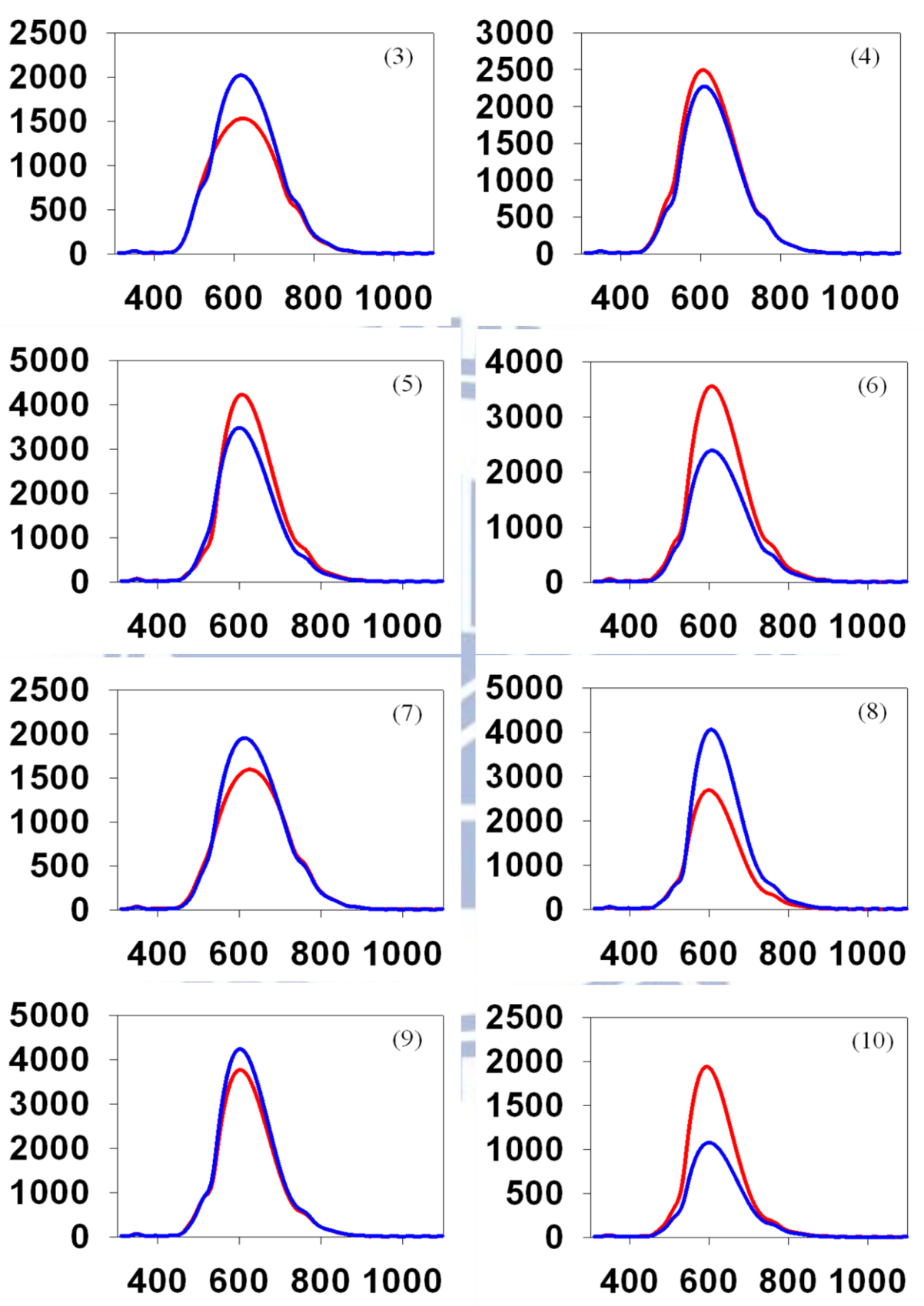
(3)
2500
2000
1500
1000
500
0
400 600 800 1000
(4)
3000
2500
2000
1500
1000
500
0
400 600 800 1000
(5)
5000
4000
3000
2000
1000
0
400 600 800 1000
(6)
4000
3000
2000
1000
0
400 600 800 1000
(7)
2500
2000
1500
1000
500
0
400 600 800 1000
(8)
5000
4000
3000
2000
1000
0
400 600 800 1000
(9)
5000
4000
3000
2000
1000
0
400 600 800 1000
(10)
2500
2000
1500
1000
500
0
400 600 800 1000

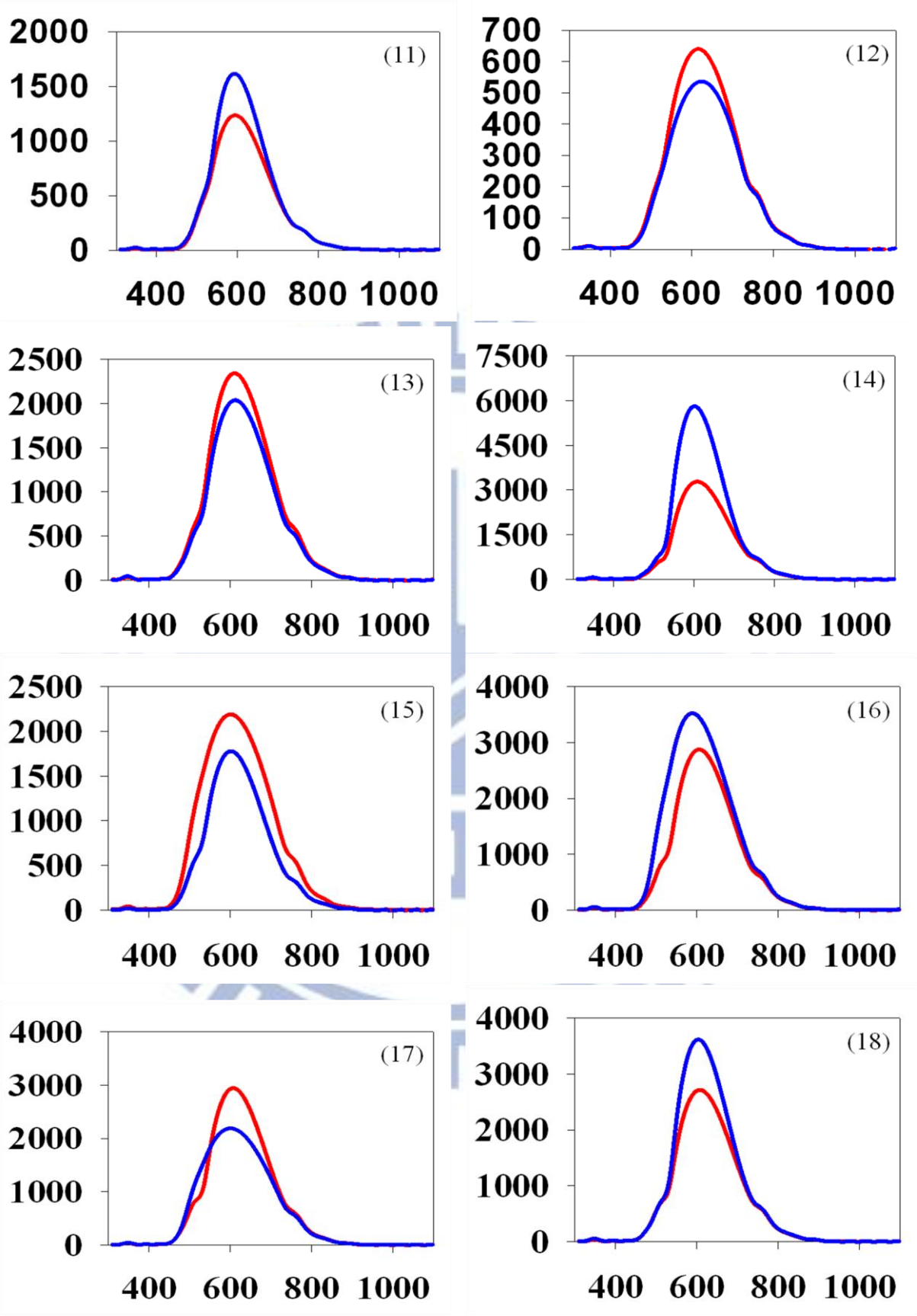
(11)
2000
1500
1000
500
0
400 600 800 1000
(12)
700
600
500
400
300
200
100
0
400 600 800 1000
(13)
2500
2000
1500
1000
500
0
400 600 800 1000
(14)
7500
6000
4500
3000
1500
0
400 600 800 1000
(15)
2500
2000
1500
1000
500
0
400 600 800 1000
(16)
4000
3000
2000
1000
0
400 600 800 1000
(17)
4000
3000
2000
1000
0
400 600 800 1000
(18)
4000
3000
2000
1000
0
400 600 800 1000

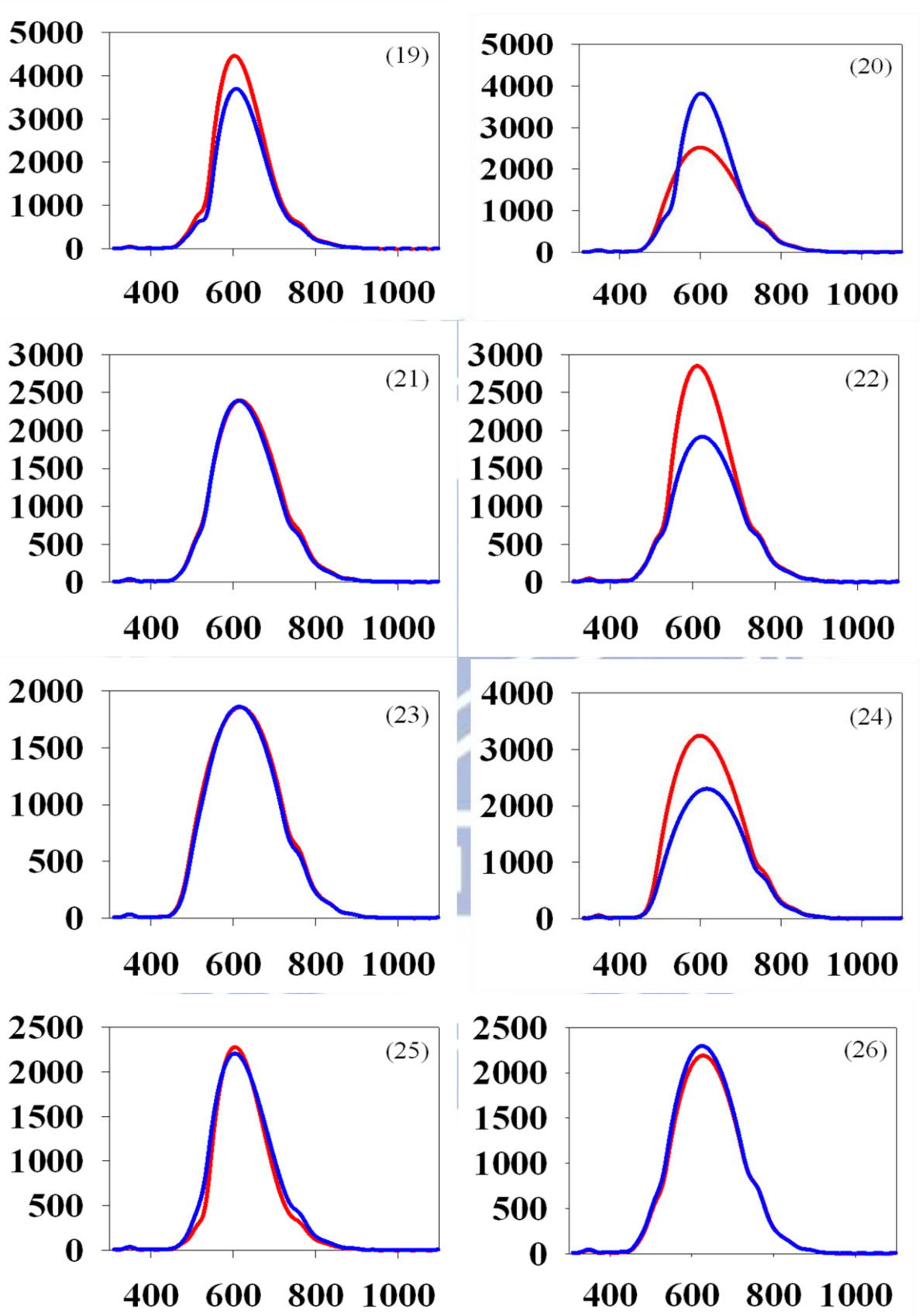
(19)
(20)
(21)
(22)
(23)
(24)
(25)
(26)
400 600 800 1000

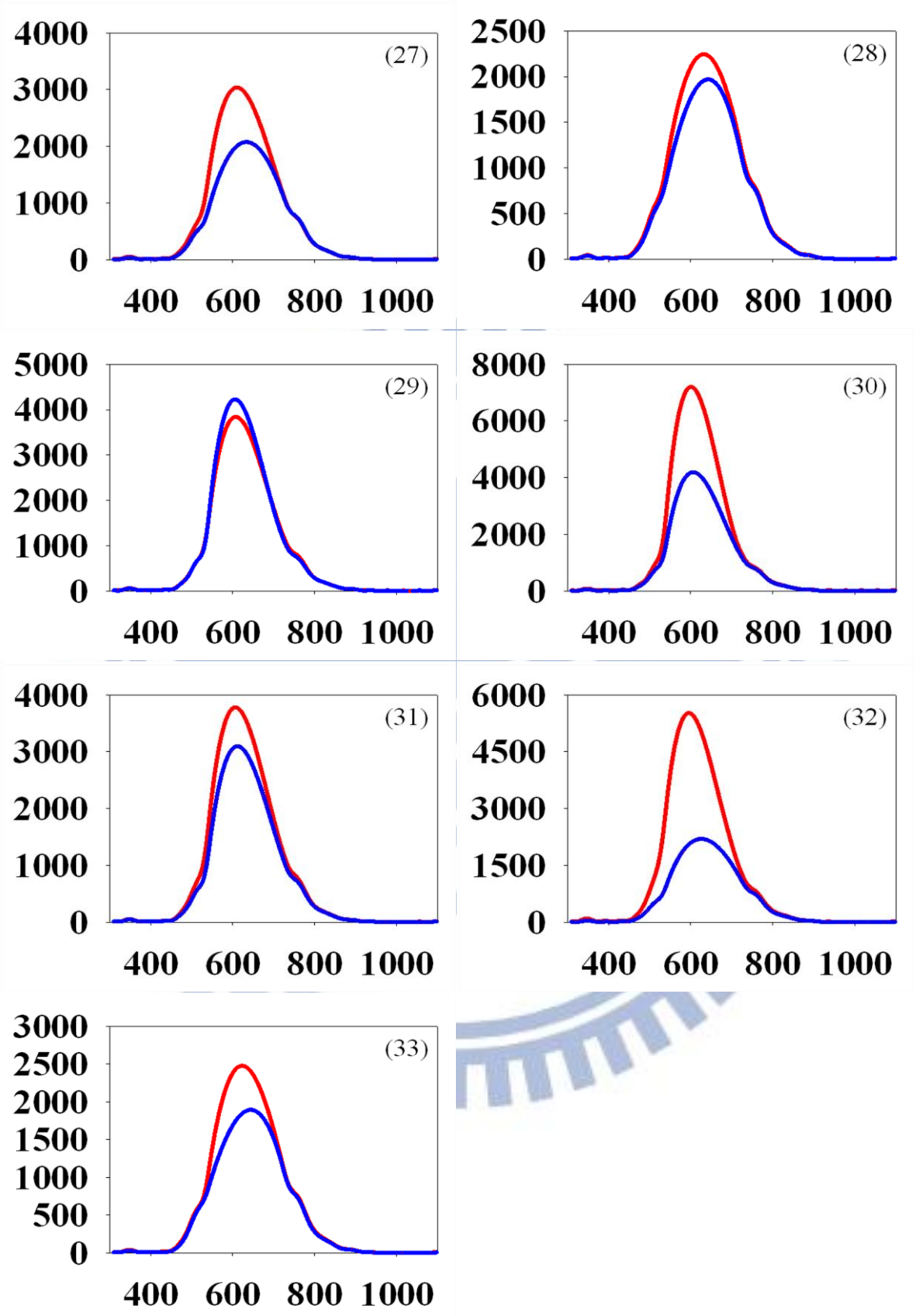

Figure 4-6: The spectral curves of each sample which have been compensated by spline in fluorescence 330~385nm excitation. The number of figure means the number of the sample. The red line means normal cells, and

blue line means cancer cells. The number means the number of patients. X axis is wavelength (nm), and Y axis is fluorescence intensity (μ w).

Table 4-5: The specificity of analysis in fluorescence 330~385nm excitation.

Number of patient	Specificity of method 2-1 (%)	Specificity of method 2-2 (%)	Specificity of method 2-3 (%)	Specificity of method 2-4 (%)
1	54.9	69.1	79.1	54.2
2	49.3	34.3	45.1	57.5
3	96.5	99.4	96.3	76.1
4	74.9	68.0	82.1	78.5
5	57.9	71.1	49.0	69.4
6	38.6	49.7	62.8	90.8
7	73.3	85.3	82.7	51.4
8	76.8	55.2	42.8	78.2
9	59.4	55.2	43.1	64.8
10	87.0	76.8	83.3	93.5
11	61.7	74.8	81.5	64.6
12	70.7	67.6	69.9	79.0
13	37.6	42.8	59.9	59.7
14	82.0	93.5	92.7	82.9
15	40.8	44.1	74.3	67.5
16	65.5	54.2	70.3	63.3
17	62.8	75.2	97.6	72.4
18	49.5	50.5	62.0	54.4
19	64.1	82.2	49.3	69.8
20	63.3	87.6	99.7	59.0
21	35.2	38.7	44.2	27.7
22	86.4	84.2	89.9	90.8
23	45.4	55.4	55.4	33.1

24	87.6	80.3	79.4	89.0
25	71.0	69.5	84.2	50.3
26	61.8	73.5	32.4	48.2
27	93.1	89.3	85.8	92.0
28	78.6	70.5	69.9	67.1
29	64.6	78.7	82.5	65.8
30	89.1	85.0	83.2	92.3
31	83.4	72.4	59.4	78.9
32	97.8	92.8	90.7	98.2
33	86.9	82.4	77.9	88.4

4.3.3 Fluorescence with 470~490nm excitation

Figure 4-7 shows the spectrum in fluorescence 470~490nm excitation. We have 3 methods to analyze the spectrum to distinguish normal cells and cancer cells. Method 3-1 compares the intensity of the peak in the wavelength range 540~570nm. Method 3-2 calculates the area under the spectral curve that we normalize. Method 3-3 calculates the full width at half maximum (FWHM) of the spectral curve.

Table 4-6 shows the result of the analysis as well as the specificity of each method in each sample. We can see that the variation of the specificity between different samples is large, and the mean of specificity in one method is too low (about 50%).

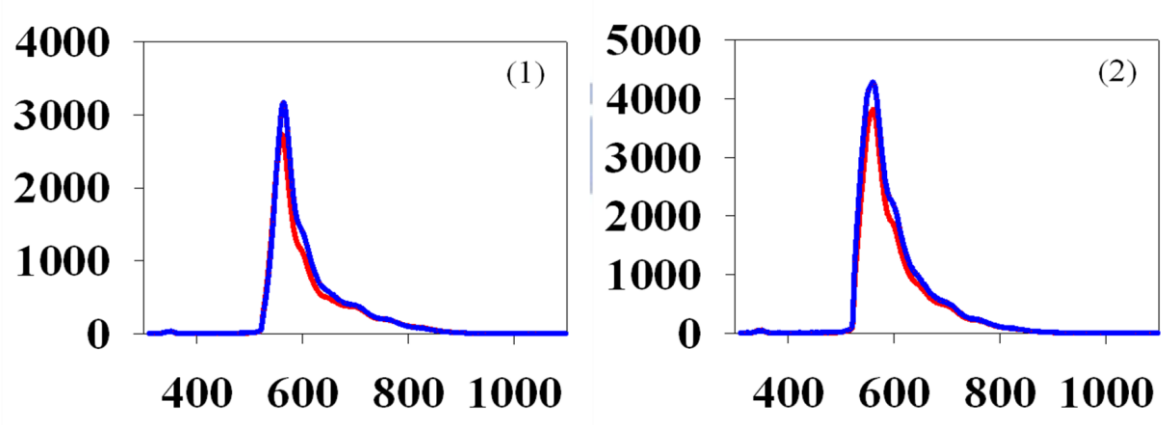

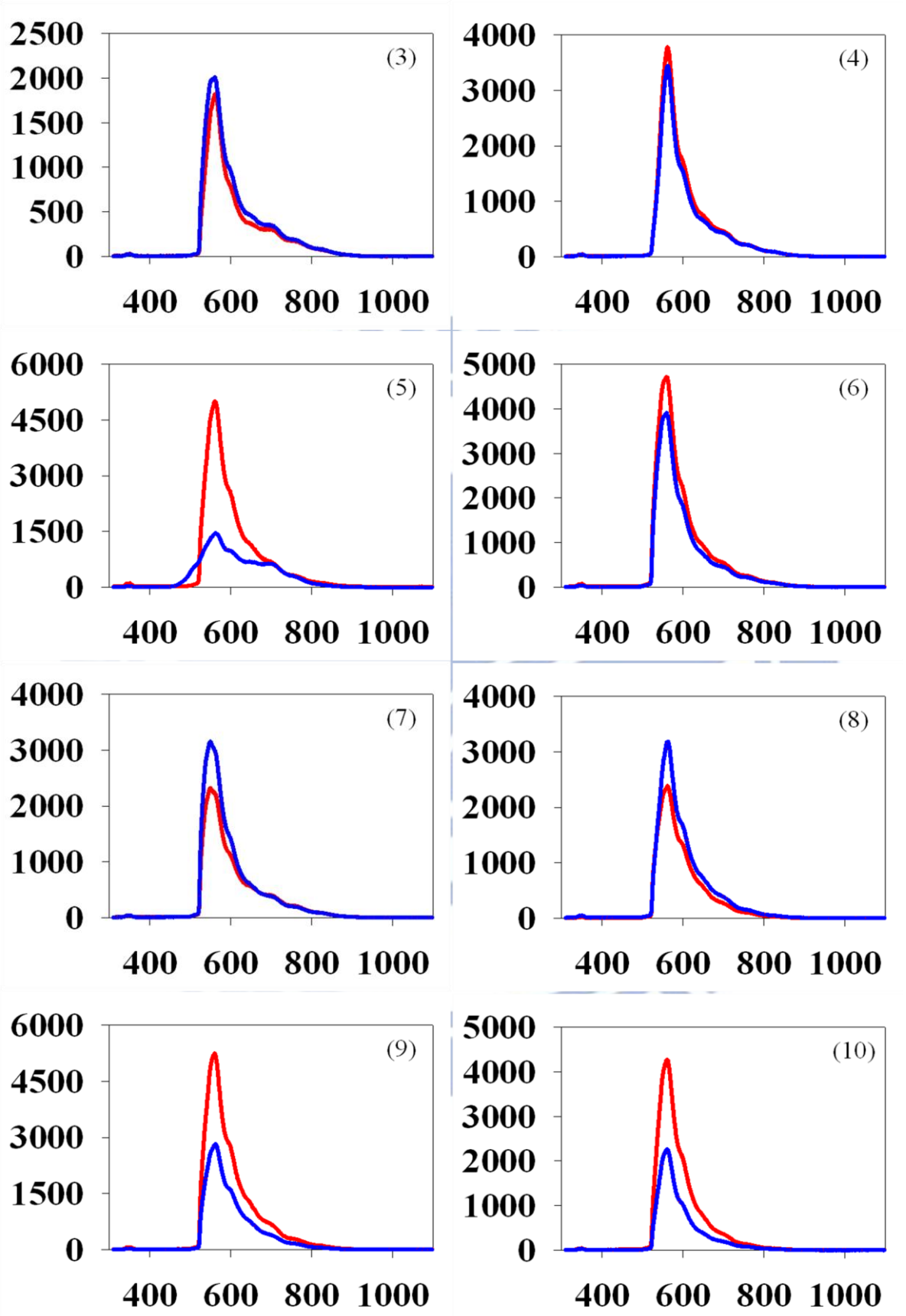
(3)
2500
2000
1500
1000
500
0
400 600 800 1000
(4)
4000
3000
2000
1000
0
400 600 800 1000
(5)
6000
4500
3000
1500
0
400 600 800 1000
(6)
5000
4000
3000
2000
1000
0
400 600 800 1000
(7)
4000
3000
2000
1000
0
400 600 800 1000
(8)
4000
3000
2000
1000
0
400 600 800 1000
(9)
6000
4500
3000
1500
0
400 600 800 1000
(10)
5000
4000
3000
2000
1000
0
400 600 800 1000

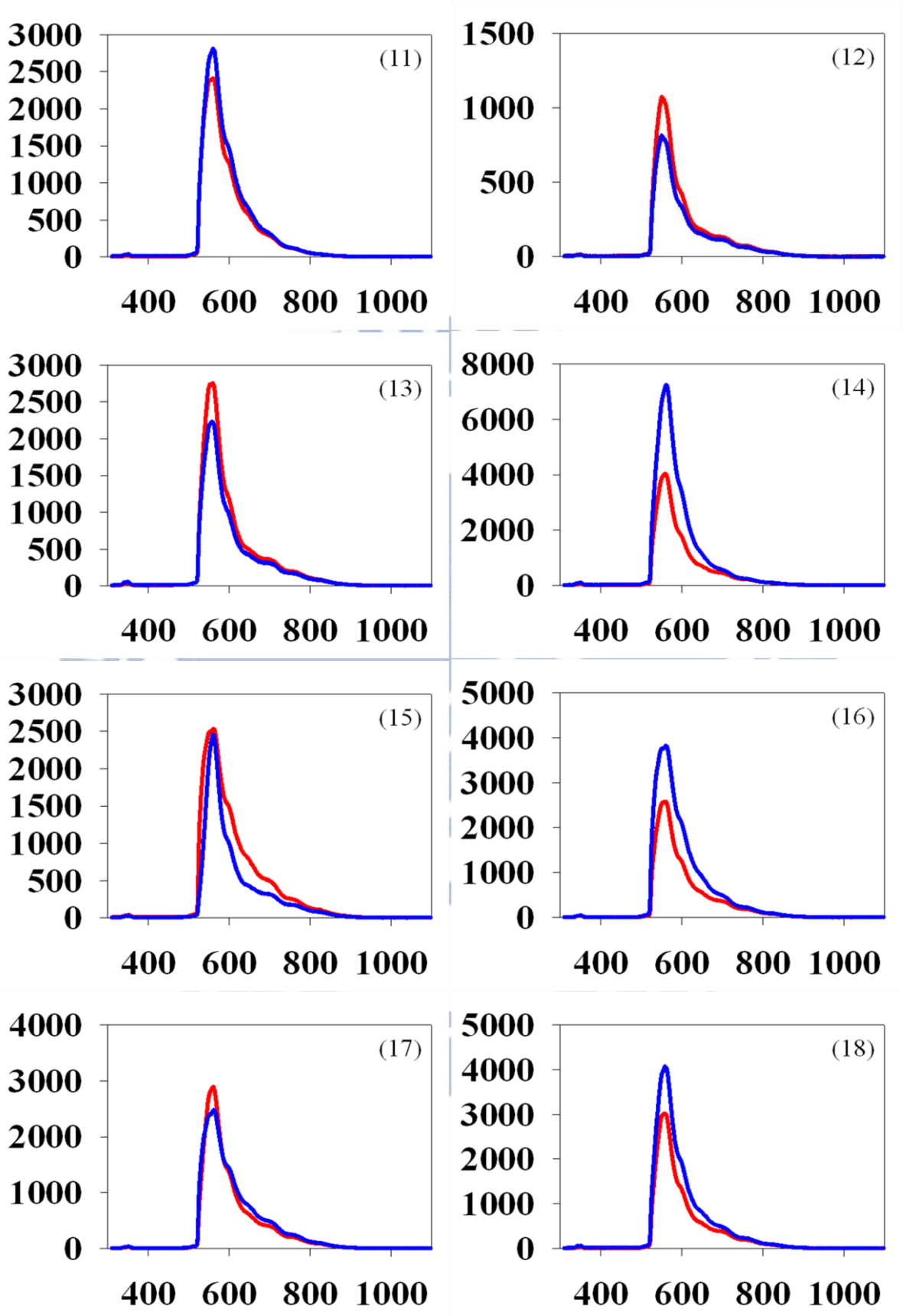
(11)
3000
2500
2000
1500
1000
500
0
400 600 800 1000
(12)
1500
1000
500
0
400 600 800 1000
(13)
3000
2500
2000
1500
1000
500
0
400 600 800 1000
(14)
8000
6000
4000
2000
0
400 600 800 1000
(15)
3000
2500
2000
1500
1000
500
0
400 600 800 1000
(16)
5000
4000
3000
2000
1000
0
400 600 800 1000
(17)
4000
3000
2000
1000
0
400 600 800 1000
(18)
5000
4000
3000
2000
1000
0
400 600 800 1000

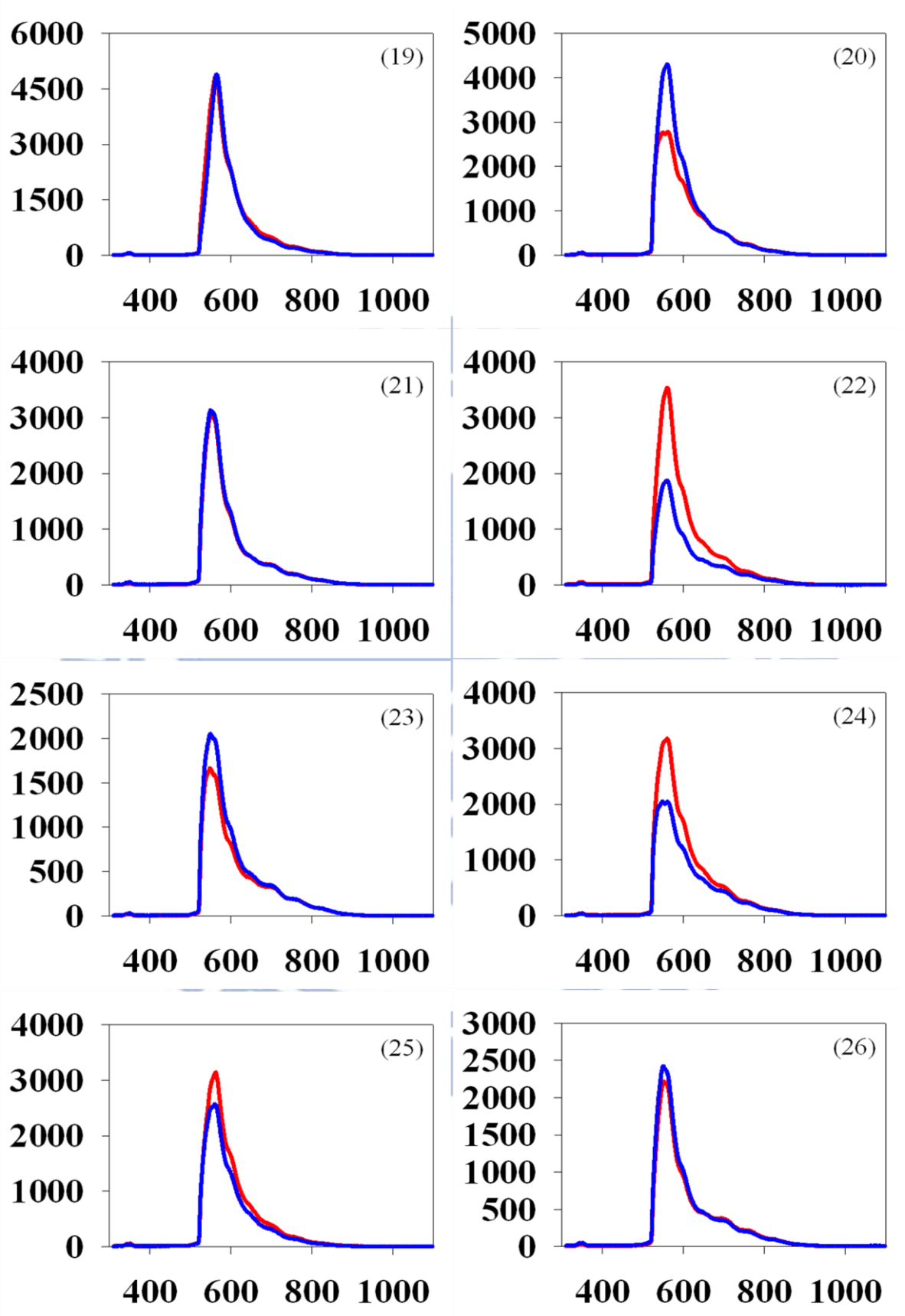
(19)
6000
4500
3000
1500
0
400 600 800 1000
(20)
5000
4000
3000
2000
1000
0
400 600 800 1000
(21)
4000
3000
2000
1000
0
400 600 800 1000
(22)
4000
3000
2000
1000
0
400 600 800 1000
(23)
2500
2000
1500
1000
500
0
400 600 800 1000
(24)
4000
3000
2000
1000
0
400 600 800 1000
(25)
4000
3000
2000
1000
0
400 600 800 1000
(26)
3000
2500
2000
1500
1000
500
0
400 600 800 1000

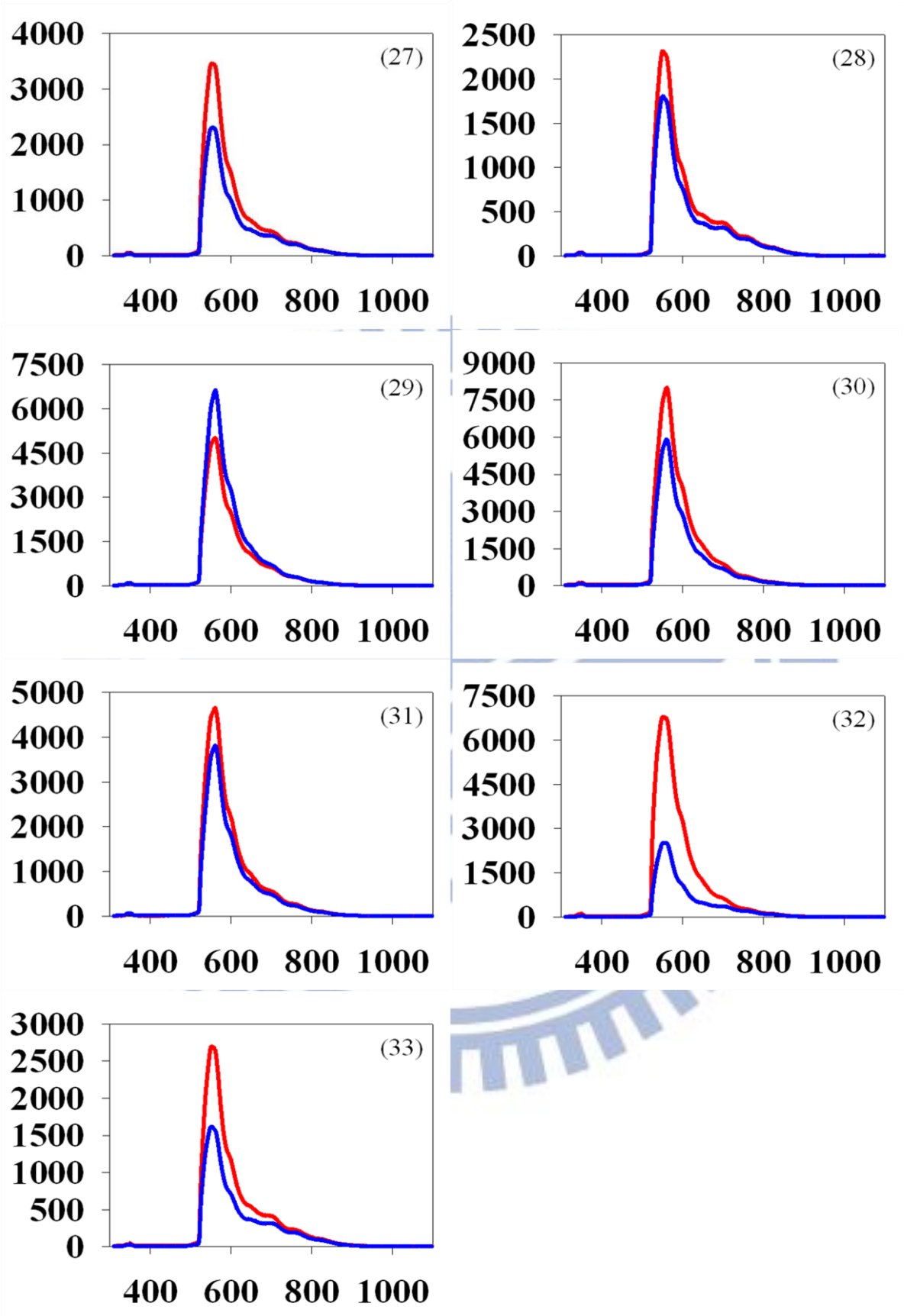

Figure 4-7: The spectral curve of each sample in fluorescence 470~490nm excitation. The number of figure means the number of the sample. The red line

means normal cells, and blue line means cancer cells. The number means the number of patients. X axis is wavelength (nm), and Y axis is fluorescence intensity (μ w).

Table 4-6: The specificity of analysis in fluorescence 330~385nm excitation.

Number of patient	Specificity of method 3-1 (%)	Specificity of method 3-2 (%)	Specificity of method 3-3 (%)	Number of patient	Specificity of method 3-1 (%)	Specificity of method 3-2 (%)	Specificity of method 3-3 (%)
1	56.9	81.6	62.0	**18**	51.1	48.6	63.1
2	51.4	51.5	85.3	**19**	48.3	83.0	84.4
3	71.3	69.7	90.4	**20**	68.6	96.8	95.0
4	77.5	86.7	76.2	**21**	24.4	35.3	40.6
5	99.2	100.0	96.7	**22**	95.4	72.7	32.2
6	61.8	46.8	42.3	**23**	53.8	65.3	54.3
7	64.8	83.5	74.3	**24**	86.3	86.4	90.0
8	54.4	35.5	82.6	**25**	68.7	49.1	38.4
9	94.7	78.7	76.7	**26**	43.8	72.4	66.0
10	92.2	63.9	70.2	**27**	90.5	76.0	35.1
11	46.6	42.4	66.4	**28**	86.2	66.0	20.8
12	76.6	64.0	50.1	**29**	74.6	85.8	74.6
13	60.6	64.9	50.0	**30**	83.7	81.1	64.8
14	83.3	92.5	75.5	**31**	71.2	68.6	50.7
15	34.0	98.3	100.0	**32**	97.1	70.7	82.6
16	58.8	53.4	90.2	**33**	89.0	69.8	43.9
17	50.9	98.9	98.9				

Chapter 5 Discussions, Conclusions and Future Works

5.1 Discussions

In calculating the fractal dimension of the image, the critical value of the threshold method has an enormous impact on the value of the fractal dimension. Determining the value of the critical value is an important issue. Because the area of which the value is 1 in the threshold method and the coordinates of the training data are both the nuclei in the basal-cell layer, we determined the critical value in accordance to the value of the training data chosen by hand.

The fractal dimension method shows a high sensitivity and specificity, except in sample number 3. The fractal dimension of number 3 in normal tissue is 1.73 and 1.67 in cancer cells. The goal of the threshold method is setting the value of the nuclei in the basal-cell layer as 1 and the other as 0; the image causes a low value of fractal dimension with a low number of nuclei. In observing the image of sample number 3, we find that the number of nuclei is low in cancerous tissue.

In the result of classification by KNN, the difference in the correct rate between normal cells and cancer cells is not large, and the specificity is only 55.34%. The distribution of nuclei in the lamina propria decides the correct rate. If the distribution shows an intensive type, it is difficult to use the KNN to distinguish the nuclei between the basal-cell layer and the lamina propria, and it causes a low correct rate. The morphology of the lamina propria shows low correlation with the erosion of cancer cells, Table 4-2. The topology of the lamina propria may change because of different composition or location.

In order to establish data for spectral diagnosis, we can mark the points on the nuclei, cytoplasm or intercellular bridge. Therefore, we have to verify the best target on the image for diagnosis. In the beginning, we mark the nuclei, cytoplasm and intercellular bridge on the image of the sample and diagnose oral cancer using the spectrum. After comparison, nuclei are chosen as the targets because of their highest sensitivity and specificity.

In the halogen spectrum, there is a large difference between normal cells and cancer cells. Except for sample number 2, methods 1 and 2 of diagnosis have high sensitivity and specificity. When we observe the normal cells in Figure 3-7(2), we see that the transmittance abnormally decreases in the wavelength range 300~700nm and 750~1100nm. In fluorescence, there is no

obvious decrease in the spectrum of normal cells. Therefore, the cause of the decrease in Figure 3-7(2) is the thickness of the sample because the thickness has an effect on transmittance, but no effect on reflectance.

We do not remove the light noise in the intensity of fluorescence because it is difficult to save light noise in fluorescence. In order to save light noise, the light source irradiates the black area of the biopsy, but there is no autofluorescence with the black area. Autofluorescence is emitted by the excited cells.

The sensitivity and specificity are higher in the diagnosis of the halogen spectrum than in the fluorescence spectrum. The average specificity of diagnosis in halogen is 79.545%, in fluorescence 330~385nm excitation is 68.48% and in fluorescence 470~490nm excitation is 70.12%. The reason for this is that we do not remove the light noise in fluorescence. Removing the light noise can remove the effect of the light source on different locations of the sample and normalize the intensity; however, the light noise cannot be recorded in fluorescence.

In defining the method of calculating the fractal dimension as in method 4-1 and the correct rate of classification by KNN as in method 4-2, according to the value of specificity, the order of methods is as follows: 1-1, 4-1, 1-2, 1-3, 3-3, 2-4, 3-1, 2-3, 2-2, 3-2, 2-1, 1-4 and 4-2. The specificity of the fractal dimension method is 91.46%, the method of calculating the halogen penetration in the wavelength range of 460~480nm (method 1-1) is 95.34% if sample number 2 is ignored, and the method of calculating the ratio of the halogen penetration in the range of 460~480nm to the halogen penetration in the range 700~710nm (method 1-2) is 86.45% if sample number 2 is ignored. Methods 1-1, 1-2 and 4-1 have the highest specificity, and the specificity is higher than the others by 13% at least. Finally, the specificity is 98.45% in combination with methods 1-1, 1-2 and 4-1.

Table 5-1 shows the comparison with other articles. Our light sources include halogen and fluorescence with 330-385nm and 470-490nm excitation, and the method includes analysis using morphology and spectrum. Compared to the research presented in other articles, our research presents more information (more light sources, larger spectral range), is more convincing (based on 33 patients and using more than 100 sets of data in one sample), more novel (analysis combining morphology and spectrum) and shows high specificity (98.45%).

Table 5-1: Comparison of other articles.

Author (year)	**Light source**	**Spectral range (nm)**	**Number of lesions**	**Methods**	**Results**
Our study (2012)	Halogen, fluorescence 330-385nm and 470-490nm excitation	400-1100	33	Fractal dimension, classification by KNN, intensity, ratio, wavelength of peak, area under spectrum, and FWHM	Sen. 92.9%, spec. 98.45%
Irene *et al*. (2001)	Fluorescence 337-620nm excitation	350-700	unknown	Combination of fluorescence, scattering, and levels of nuclear crowding and enlargement	Sensitivity 100%, specificity 100%
Hamed *et al*. (2011)	Halogen	1000-2500	10	Standard deviation, support vector machine, and first derivatives and integral	Spec. 82% in SD, spec.82% in SVM, and spec. 88% in integral
Kevin *et al*. (2009)	Fluorescence 465-645nm excitation	>600	7	567/515 nm ratio	Showing a good correlation between various disease states
Kojiro *at al*. (2002)	Fluorescence 404nm	500-700	18	Intensity at 582, 634, and 672nm	Cancer changes: peaks at 634 and 672 increased and peaks at 520 and 582nm decreased
Chich-Yu Wang *et al*. (1999)	Fluorescence 280-400nm excitation	300-700	96	Combination of PLS andlysis and logistic regression	Accuracy rate 81.3
Brigitte *et al*. (2001)	Fluorescence 375-478nm excitation	450-750	13	500-549/657-700nm ratio	Sens. 97%, spec. 95%

5.1.1 Cocktail method in accordance to the sample data

The cocktail method combines the methods with fluorescence excitation , and the methods show higher specificity and better correlation with sample data. The sample data includes the age of patient, the differentiated level, the location of biopsy, the stage of oral cancer, T, N, and M. T is the diagnosis of tumor, N is the diagnosis of regional lymph nodes, and M is the diagnosis of distant metastasis. For finding the correlation between specificity of the methods and the sample data, the Figures 5-1 to 5-7 show the specificity of methods in different sample data. In the Figure, X axis is the specificity of methods, and Y axis is the ratio of people with the specificity above the value in X axis. For example, Figure 5-1(b), the ratio of people which is in age 30-39 in method 2-1 is 80% with specificity above 60%, 60% with specificity above 70%, and 20% with specificity above 90%. We define the method which has highest summing Y values in X values 80 and 90 as the most effective method.

Table 5-2 shows the most effective method for detecting cancer in each sample data. According to Table 5-2, we get the effective methods analyzing each sample. For example, one sample data are 59 years, poorly differentiated, tongue, stage 1, and T0N0M0, and the effective methods are method 2-4, 3-1, 3-2, and 3-3. We combine the effective method and compute the specificity, Table 5-3. The average of specificity is 87% which is higher 15 % than the specificity in method 2-1 to 3-3, Table 5-4.

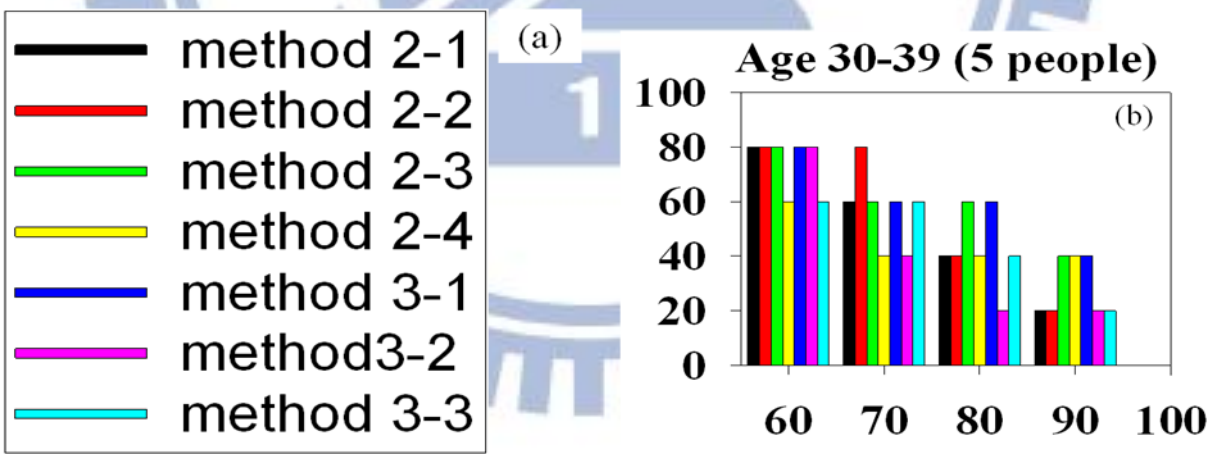

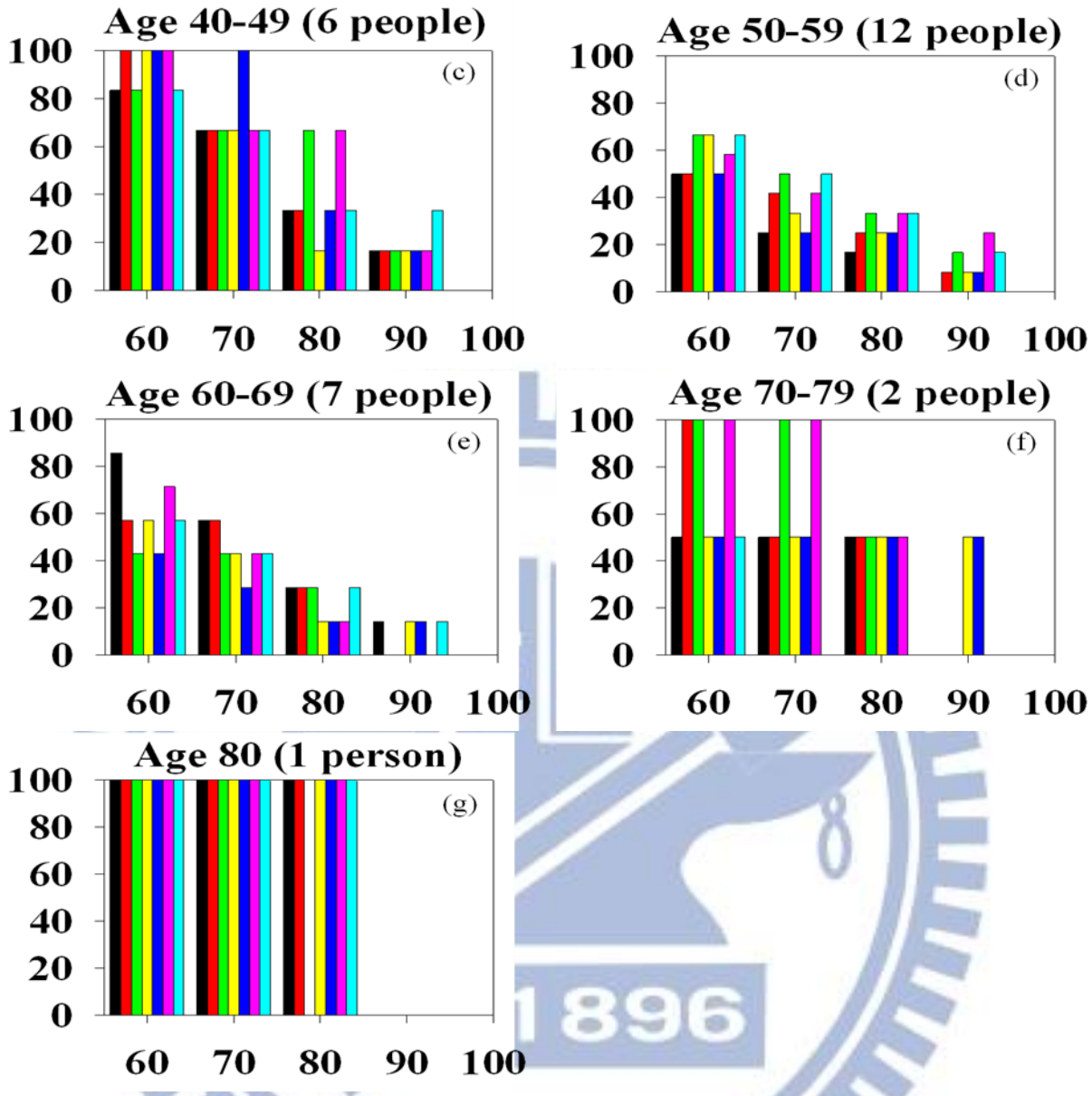

Figure 5-1: The ratio of people in different age ranges. X axis is specificity, and Y axis is the ratio of people.

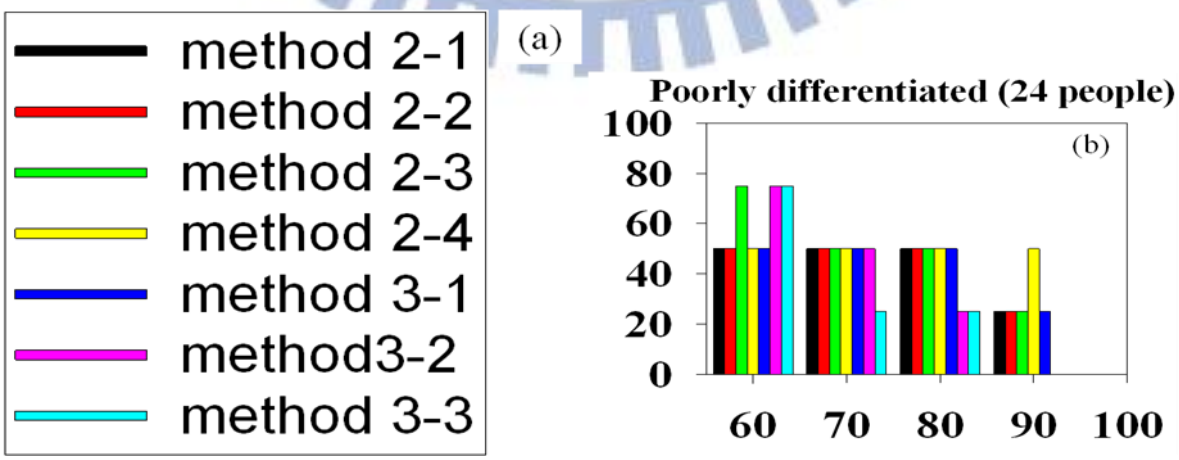

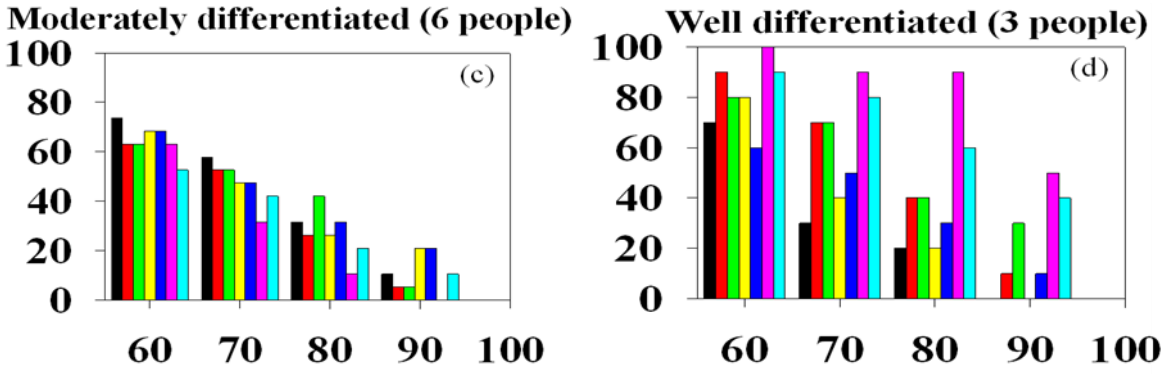

Figure 5-2: The ratio of people in different differentiation. X axis is specificity, and Y axis is the ratio of people.

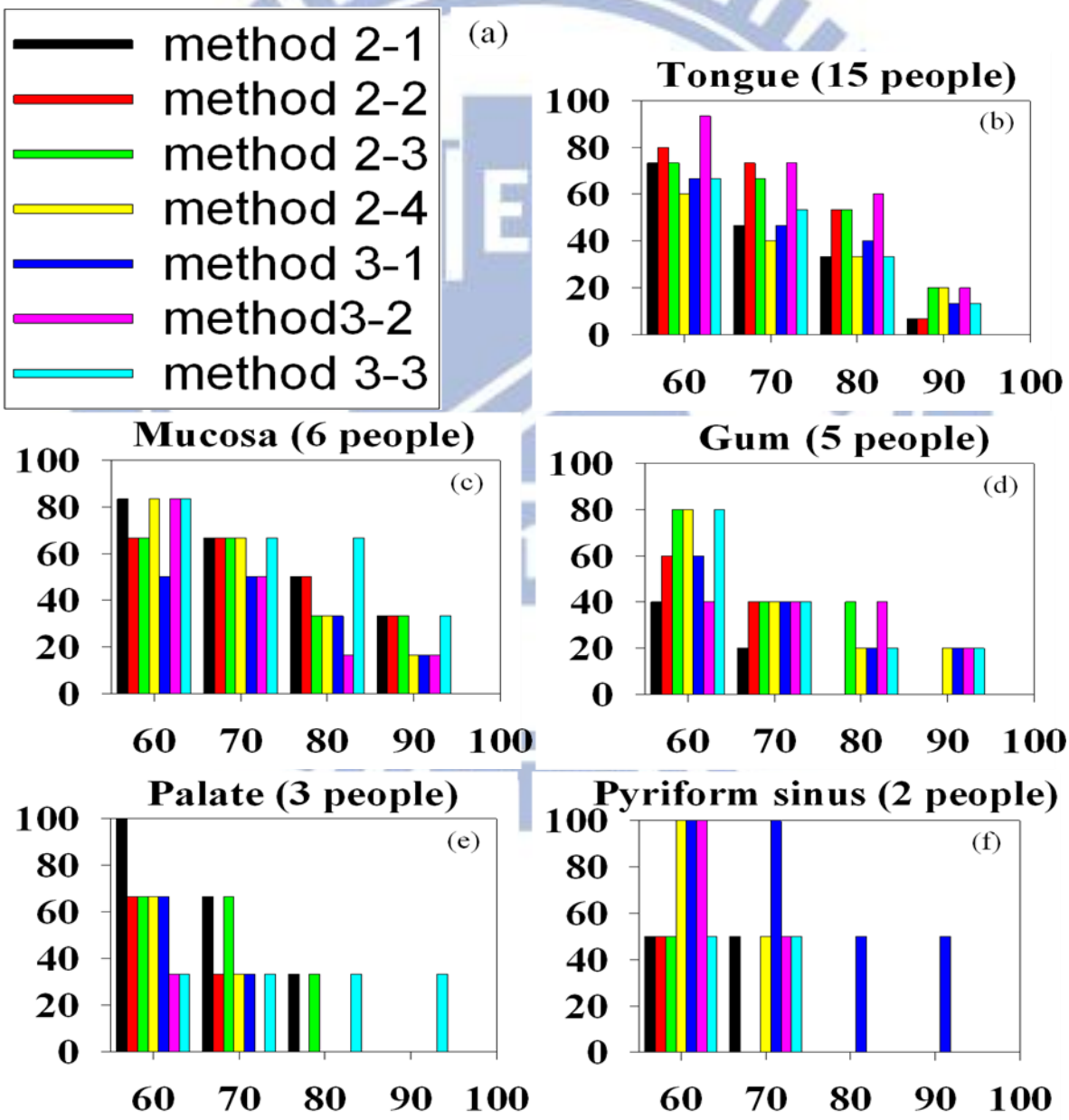

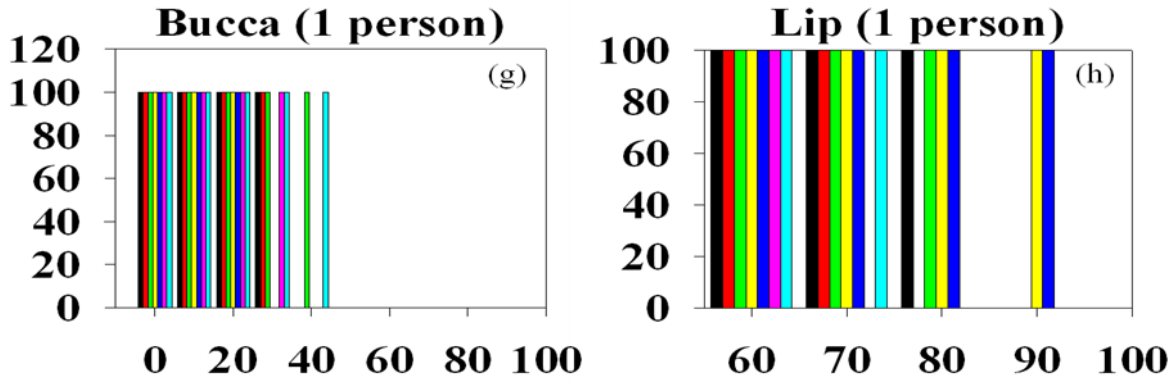

Figure 5-3: The ratio of people in different locations. X axis is specificity, and Y axis is the ratio of people.

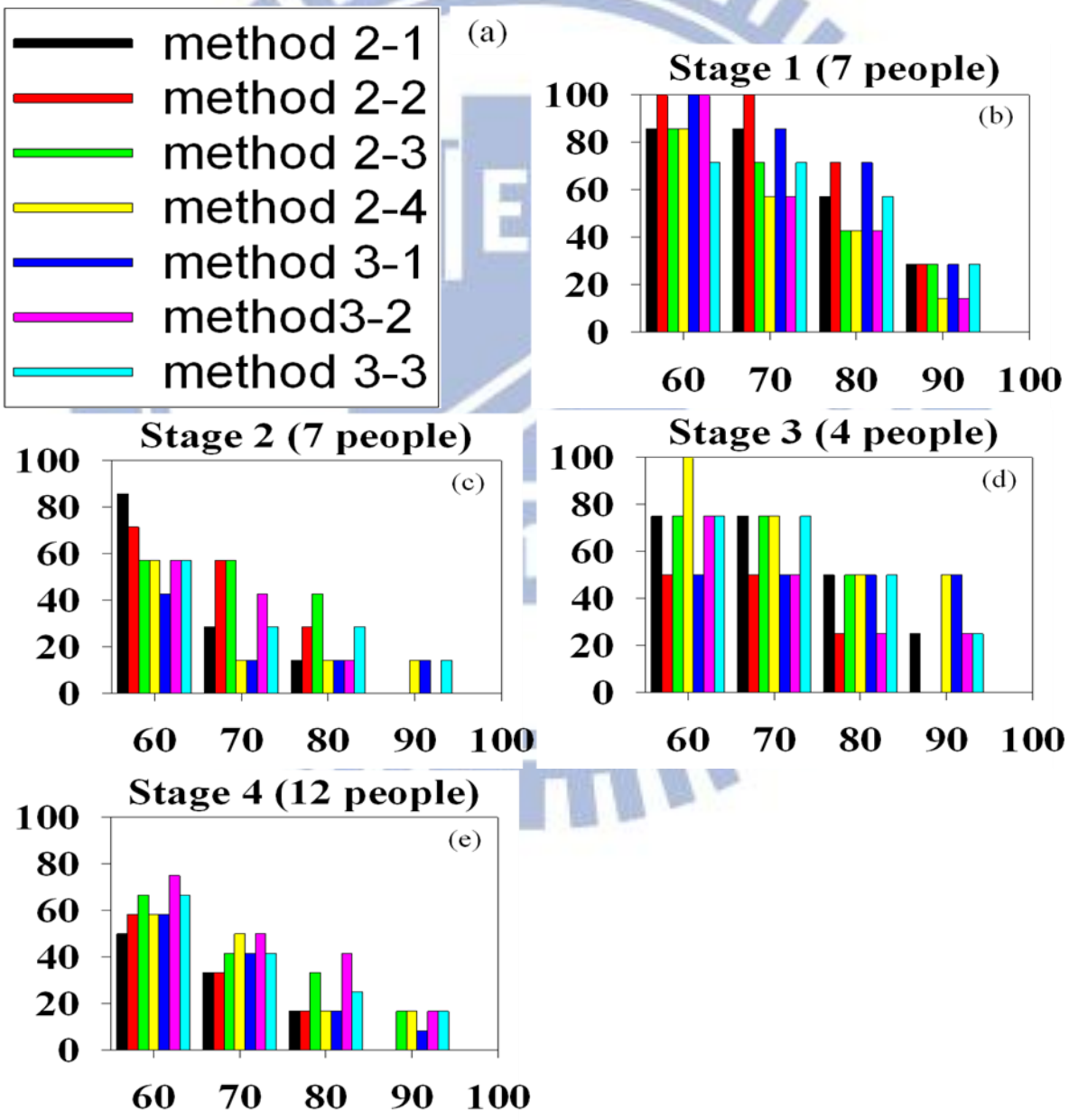

Figure 5-4: The ratio of people in different stage. X axis is specificity, and Y axis is the ratio of people.

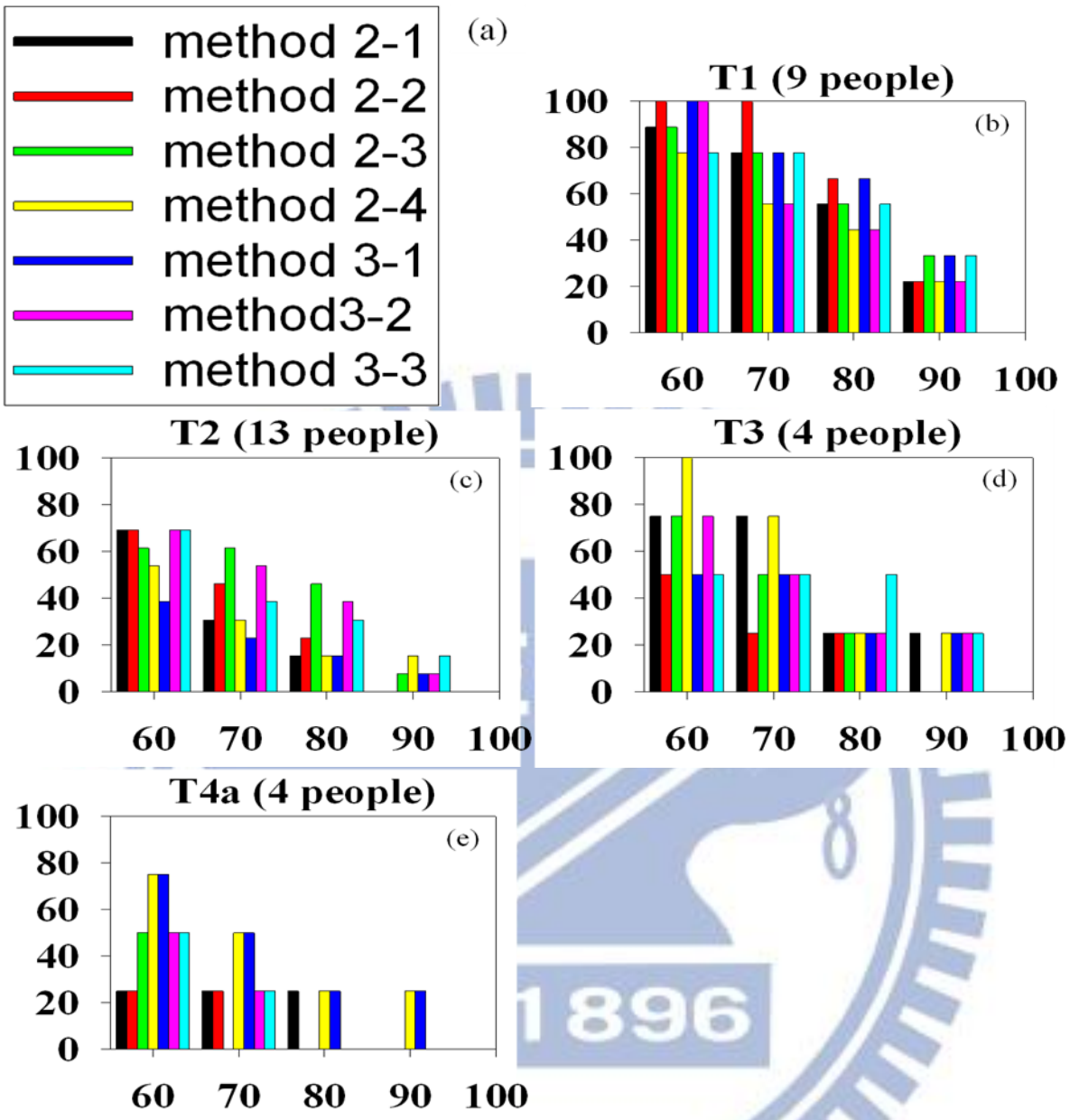

Figure 5-5: The ratio of people in different T. X axis is specificity, and Y axis is the ratio of people.

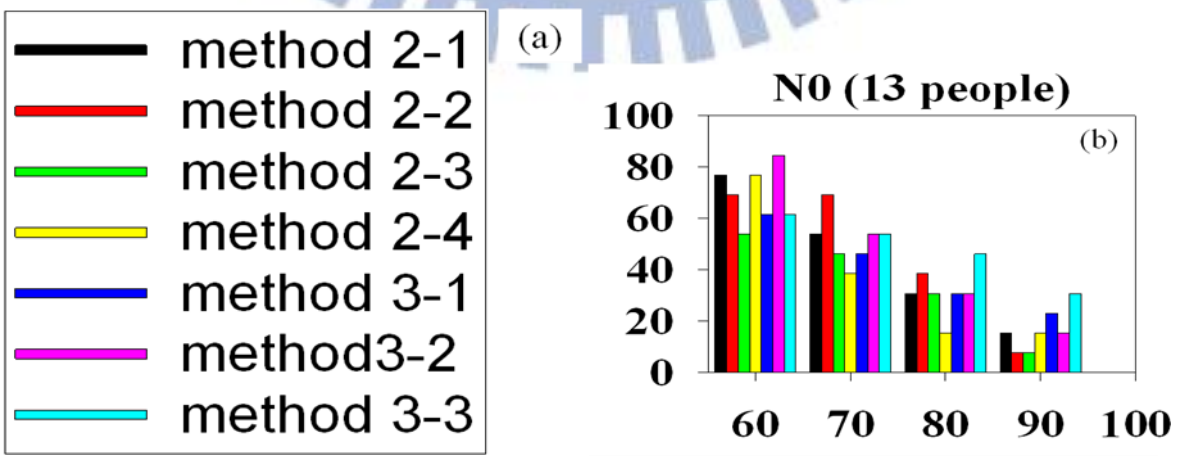

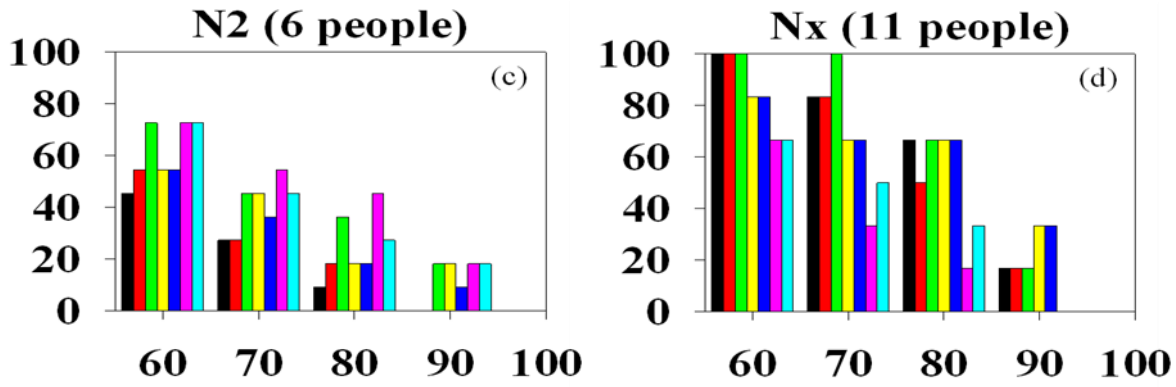

Figure 5-6: The ratio of people in different N. X axis is specificity, and Y axis is the ratio of people.

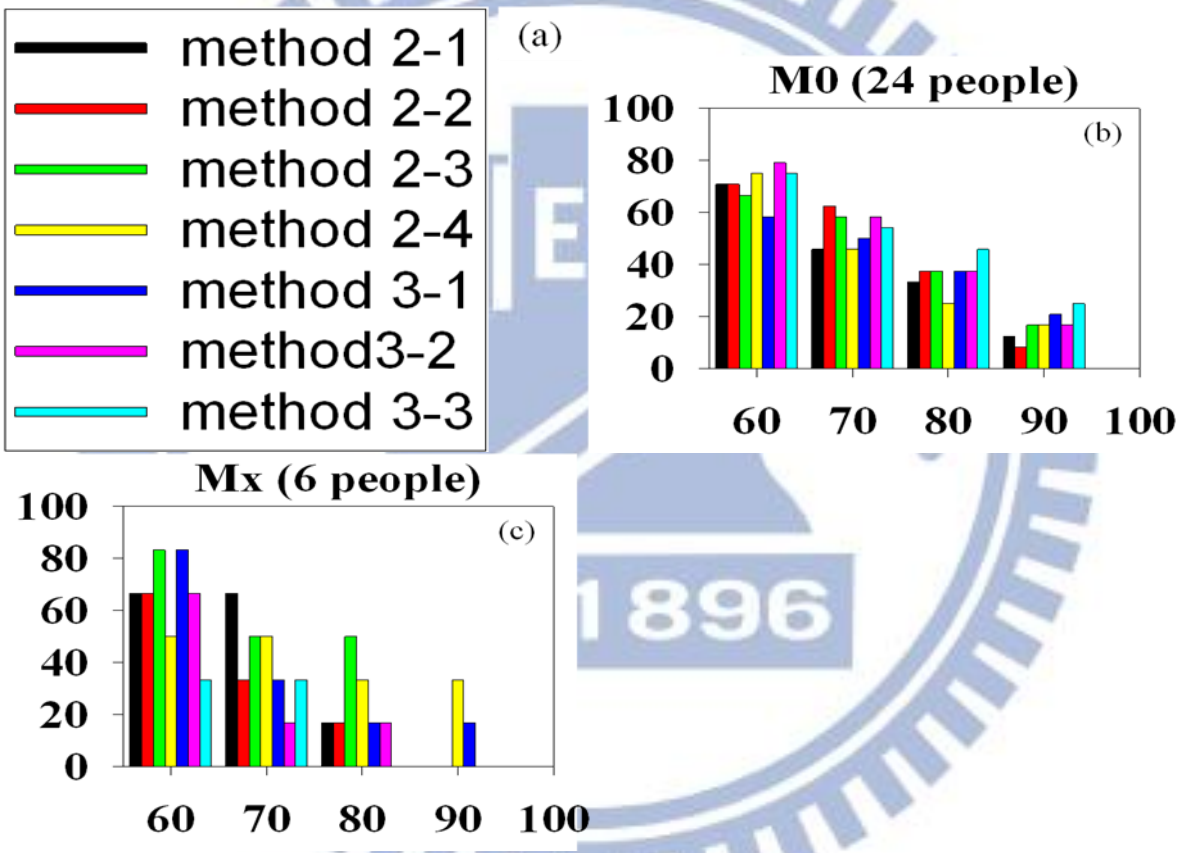

Figure 5-7: The ratio of people in different M. X axis is specificity, and Y axis is the ratio of people.

Table 5-2: The most effective method with each sample data.

Age	30-39	40-49	50-59	60-69	70-79	80	
Method	3-1	3-2, 3-3	3-2	3-3	2-4, 3-1	no	
Differentiated level	Poor	Moderate	Well				
Method	2-4	3-1	3-2				
Location of biopsies	Tongue	Mucosa	Gum	Palate	Pyriform sinus	Bucca	Lip
Method	3-2	3-3	3-2	3-3	3-1	no	2-4, 3-1
Stage of cancer	Stage 1	Stage 2	Stage 3	Stage 4			
Method	3-1	3-3	2-4	3-2			
Tumor	T1	T2	T3	T4a			
Method	3-1	3-2	3-3	2-4, 3-1			
Regional lymph nodes	N0	N2	Nx				
Method	3-3	3-2	2-4, 3-1				
Distant metastasis	M0	Mx					
Method	3-3	2-4					

Table 5-3: The combined methods of cocktail method and the specificity for each sample.

Sample	Combined Methods	Specificity (%)	Sample	Combined Methods	Specificity (%)
1	2-4, 3-1, 3-2, 3-3	85.4	18	2-4, 3-3	56.12
2	3-3	85.3	19	3-2, 3-3	97.7
3	3-1, 3-2, 3-3	95.3	20	3-1, 3-2, 3-3	98.3
4	3-1, 3-2, 3-3	99.2	21	3-2, 3-3	30.19
5	3-1, 3-2, 3-3	100	22	2-4, 3-1, 3-2, 3-3	90.1
6	2-4, 3-1, 3-2	100	23	3-1, 3-2, 3-3	59.73
7	2-4, 3-1, 3-2, 3-3	86.5	24	3-1, 3-2, 3-3	96.7
8	2-4, 3-1, 3-3	90.1	25	2-4, 3-1, 3-2, 3-3	100
9	2-4, 3-1, 3-2, 3-3	100	26	3-2, 3-3	82.22
10	2-4, 3-1, 3-3	98.8	27	2-4, 3-1, 3-2, 3-3	92.9
11	2-4, 3-3	75	28	2-4, 3-1, 3-2	79.08
12	2-4, 3-1	88.28	29	3-2, 3-3	89.4
13	3-1, 3-2	70.83	30	2-4, 3-2, 3-3	98.9
14	3-2	94.1	31	2-4, 3-1, 3-2, 3-3	80.1
15	2-4, 3-2, 3-3	100	32	2-4, 3-1, 3-3	99.6
16	3-1, 3-2, 3-3	71.1	33	3-1, 3-2, 3-3	81.1
17	3-1, 3-2, 3-3	98.4			

Table 5-4: The comparison of the methods.

	Method 2-1	**Method 2-2**	**Method 2-3**	**Method 2-4**
Mean of specificity (%)	68.1	70	71.5	70
Standard deviation of specificity	3.11	2.96	3.2	3.04
	Method 3-1	**Method 3-2**	**Method 3-3**	**Cocktail method**
Mean of specificity (%)	68.7	70.9	67.4	87
Standard deviation of specificity	3.40	3.16	3.76	2.72

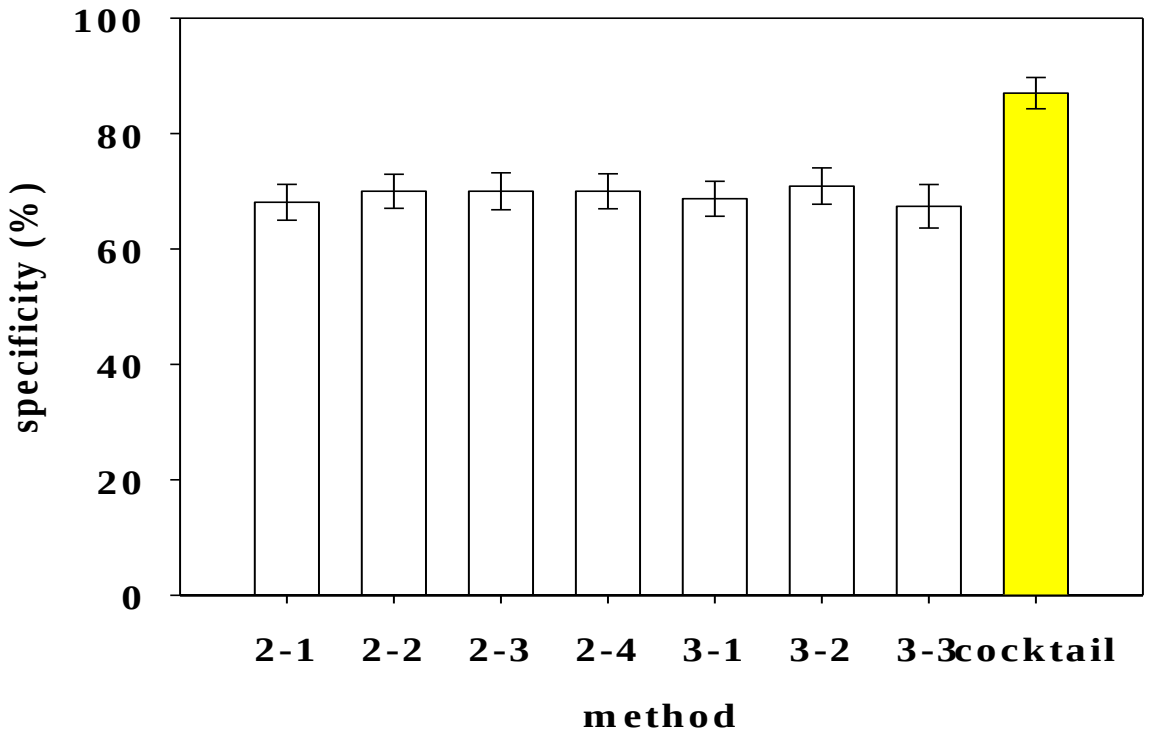

Figure 5-8: The comparison of the methods with vertical bars.

5.1.2 Cause of halogen transmittance over 1.0

In Figures 4-3(2), (11) and (12), we see that the halogen transmittance is higher than 1.0 in the wavelength range 680~730nm, and that it is abnormal. Because the transmittance is calculated by the spectrum, subtracting black noise and dividing the light noise, the value of transmittance is usually between 0 and 1. When we compared the spectrum normalized in halogen and fluorescence in 330-385nm excitation, we found that the peaks at 680-730nm are similar, as

shown in Figure 5-1. Therefore, we estimated transmittance of more than 1.0 caused by fluorescence excitation.

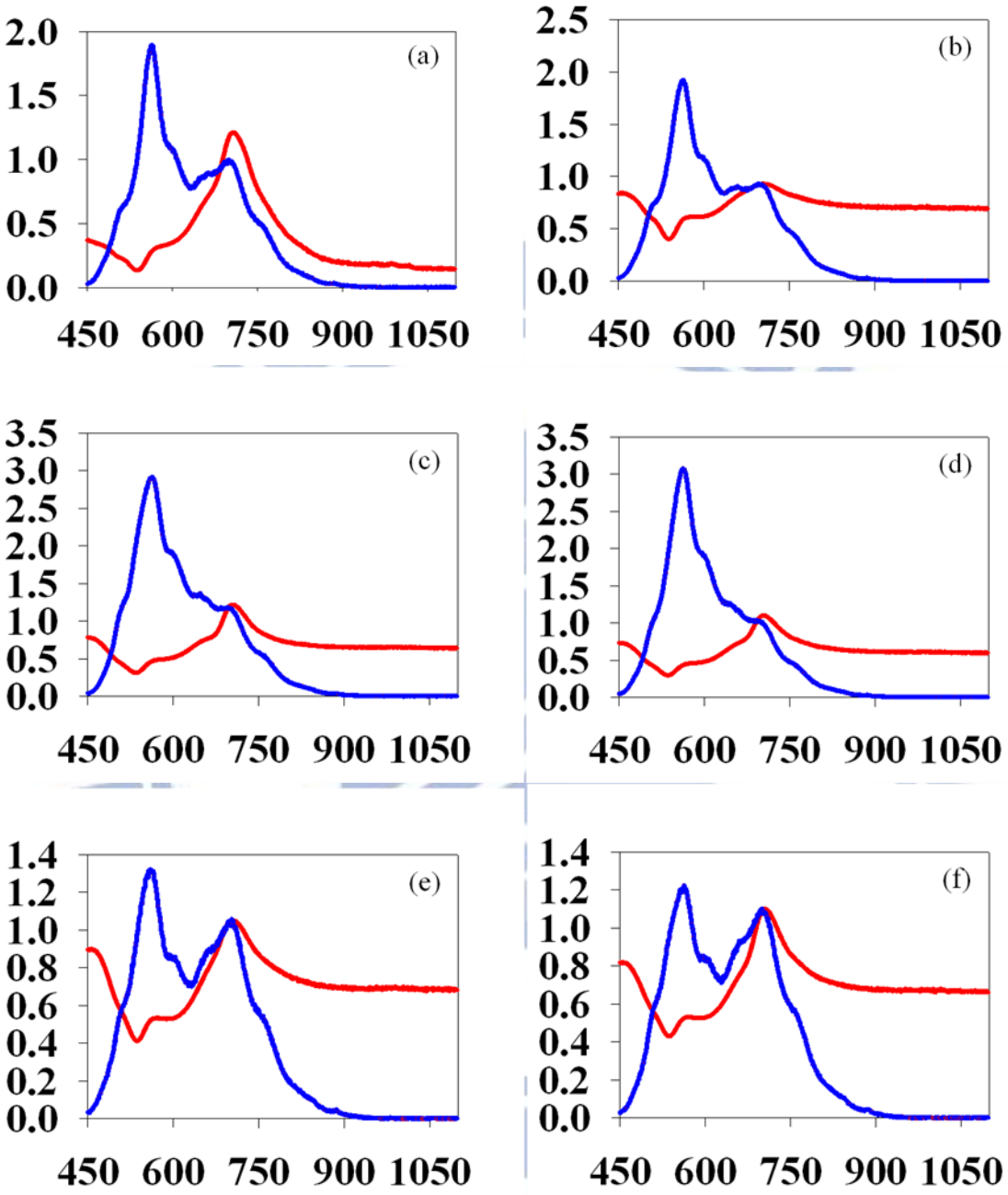

Figure 5-9: The comparison of spectrum in the halogen and fluorescence (a) Normal cells in the sample 2. (b) Cancer cells in the sample 2. (c) Normal cells in the sample 11. (d) Cancer cells in the sample 11. (e) Normal cells in the sample 12. (f) Cancer cells in the sample 12. The red line means halogen spectrum, and blue line means fluorescence spectrum. X axis is wavelength (nm), and Y axis is normalized intensity.

5.2 Conclusions and future works

In this study, we aimed to detect oral cancer using ERL-MHIS. The ERL-MHIS includes: a microscope, relay lens, spectrometer and EMCCD. With the relay lens, we can scan the image of a sample without the relative movement between the biopsies and the scanning system. After saving the hyperspectral information, we used algorithms to diagnose the oral cancer. We observed the change of morphology and spectrum in the sample. The methods of morphology include the fractal dimension and the correct rate of classification by KNN. Because cancer cells destroy the structure of epithelial tissues, method 4-1 of calculating fractal dimension shows high sensitivity in distinguishing between normal and cancerous tissues. The methods of spectrum include: comparing the intensity, the ratio, the wavelength of a specific peak, the area under spectral curve and the FWHM. The spectral data include halogen transmittance and fluorescent spectrum with 330~385nm and 470~490nm excitation. After removing the noise, we found the decrease of halogen transmittance at 470-490nm.

After combining the methods of the penetration in the wavelength range of 460~480nm, the ratio of the penetration in the range 460~480nm to the penetration in the range 700~710nm and fractal dimension, the sensitivity and specificity were both more than 95%. ERL-MHIS with diagnoses using morphology and spectrum successfully distinguished normal and cancerous tissues. However, because of the irregular shape of nuclei, it is hard to automatically choose nuclei as training data. All of the methods are needed to choose the training data by hand, and it significantly influences sensitivity. In the fractal dimension method, the value of the critical point in the threshold method is decided according to the training data. In classification by KNN, we also need training data. In the spectral method, the coordinates of analyzed data are all chosen by hand. In the future, we will try to design a portable and real-time instrument and diagnose oral cancer automatically without biopsies or training data chosen by hand.

References

[1] http://www.iosh.gov.tw/Book/Message_Publish.aspx?P=118&U=1272.

[2] http://website.tpech.gov.tw/cancer/癌症預防與篩檢/口腔癌簡介.html.

[3] R.-S. Tsai, *Anatomy*. New Taipei City: Chiuanwei Books Ltd, 2006.

[4] D. C. G. de Veld, M. Skurichina, M. J. H. Witjes, R. P. W. Duin, D. Sterenborg, W. M. Star, and J. L. N. Roodenburg, "Autofluorescence characteristics of healthy oral mucosa at different anatomical sites," *Lasers in Surgery and Medicine*, vol. 32(5), pp. 367-376, 2003.

[5] A. Stevens and J. Lowe, *Human Histology*. Singapore: Elsevier 2007.

[6] D. C. G. De Veld, M. J. H. Witjes, H. Sterenborg, and J. L. N. Roodenburg, "The status of in vivo autofluorescence spectroscopy and imaging for oral oncology," *Oral Oncology*, vol. 41(2), pp. 117-131, 2005.

[7] T. C. Kennedy, S. Lam, and F. R. Hirsch, "Review of recent advances in fluorescence bronchoscopy in early localization of central airway lung cancer," *Oncologist*, vol. 6(3), pp. 257-262, 2001.

[8] S. Lam and B. Palcic, "Autofluorescence bronchoscopy in the detection of squamous metaplasia and dysplasia in current and former smokers," *Journal of the National Cancer Institute*, vol. 91(6), pp. 561-562, 1999.

[9] M. Sato, A. Sakurada, M. Sagawa, M. Minowa, H. Takahashi, T. Oyaizu, Y. Okada, Y. Matsumura, T. Tanita, and T. Kondo, "Diagnostic results before and after introduction of autofluorescence bronchoscopy in patients suspected of having lung cancer detected by sputum cytology in lung cancer mass screening," *Lung Cancer*, vol. 32(3), pp. 247-253, 2001.

[10] S. Lam, T. Kennedy, M. Unger, Y. E. Miller, D. Gelmont, V. Rusch, B. Gipe, D. Howard, J. C. LeRiche, A. Coldman, and A. F. Gazdar, "Localization of bronchial intraepithelial neoplastic lesions by fluorescence bronchoscopy," *Chest*, vol. 113(3), pp. 696-702, 1998.

[11] T. G. Sutedja, H. Codrington, E. K. Risse, R. H. Breuer, J. C. van Mourik, R. P. Golding, and P. E. Postmus, "Autofluorescence bronchoscopy improves staging of radiographically occult lung cancer and has an impact on therapeutic strategy," *Chest*, vol. 120(4), pp. 1327-1332, 2001.

[12] B. J. W. Venmans, T. J. M. van Boxem, E. F. Smit, P. E. Postmus, and T. G. Sutedja, "Bronchial intraepithelial neoplastic lesions in head and neck cancer patients: Results of autofluorescence bronchoscopy," *Annals of Otology Rhinology and Laryngology*, vol. 110(7), pp. 635-638, 2001.

[13] W. Zheng, W. Lau, C. Cheng, K. C. Soo, and M. Olivo, "Optimal excitation-emission wavelengths for autofluorescence diagnosis of bladder tumors," *International Journal of Cancer*, vol. 104(4), pp. 477-481, 2003.

[14] G. Bottiroli, A. C. Croce, D. Locatelli, R. Marchesini, E. Pignoli, S. Tomatis, C. Cuzzoni, S. Dipalma, M. Dalfante, and P. Spinelli, "NATURAL FLUORESCENCE OF NORMAL AND NEOPLASTIC HUMAN COLON - A COMPREHENSIVE EX-VIVO STUDY," *Lasers in Surgery and Medicine*, vol. 16(1), pp. 48-60, 1995.

[15] B. W. Chwirot, Z. Michniewicz, M. Kowalska, and J. Nussbeutel, "Detection of colonic malignant lesions by digital imaging of UV laser-induced autofluorescence," *Photochemistry and Photobiology*, vol. 69(3), pp. 336-340, 1999.

[16] B. W. Chwirot, M. Kowalska, N. Sypniewska, Z. Michniewicz, and M. Gradziel, "Spectrally resolved fluorescence imaging of human colonic adenomas," *Journal of*

Photochemistry and Photobiology B-Biology, vol. 50(2-3), pp. 174-183, 1999.

[17] R. M. Cothren, M. V. Sivak, J. VanDam, R. E. Petras, M. Fitzmaurice, J. M. Crawford, J. Wu, J. F. Brennan, R. P. Rava, R. Manoharan, and M. S. Feld, "Detection of dysplasia at colonoscopy using laser-induced fluorescence: A blinded study," *Gastrointestinal Endoscopy*, vol. 44(2), pp. 168-176, 1996.

[18] C. Eker, S. Montan, E. Jaramillo, K. Koizumi, C. Rubio, S. Andersson-Engels, K. Svanberg, S. Svanberg, and P. Slezak, "Clinical spectral characterisation of colonic mucosal lesions using autofluorescence and delta aminolevulinic acid sensitisation," *Gut*, vol. 44(4), pp. 511-518, 1999.

[19] K. Izuishi, H. Tajiri, T. Fujii, N. Boku, A. Ohtsu, T. Ohnishi, M. Ryu, T. Kinoshita, and S. Yoshida, "The histological basis of detection of adenoma and cancer in the colon by autofluorescence endoscopic imaging," *Endoscopy*, vol. 31(7), pp. 511-516, 1999.

[20] T. D. Wang, J. M. Crawford, M. S. Feld, Y. Wang, I. Itzkan, and J. Van Dam, "In vivo identification of colonic dysplasia using fluorescence endoscopic imaging," *Gastrointestinal Endoscopy*, vol. 49(4), pp. 447-455, 1999.

[21] S. Abe, K. Izuishi, H. Tajiri, T. Kinoshita, and T. Matsuoka, "Correlation of in vitro autofluorescence endoscopy images with histopathologic findings in stomach cancer," *Endoscopy*, vol. 32(4), pp. 281-286, 2000.

[22] M. Kobayashi, H. Tajiri, E. Seike, M. Shitaya, S. Tounou, M. Mine, and K. Oba, "Detection of early gastric cancer by a real-time autofluorescence imaging system," *Cancer Letters*, vol. 165(2), pp. 155-159, 2001.

[23] C. Ell, "Improving endoscopic resolution and sampling: fluorescence techniques," *Gut*, vol. 52(pp. 30-33, 2003.

[24] H. S. Zeng, A. Weiss, R. Cline, and C. E. MacAulay, "Real-time endoscopic fluorescence imaging for early cancer detection in the gastrointestinal tract," *Bioimaging*, vol. 6(4), pp. 151-165, 1998.

[25] I. Pavlova, K. Sokolov, R. Drezek, A. Malpica, M. Follen, and R. Richards-Kortum, "Microanatomical and biochemical origins of normal and precancerous cervical autofluorescence using laser-scanning fluorescence confocal microscopy," *Photochemistry and Photobiology*, vol. 77(5), pp. 550-555, 2003.

[26] D. Roblyer, C. Kurachi, V. Stepanek, M. D. Williams, A. K. El-Naggar, J. J. Lee, A. M. Gillenwater, and R. Richards-Kortum, "Objective Detection and Delineation of Oral Neoplasia Using Autofluorescence Imaging," *Cancer Prevention Research*, vol. 2(5), pp. 423-431, 2009.

[27] C. F. Poh, L. W. Zhang, D. W. Anderson, J. S. Durham, R. M. Williams, R. W. Priddy, K. W. Berean, S. S. Ng, O. L. Tseng, C. MacAulay, and M. P. Rosin, "Fluorescence visualization detection of field alterations in tumor margins of oral cancer patients," *Clinical Cancer Research*, vol. 12(22), pp. 6716-6722, 2006.

[28] P. M. Lane, T. Gilhuly, P. Whitehead, H. S. Zeng, C. F. Poh, S. Ng, P. M. Williams, L. W. Zhang, M. P. Rosin, and C. E. MacAulay, "Simple device for the direct visualization of oral-cavity tissue fluorescence," *Journal of Biomedical Optics*, vol. 11(2), 2006.

[29] D. L. Heintzelman, U. Utzinger, H. Fuchs, A. Zuluaga, K. Gossage, A. M. Gillenwater, R. Jacob, B. Kemp, and R. R. Richards-Kortum, "Optimal excitation wavelengths for in vivo detection of oral neoplasia using fluorescence spectroscopy," *Photochemistry and Photobiology*, vol. 72(1), pp. 103-113, 2000.

[30] S. K. Majumder, S. K. Mohanty, N. Ghosh, P. K. Gupta, D. K. Jain, and F. Khan, "A pilot study on the use of autofluorescence spectroscopy for diagnosis of the cancer of human oral cavity," *Current Science*, vol. 79(8), pp. 1089-1094, 2000.

[31] S. K. Majumder, N. Ghosh, S. Kataria, and P. K. Gupta, "Nonlinear pattern recognition for laser-induced fluorescence diagnosis of cancer," *Lasers in Surgery and Medicine,* vol. 33(1), pp. 48-56, 2003.
[32] V. R. Kolli, H. E. Savage, T. J. Yao, and S. P. Schantz, "NATIVE CELLULAR FLUORESCENCE OF NEOPLASTIC UPPER AERODIGESTIVE MUCOSA," *Archives of Otolaryngology-Head & Neck Surgery,* vol. 121(11), pp. 1287-1292, 1995.
[33] V. R. Kolli, A. R. Shaha, H. E. Savage, P. G. Sacks, M. A. Casale, and S. P. Schantz, "NATIVE CELLULAR FLUORESCENCE CAN IDENTIFY CHANGES IN EPITHELIAL THICKNESS IN-VIVO IN THE UPPER AERODIGESTIVE TRACT," *American Journal of Surgery,* vol. 170(5), pp. 495-498, 1995.
[34] J. K. Dhingra, D. F. Perrault, K. McMillan, E. E. Rebeiz, S. Kabani, R. Manoharan, I. Itzkan, M. S. Feld, and S. M. Shapshay, "Early diagnosis of upper aerodigestive tract cancer by autofluorescence," *Archives of Otolaryngology-Head & Neck Surgery,* vol. 122(11), pp. 1181-1186, 1996.
[35] T. Tsai, H. M. Chen, C. Y. Wang, J. C. Tsai, C. T. Chen, and C. P. Chiang, "In vivo autofluorescence Spectroscopy of oral premalignant and malignant lesions: Distortion of fluorescence intensity by submucous fibrosis," *Lasers in Surgery and Medicine,* vol. 33(1), pp. 40-47, 2003.
[36] A. Gillenwater, R. Jacob, R. Ganeshappa, B. Kemp, A. K. El-Naggar, J. L. Palmer, G. Clayman, M. F. Mitchell, and R. Richards-Kortum, "Noninvasive diagnosis of oral neoplasia based on fluorescence spectroscopy and native tissue autofluorescence," *Archives of Otolaryngology-Head & Neck Surgery,* vol. 124(11), pp. 1251-1258, 1998.
[37] S. P. Schantz, V. Kolli, H. E. Savage, G. P. Yu, J. P. Shah, D. E. Harris, A. Katz, R. R. Alfano, and A. G. Huvos, "In vivo native cellular fluorescence and histological characteristics of head and neck cancer," *Clinical Cancer Research,* vol. 4(5), pp. 1177-1182, 1998.
[38] M. Inaguma and K. Hashimoto, "Porphyrin-like fluorescence in oral cancer - In vivo fluorescence spectral characterization of lesions by use of a near-ultraviolet excited autofluorescence diagnosis system and separation of fluorescent extracts by capillary electrophoresis," *Cancer,* vol. 86(11), pp. 2201-2211, 1999.
[39] C. S. Betz, M. Mehlmann, K. Rick, H. Stepp, G. Grevers, R. Baumgartner, and A. Leunig, "Autofluorescence imaging and spectroscopy of normal and malignant mucosa in patients with head and neck cancer," *Lasers in Surgery and Medicine,* vol. 25(4), pp. 323-334, 1999.
[40] D. R. Ingrams, J. K. Dhingra, K. Roy, D. F. Perrault, I. D. Bottrill, S. Kabani, E. E. Rebeiz, M. M. Pankratov, S. M. Shapshay, R. Manoharan, I. Itzkan, and M. S. Feld, "Autofluorescence characteristics of oral mucosa," *Head and Neck-Journal for the Sciences and Specialties of the Head and Neck,* vol. 19(1), pp. 27-32, 1997.
[41] H. J. van Staveren, R. L. P. van Veen, O. C. Speelman, M. J. H. Witjes, W. M. Star, and J. L. N. Roodenburg, "Classification of clinical autofluorescence spectra of oral leukoplakia using an artificial neural network: a pilot study," *Oral Oncology,* vol. 36(3), pp. 286-293, 2000.
[42] C. Y. Wang, T. Tsai, H. M. Chen, C. T. Chen, and C. P. Chiang, "PLS-ANN based classification model for oral submucous fibrosis and oral carcinogenesis," *Lasers in Surgery and Medicine,* vol. 32(4), pp. 318-326, 2003.
[43] I. Georgakoudi, B. C. Jacobson, J. Van Dam, V. Backman, M. B. Wallace, M. G. Muller, Q. Zhang, K. Badizadegan, D. Sun, G. A. Thomas, L. T. Perelman, and M. S. Feld, "Fluorescence, reflectance, and light-scattering spectroscopy for evaluating

dysplasia in patients with Barrett's esophagus," *Gastroenterology*, vol. 120(7), pp. 1620-1629, 2001.

[44] H. Akbari, K. Uto, Y. Kosugi, K. Kojima, and N. Tanaka, "Cancer detection using infrared hyperspectral imaging," *Cancer Science*, vol. 102(4), pp. 852-857, 2011.

[45] K. R. Koh, T. C. Wood, R. D. Goldin, G. Z. Yang, and D. S. Elson, "Visible and near infrared autofluorescence and hyperspectral imaging spectroscopy for the investigation of colorectal lesions and detection of exogenous fluorophores," in *Advanced Biomedical and Clinical Diagnostic Systems Vii*. vol. 7169, A. MahadevanJansen, *et al.*, Eds., ed Bellingham: Spie-Int Soc Optical Engineering, 2009.

[46] K. Onizawa, N. Okamura, H. Saginoya, H. Yusa, T. Yanagawa, and H. Yoshida, "Analysis of fluorescence in oral squamous cell carcinoma," *Oral Oncology*, vol. 38(4), pp. 343-348, 2002.

[47] B. Mayinger, P. Horner, M. Jordan, C. Gerlach, T. Horbach, W. Hohenberger, and E. G. Hahn, "Light-induced autofluorescence spectroscopy for the endoscopic detection of esophageal cancer," *Gastrointestinal Endoscopy*, vol. 54(2), pp. 195-201, 2001.

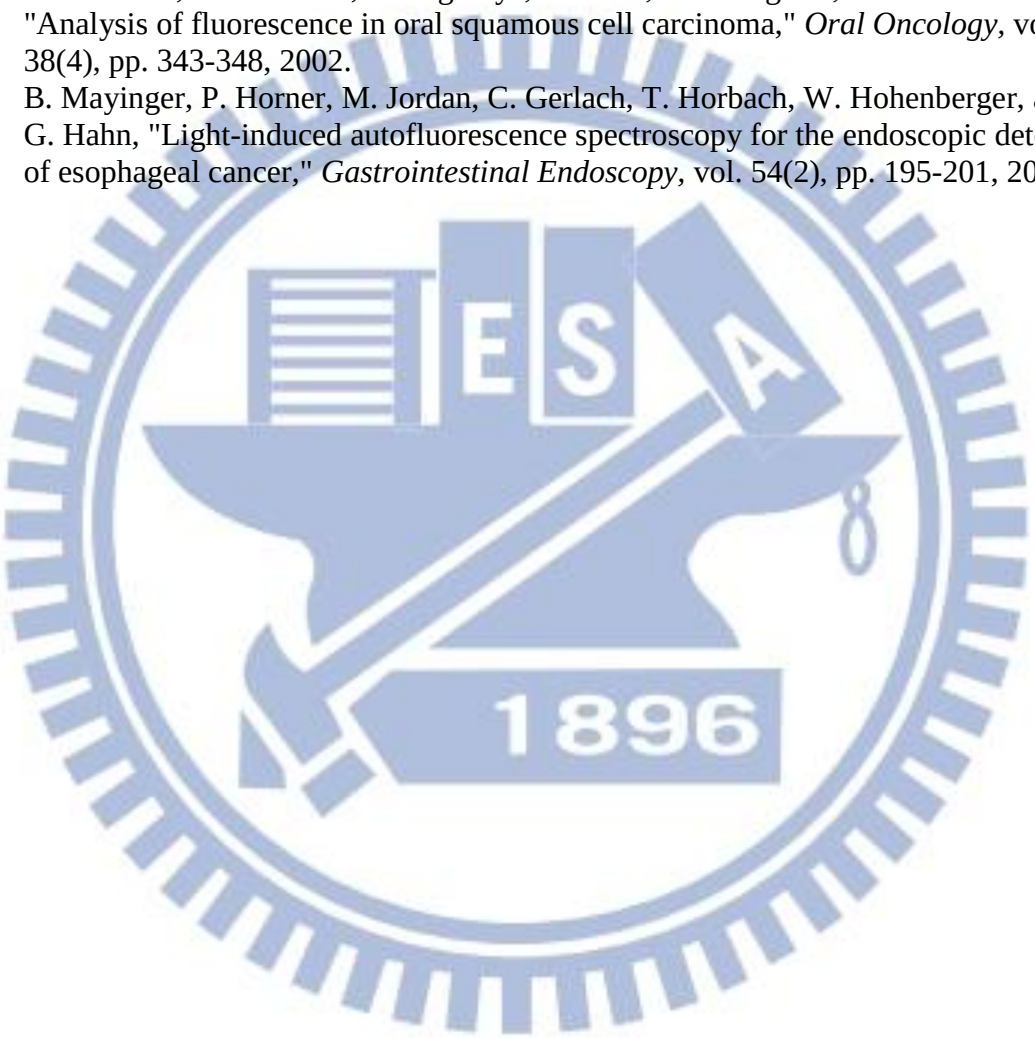

Publications

Publications

Conference Papers

1. **Chih-Hsien Chen**, Yao-Fang Hsieh, Ou-Yang Mang, Jeng-Ren Duann,Jin-Chern Chiou, Yung-Jiun Lin, Ming-Hsui Tsai, Da-Tian Bau, Chang-Fang Chiu, Guan-Chin Teseng, Nai-Wen Chang, Wen-Chung Kao, and Shun-De Wu, " The experiment of analyzing oral cancer's spectral characteristics by using UV fluorescence excitation," *International Conference on Photonics*, Tainan, Taiwan, Dec. 8-10, 2011.
2. **Chih-Hsien Chen**, Sing-Tsung Lee, Yao-Fang Hsieh, Mang Ou-Yang, Jeng-Ren Duann, Jin-Chern Chiou, Yung-Jiun Lin, Ming-Hsui Tsai, Chang-Fang Chiu, Guan-Chin Teseng, Nai-Wen Chang, Wen-Chung Kao, and Shun-De Wu," Analysis of Spectral Image for Evaluation of Oral Cancer," *Conference of Symposium on Engineering Medicine and Biology Applications*, Taichung, Taiwan, Feb. 11-13 ,2012

Patents

1. 歐陽盟，謝耀方，**陳誌賢**，“一種繼光鏡掃瞄超光譜數位典藏裝置與方法”，專利申請中，中華民國，民國99年。